Electronic Supplementary Material (ESI) for Inorganic Chemistry Frontiers.

Supporting Information For:

Recyclable MOF@Polymer Thin Film Composite for Nanomolar On-Site Fluorometric Detection of Heavy Metal Ion and Anti-Histamine Drug and Efficient Heterogeneous Catalysis of Friedel-Crafts Alkylation

Sk Sakir Hossain,[a] *Veerappan Karthik,*[b] *Amarajothi Dhakshinamoorthy**[b,c] *and Shyam Biswas**[a]

[a] Department of Chemistry, Indian Institute of Technology Guwahati, 781039 Assam, India.

[b] School of Chemistry, Madurai Kamaraj University, Madurai 625021, Tamil Nadu, India.

[c] Departamento de Química, Universitat Politècnica de València, C/Camino de Vera, s/n, 46022, Valencia, Spain

*Corresponding author. Tel: 91-3612583309

E-mail address: sbiswas@iitg.ac.in (SB); admguru@gmail.com (AD)

Materials and Characterization Methods:

All of the chemicals were purchased from commercial suppliers and used directly. The experimental techniques used in this study included X-ray diffraction (XRD) using a Rigaku Smartlab X-ray diffractometer, Attenuated Total Reflectance Infrared (ATR-IR) spectroscopy using a Perkin Elmer UATR Two, thermogravimetric analysis (TGA) using a Perkin Elmer TGA 4000 thermogravimetric analyzer, nitrogen sorption isotherm analysis using a Quantachrome Autosorb iQ-MP volumetric gas adsorption equipment, fluorescence sensing studies using a HORIBA JOBIN YVON Fluoromax-4 spectrofluorometer, scanning electron microscopy (SEM) imaging using a Zeiss (Sigma 300) scanning electron microscope, and Nuclear Magnetic Resonance (NMR) using a Bruker Avance III 500 NMR spectrometer. Fluorescence lifetimes were measured using Picosecond Time-resolved and Steady State Luminescence Spectrometer on an Edinburg Instruments Lifespec II & FSP 920 instrument. The Pawley refinement method was carried out using Materials Studio software. The XRD analysis was performed using Cu-K_α radiation (λ = 1.54056 Å), with an operating voltage of 40 kV and an operating current of 125 mA. TGA was conducted in the temperature range of 25-800 °C under N_2 atmosphere at a heating rate of 4 °C min^{-1}, while N_2 sorption isotherms were measured at -196 °C after degassing the compound at 100 °C under a high vacuum for 24 hours. UPS work was performed with PHI-5000 Versaprobe III (ULVAC-PHI Inc.) using He(I) (21.22eV) excitation. The ATR-IR was performed in the 400-4000 cm^{-1} range at room temperature. Very strong (vs), strong (s), medium (m), weak (w), shoulder (sh), and broad (br) were used to designate the corresponding absorption bands. For catalytic investigations, the conversion and selectivity were determined with the help of Agilent 7820A gas chromatograph using nitrogen as carrier gas. The products were confirmed by analyzing the reaction mixture with Agilent 5890 GC-MS.

Synthetic Procedure for 2-(3-Acetylthioureido)Terephthalic Acid Linker:

The linker was synthesized with the help of previously reported literature with a slight modification (Scheme 1).[1] Briefly, 3.58 g (44 mmol) of sodium thiocyanate was taken in a 250 mL round bottom flask containing 50 mL of acetone. Then, 1.57 mL (22 mmol) of acetyl chloride was added to the previous mixture and the resulting mixture was refluxed under stirring for 2 h. Meanwhile, 1 g (5.52 mmol) of 2-amino terephthalic acid was dissolved in 50 mL of tetrahydrofuran (THF). After two hours, the mixture was cooled down to room temperature, and the THF mixture was added to it. The resulting mixture was stirred for another two hours at room temperature. After completion of 2 h, the mixture was poured into 200 mL of ice-cold water and kept it for 30 min. Thereafter, pale yellow precipitation was found and the product was collected by vacuum filtration, washed several times with distilled water. Finally, the product was dried in an oven at 80 °C. Yield: 1.34 g (4.71 mmol, 83%). ^{1}H NMR (500 MHz, DMSO-d_6): δ (ppm) = 8.11 (d, 1H, J = 10 Hz), 8.02 (s, 1H), 7.95 (d, 1H, J = 10 Hz), 11.98 (s, 1H), and 13.69 (s, 1H). ^{13}C NMR (125 MHz, DMSO-d_6): δ (ppm) = 23.91, 121.63, 125.15, 126.76, 129.98, 137.55, 147.85, 153.95, 166.30, 171.21, 184.76. The ^{1}H NMR and ^{13}C NMR spectra are shown below as Figures S1 and S2.

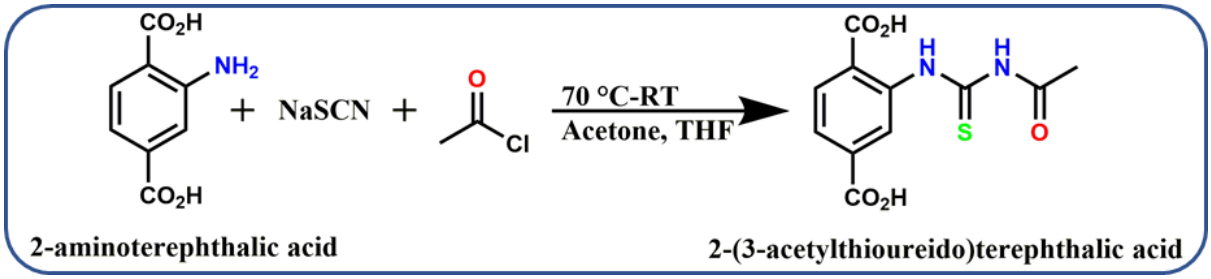

Scheme 1. Reaction scheme for the linker synthesis.

Preparation MOF (1') Suspension for Fluorescence Experiments:

The Hg^{2+} sensing experiment was performed in aqueous medium while ranitidine sensing was executed in HEPES buffer medium. For Hg^{2+} sensing, 1 mg of probe **1'** was suspended in a 5 mL glass vial containing 4 mL of water and placed in sonication bath for 30 min. After that the vial was kept overnight at room temperature to make the suspension stable. The fluorescence experiment was carried out using 100 µL of above-mentioned suspension in a quartz containing 3 mL distilled water. All the fluorescence measurements were executed in the range of 342-550 nm upon exciting the suspension at 322 nm. For competitive analysis, different analyte solutions (10 mM) were added to the above suspension and recorded the emission response in the same range. Similar protocol has been used for ranitidine sensing with some modification. In this case, HEPES buffer medium was used and 5 mM solutions of different analytes were used for the selectivity test.

Fluorometric Detection of Ranitidine in Human Blood Serum Sample:

From the right arm vein of a healthy human with blood group A^+, 10 mL of blood sample was collected. The sample was centrifuged at 10,000 rpm for 15 min to obtain blood plasma, from which the light-yellow blood serum was collected and stored in a Falcon tube at -20 °C. To conduct fluorescence detection experiments, varying concentrations of ranitidine were added to different aliquots of the human blood serum sample containing a MOF suspended in HEPES buffer (pH = 7.4).

Fluorometric Detection of Ranitidine in Human Urine Sample:

A 10 mL urine sample was collected from a healthy individual and treated with 500 mL of HNO_3 to eliminate any interfering living organisms. The sample was then centrifuged at 8000 rpm for 10 min, and the supernatant was used for the experiments. To conduct fluorescence experiments, various amounts of ranitidine were added to the urine samples containing a HEPES buffer suspension of the probe.

Catalytic Procedure:

In a typical experiment, 10 mL Schlenk tube was charged with 10 mg of **1'** which is followed by, 0.1 mmol of IND, 0.105 mmol of NS and 0.1 mL of toluene. Subsequently, this heterogeneous slurry was thoroughly agitated and placed in an oil bath maintained at 70 °C for 24 h. The samples were collected from the reaction mixture then analysed by Agilent 7820A model to assess the conversion and selectivity of the products. Furthermore, gas chromatography coupled with mass spectrometry (GC-MS; Agilent 5977B spectrometer) was

carried out to confirm the formed products. For the recycling experiments, the above explained catalytic procedure was repeated with **1'** separated after the reaction, washed three times with fresh acetonitrile, and dried at 80 °C for 5 h. This dried catalyst was then reused in successive cycles alongside with the fresh IND and NS.

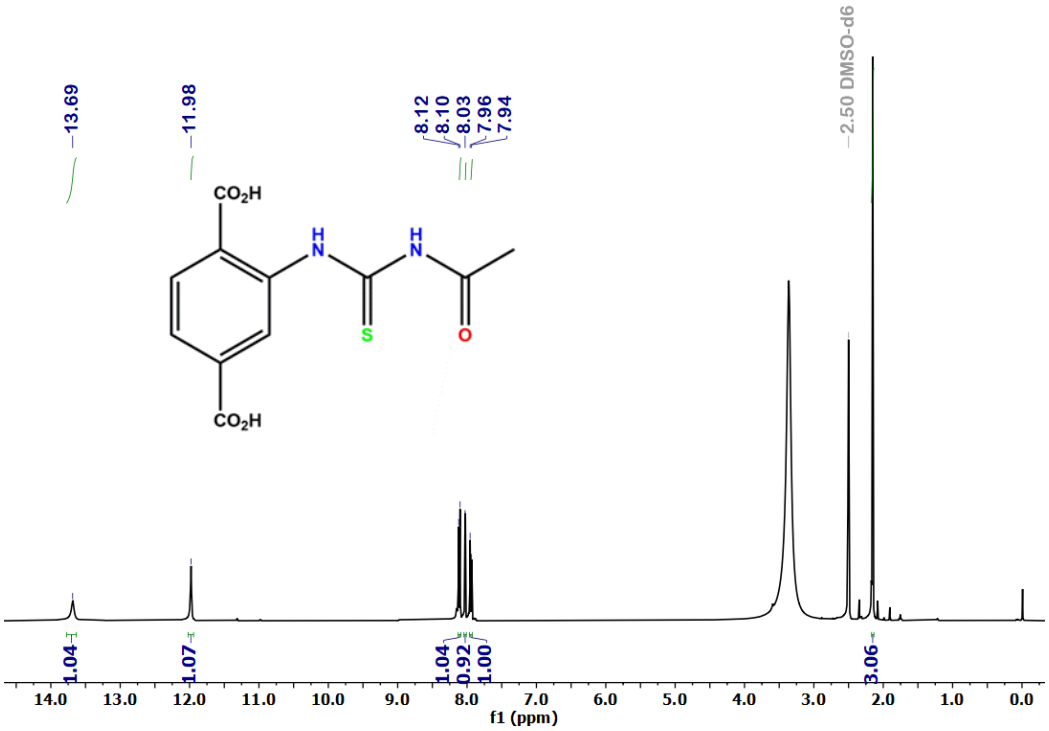

Figure S1. ^{1}H NMR spectrum (500 MHz, DMSO-d_6) of synthesized linker.

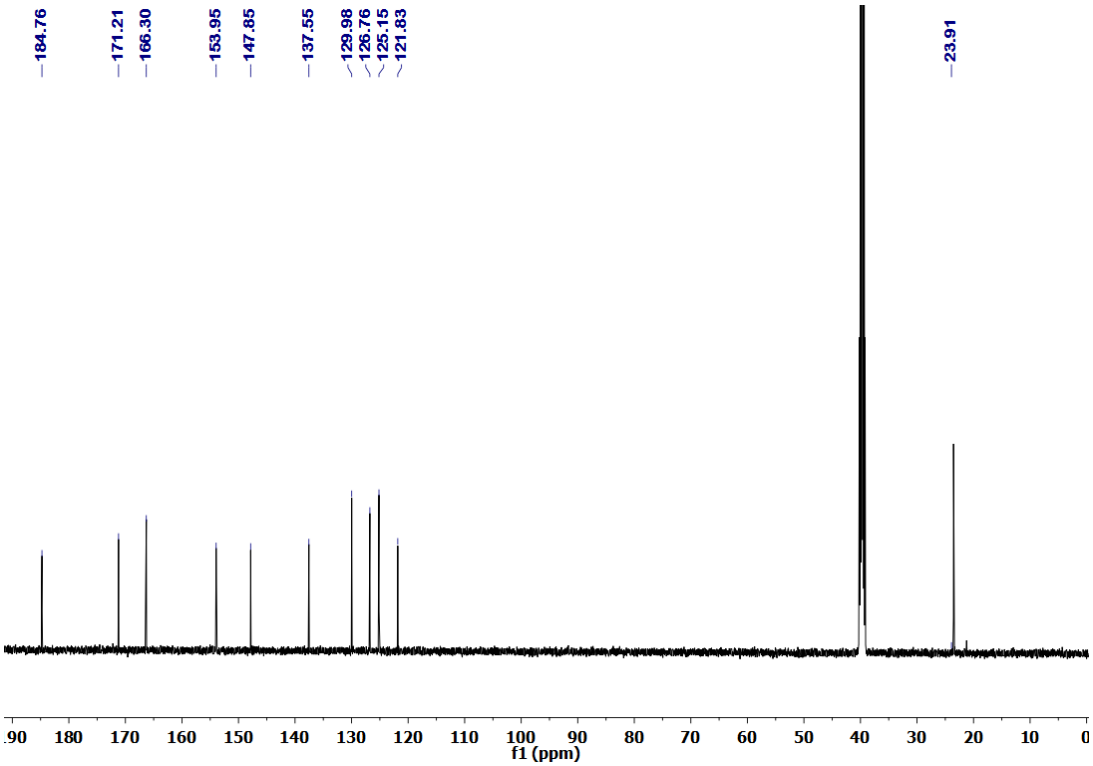

Figure S2. ^{13}C NMR spectrum (125 MHz, DMSO-d_6) of synthesized linker.

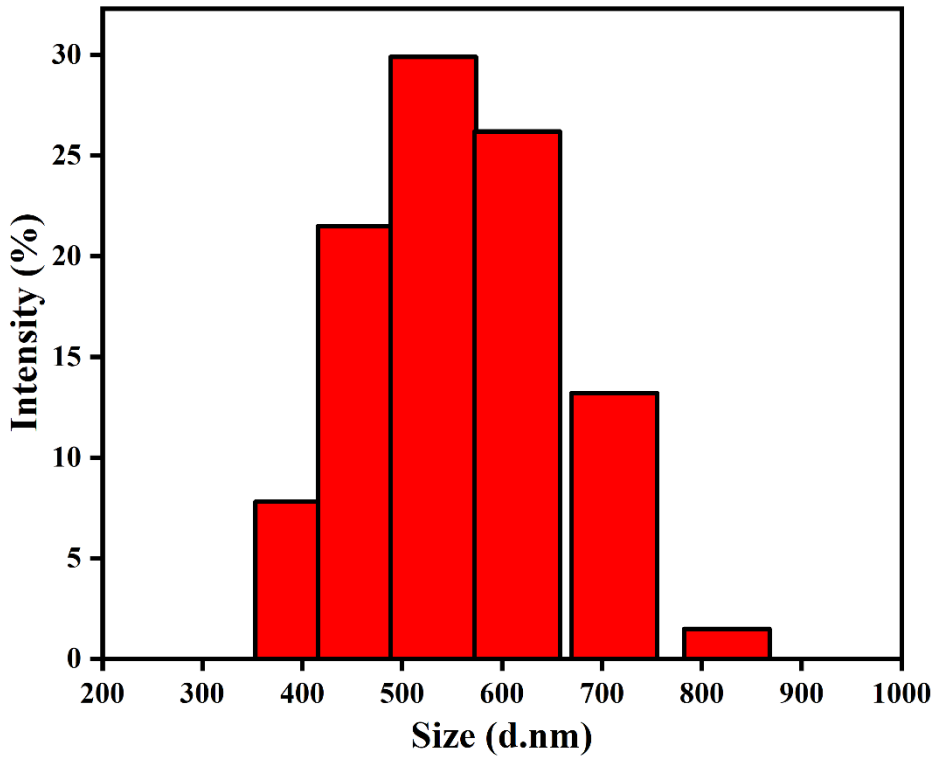

Figure S3. Particle size distribution of the aqueous dispersion of **1′** measured by DLS method.

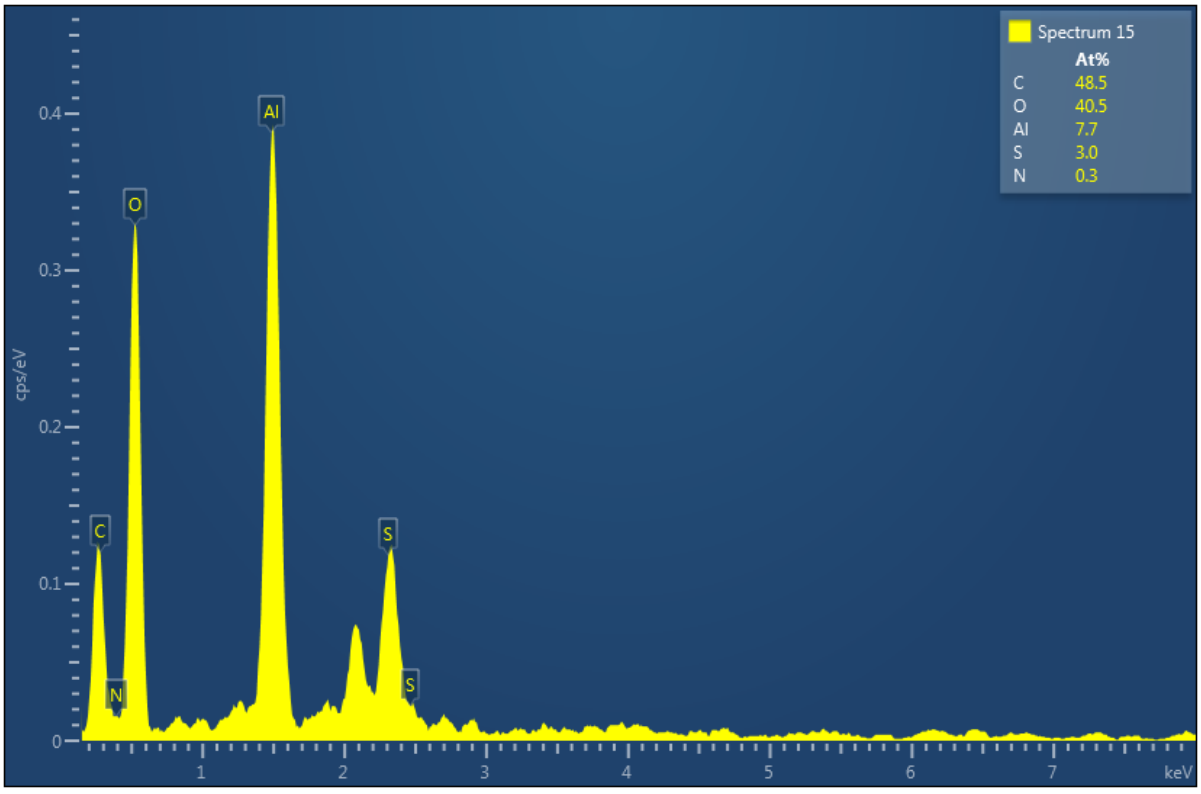

Figure S4. EDX spectrum of **1'**.

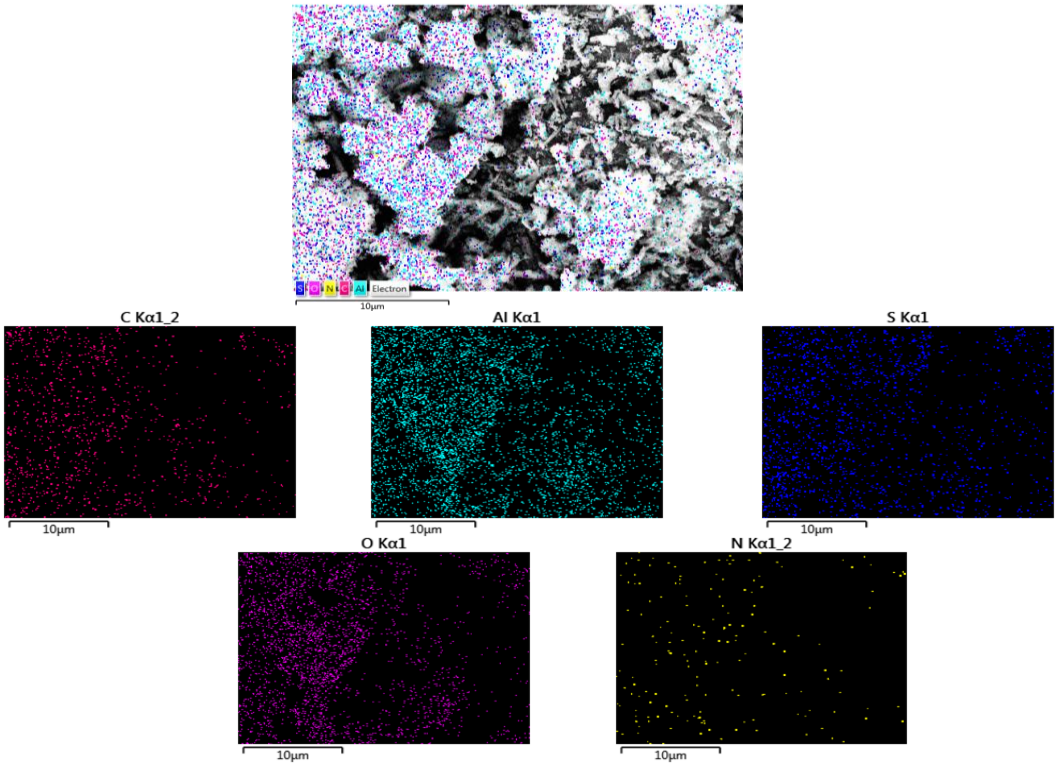

Figure S5. EDX elemental mapping of expected elements present in **1'**.

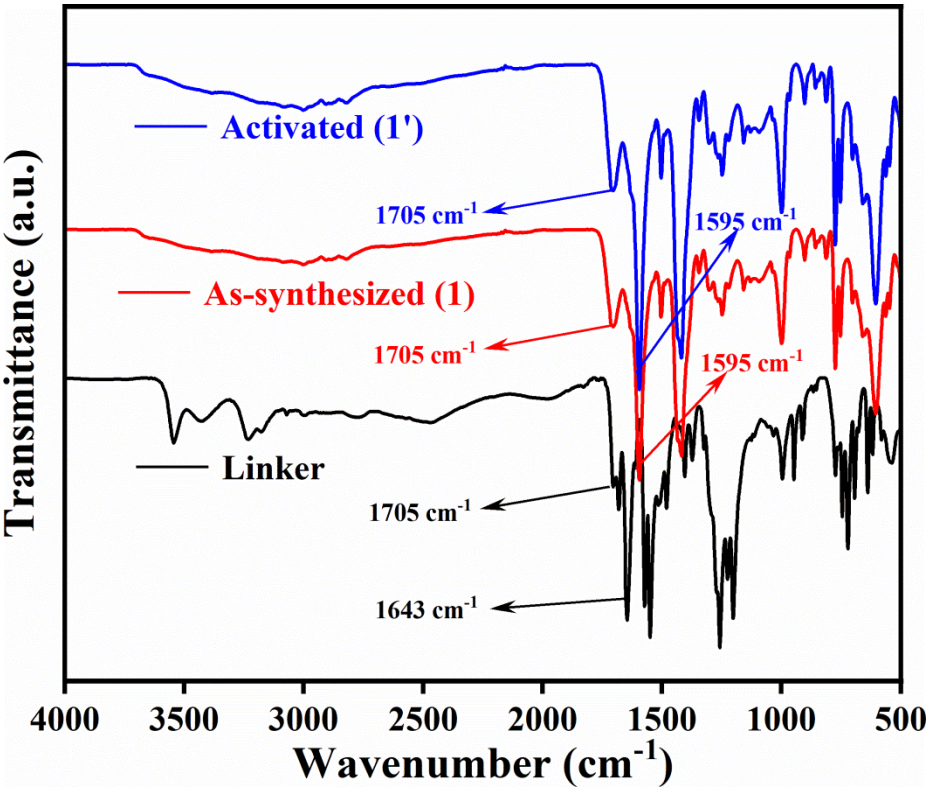

Figure S6. ATR-IR spectra of linker, **1** and **1'**.

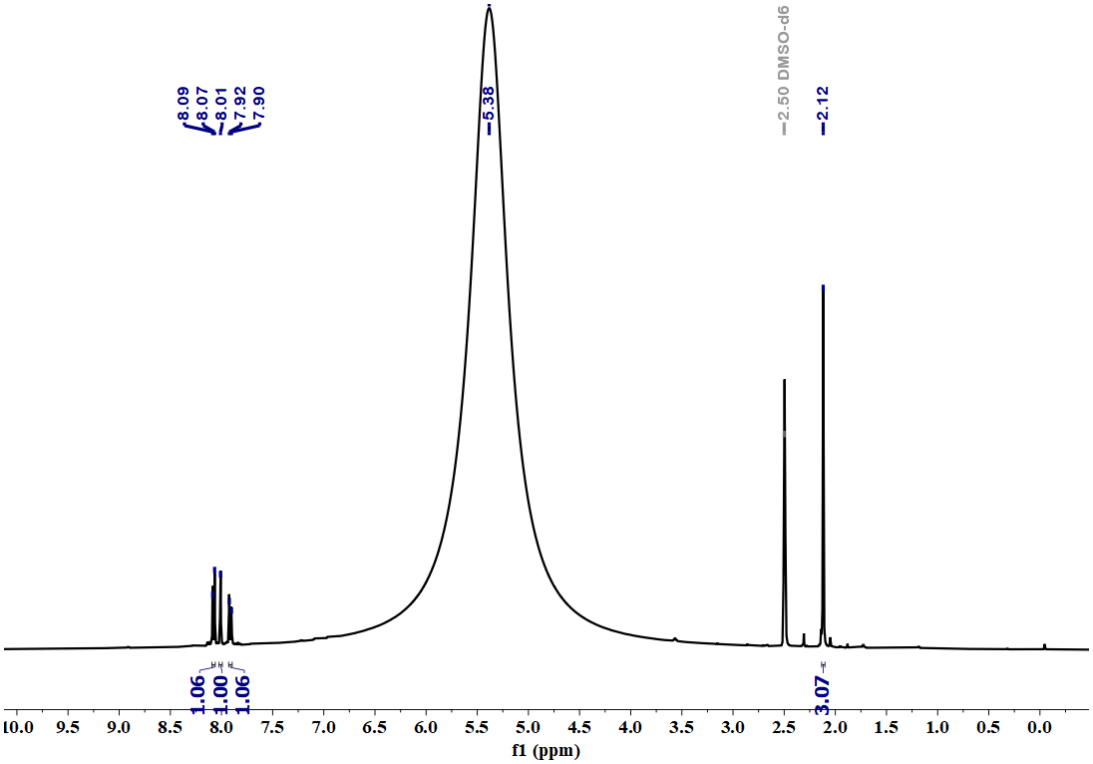

Figure S7. ^{1}H NMR spectrum of digested **1'** (digested using 100 µL of 40% HF in 500 µL of DMSO-d_6).

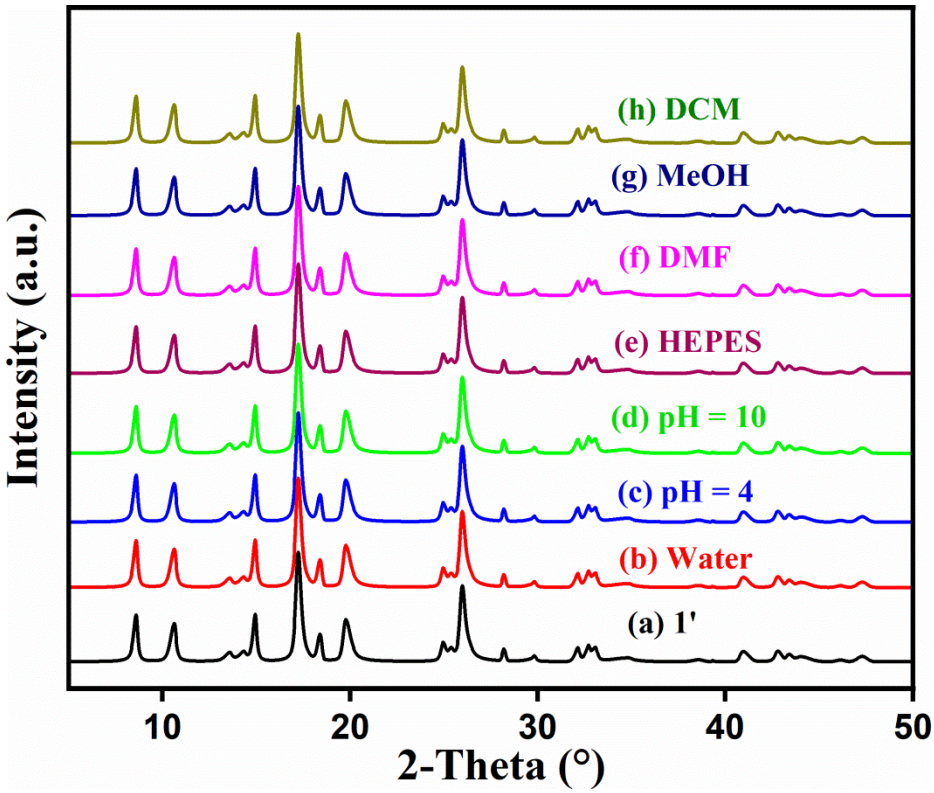

Figure S8. PXRD patterns of **1'** and the obtained samples after stirring in different conditions.

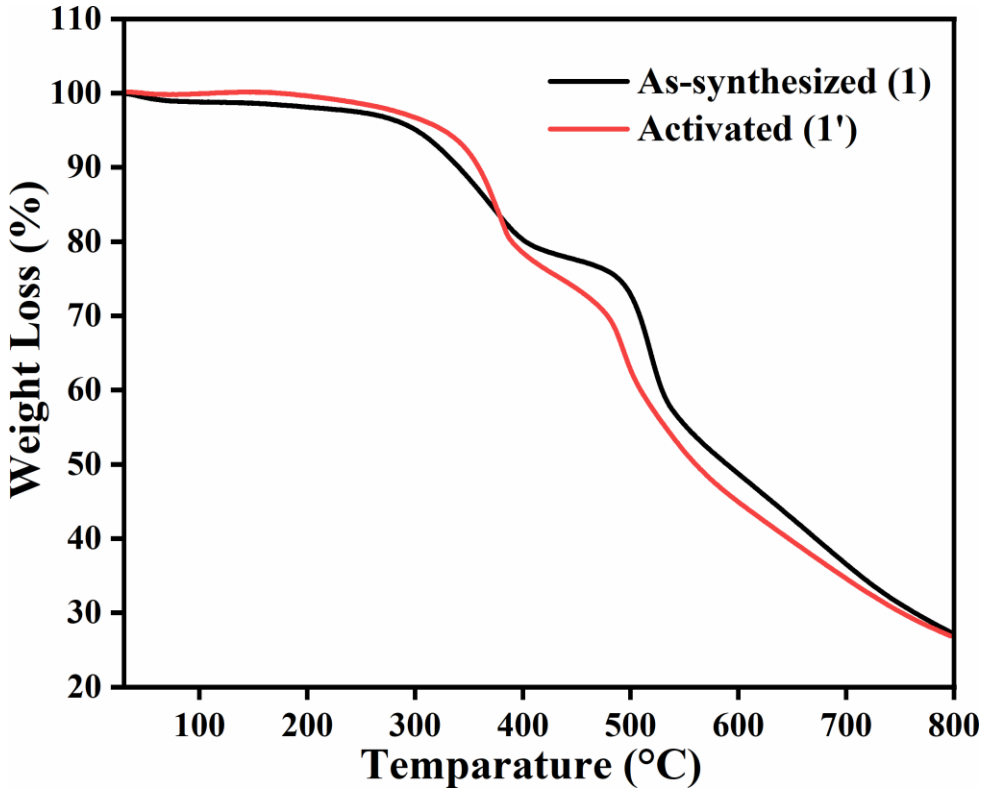

Figure S9. TGA curves of **1** and **1'** recorded under N_2 atmosphere in the temperature range of 30-800 ℃ with a heating rate 4 ℃/min.

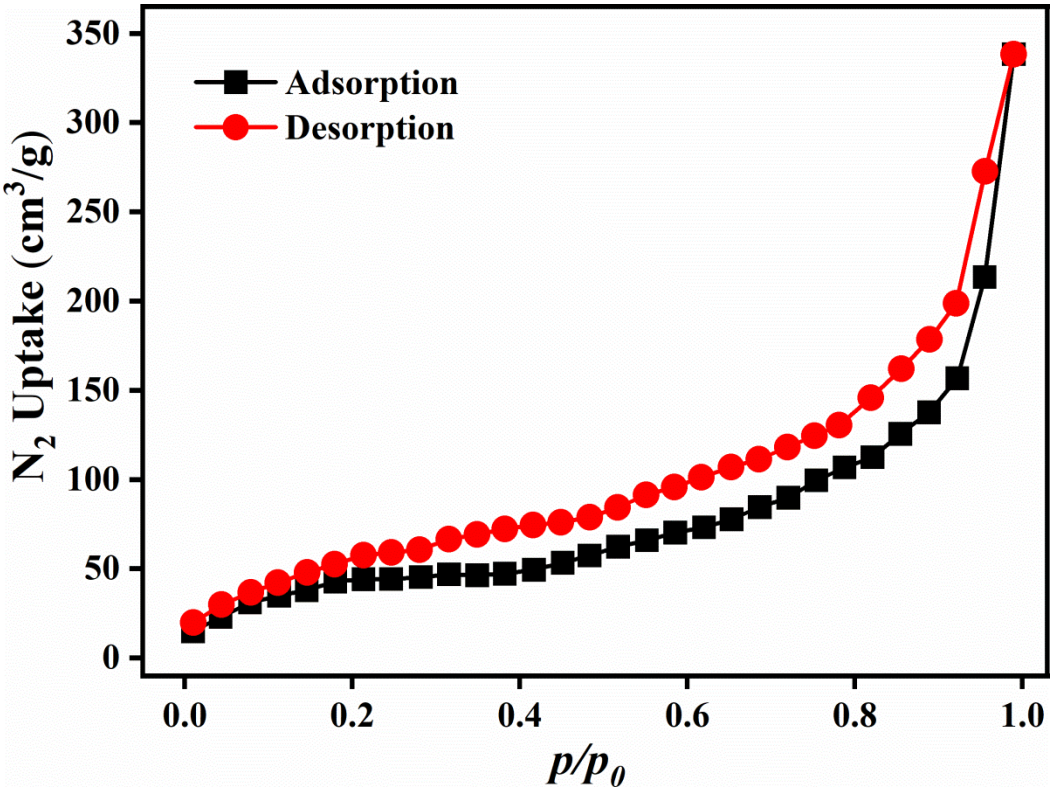

Figure S10. N_2 sorption isotherms of **1'** measured at -196 ℃.

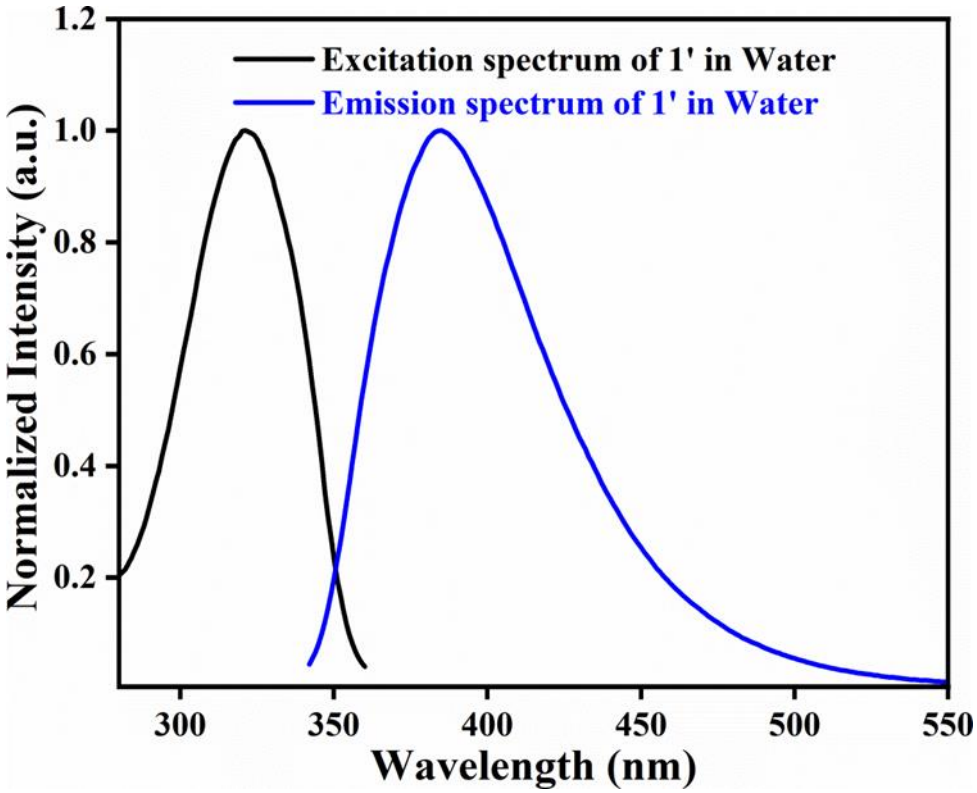

Figure S11. Fluorescence excitation and emission spectra of **1'** in water.

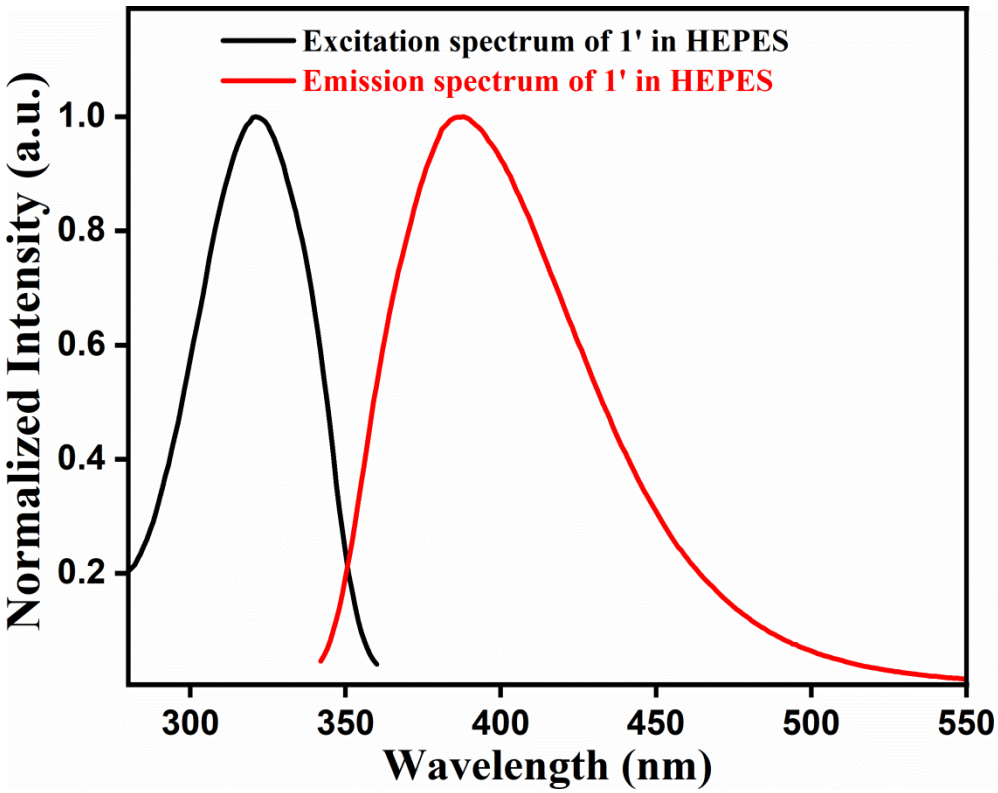

Figure S12. Fluorescence excitation and emission spectra of **1'** in HEPES buffer medium (pH = 7.4).

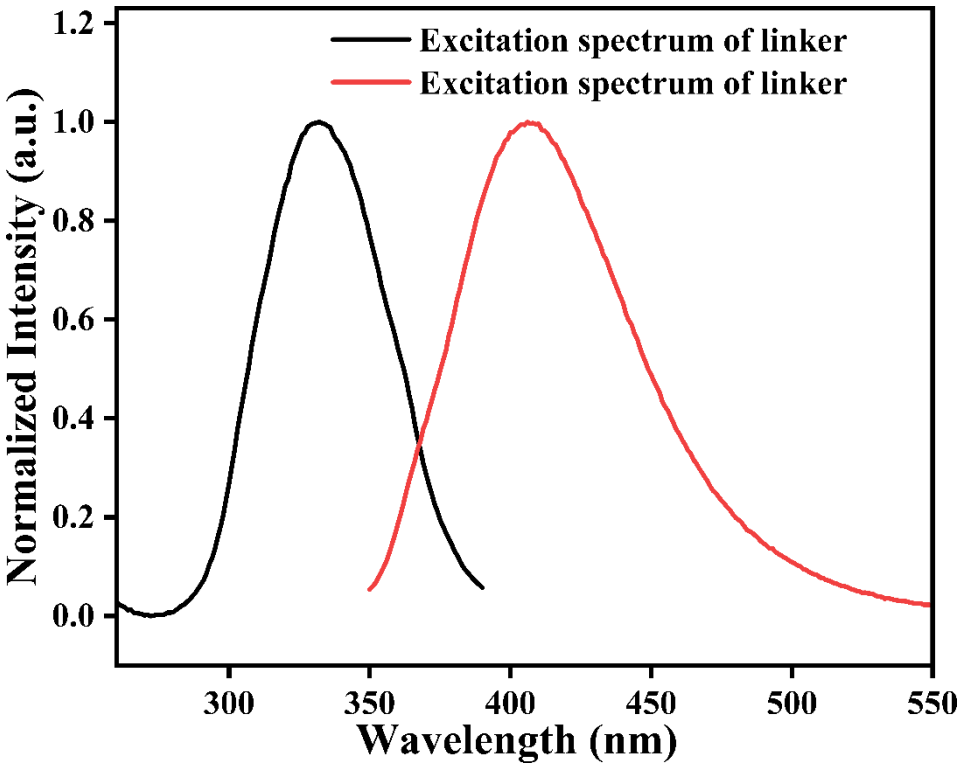

Figure S13. Fluorescence excitation and emission spectra of linker in water.

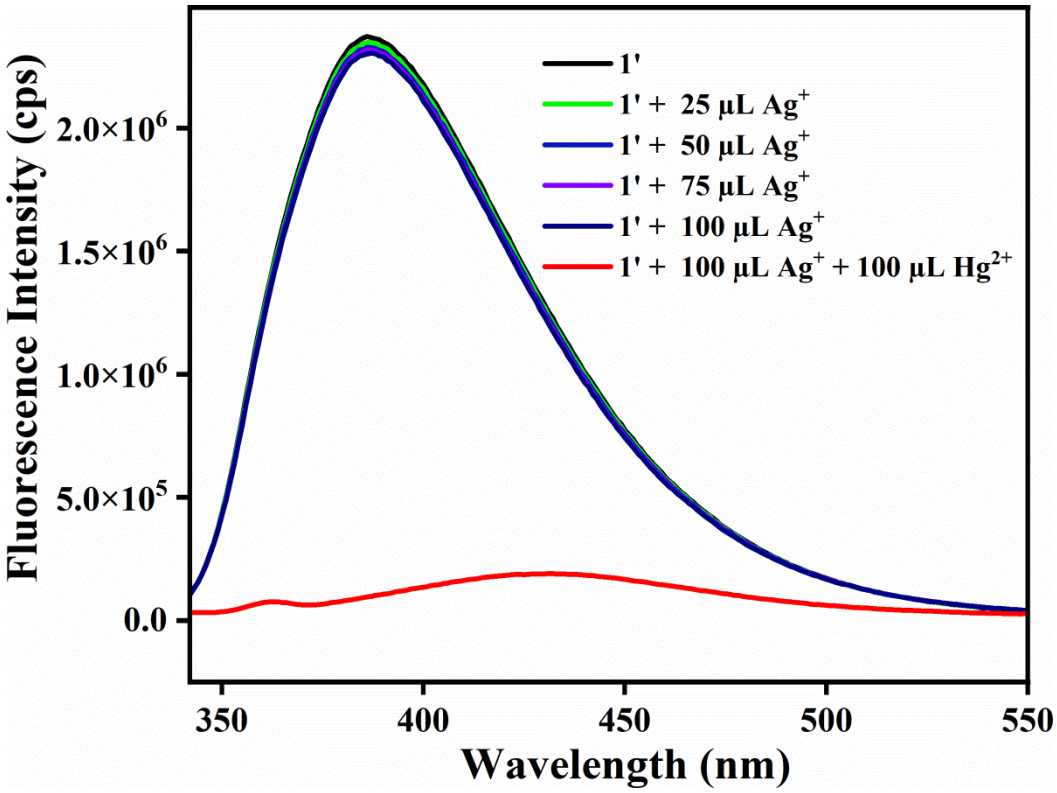

Figure S14. Fluorometric turn-off response of **1'** towards Hg^{2+} (10 mM) in the presence of Ag^{+} (10 mM) in aqueous medium.

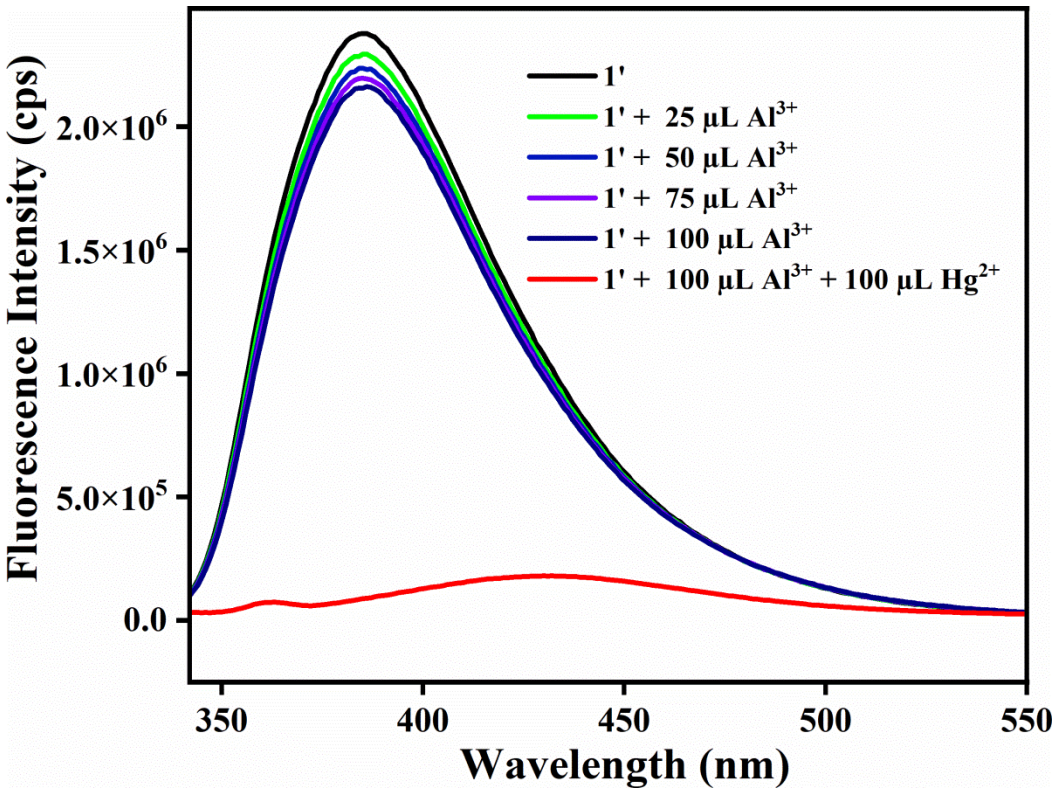

Figure S15. Fluorometric turn-off response of **1'** towards Hg^{2+} (10 mM) in the presence of Al^{3+} (10 mM) in aqueous medium.

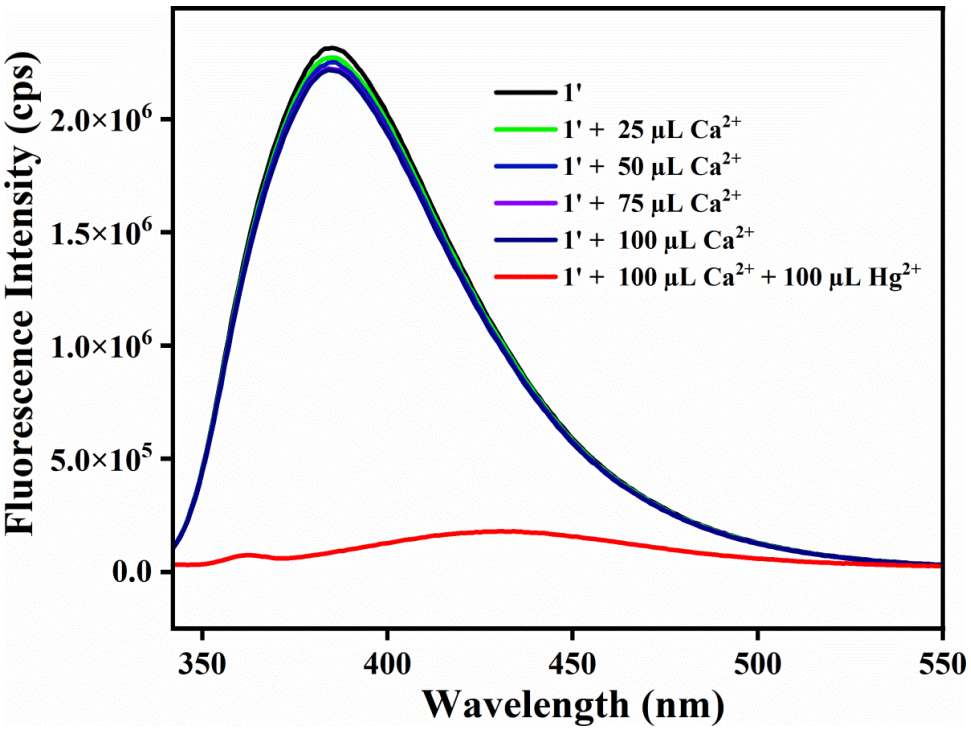

Figure S16. Fluorometric turn-off response of **1'** towards Hg^{2+} (10 mM) in the presence of Ca^{2+} (10 mM) in aqueous medium.

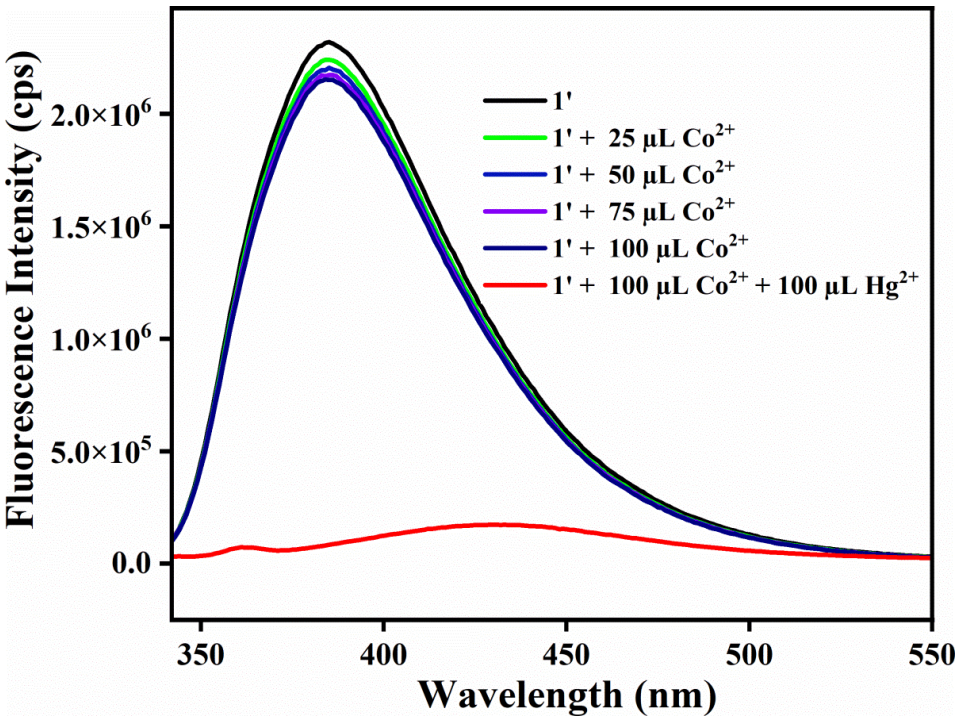

Figure S17. Fluorometric turn-off response of **1'** towards Hg^{2+} (10 mM) in the presence of Co^{2+} (10 mM) in aqueous medium.

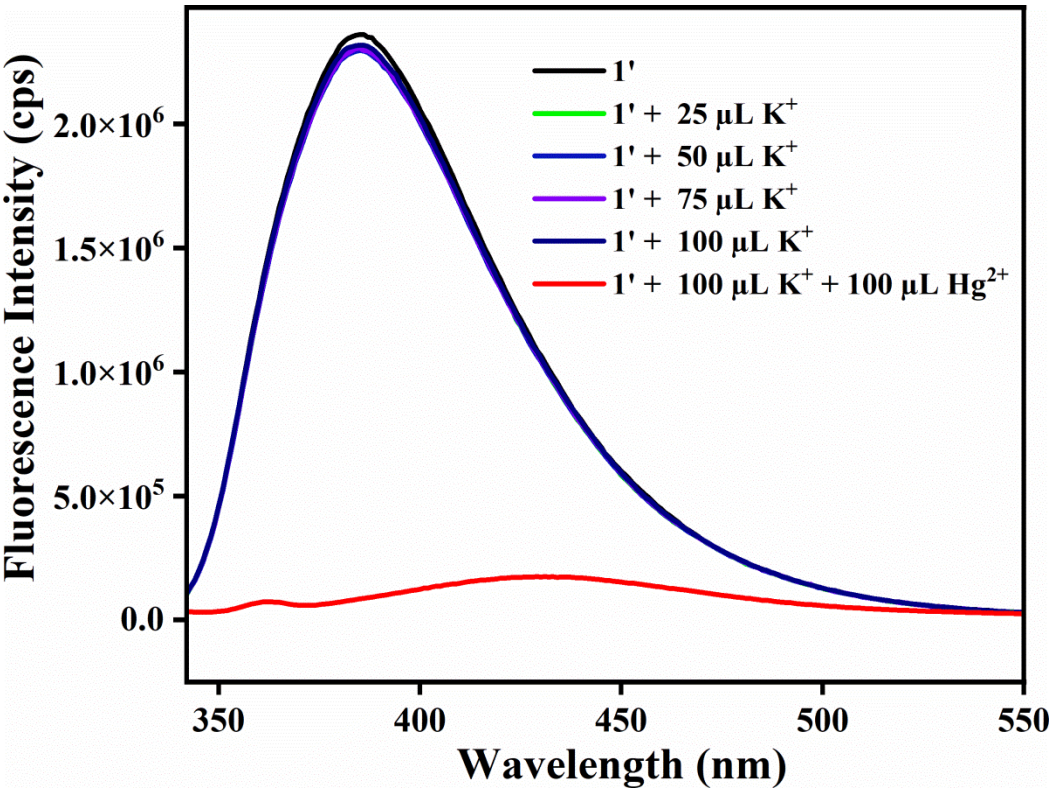

Figure S18. Fluorometric turn-off response of **1'** towards Hg^{2+} (10 mM) in the presence of K^{+} (10 mM) in aqueous medium.

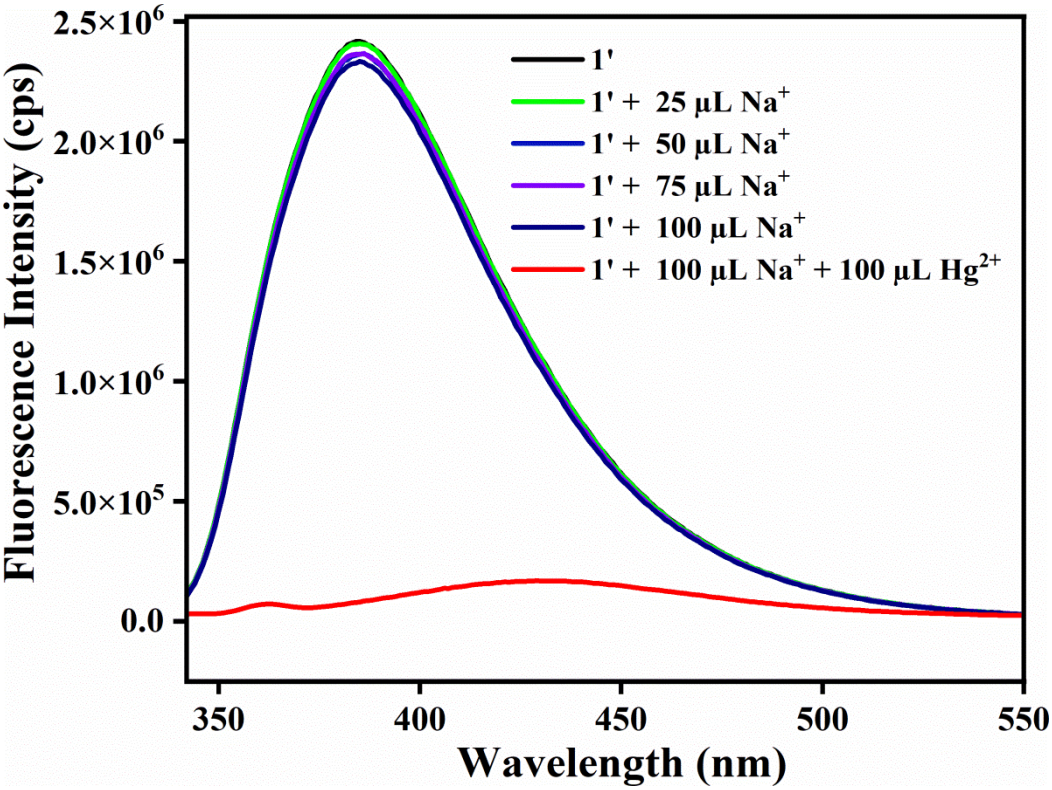

Figure S19. Fluorometric turn-off response of **1'** towards Hg^{2+} (10 mM) in the presence of Na^{+} (10 mM) in aqueous medium.

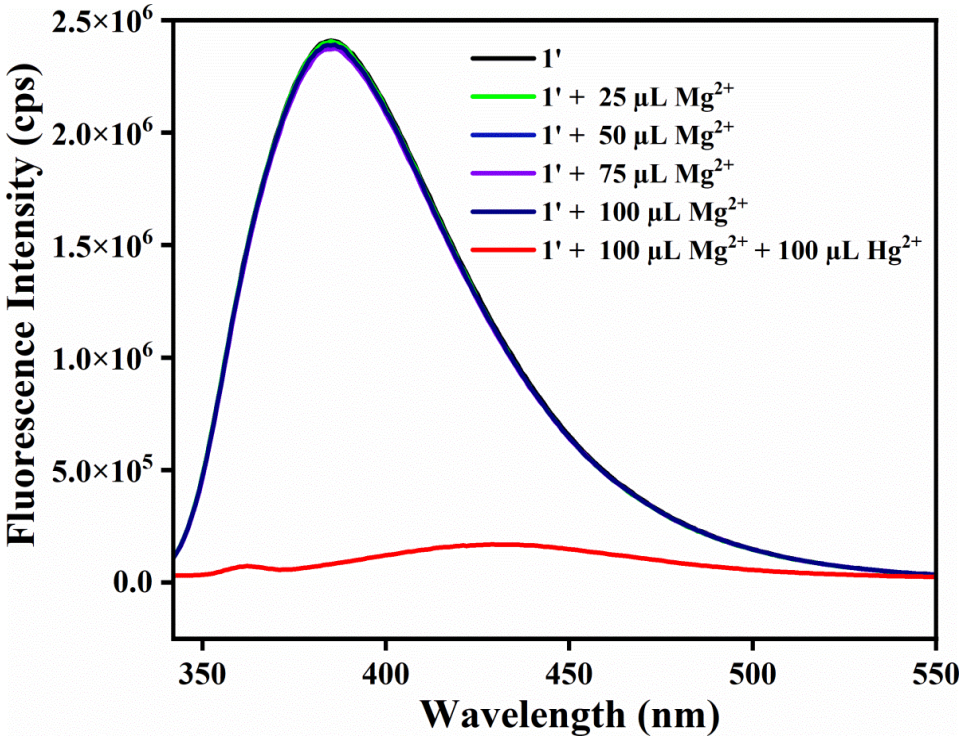

Figure S20. Fluorometric turn-off response of **1'** towards Hg^{2+} (10 mM) in the presence of Mg^{2+} (10 mM) in aqueous medium.

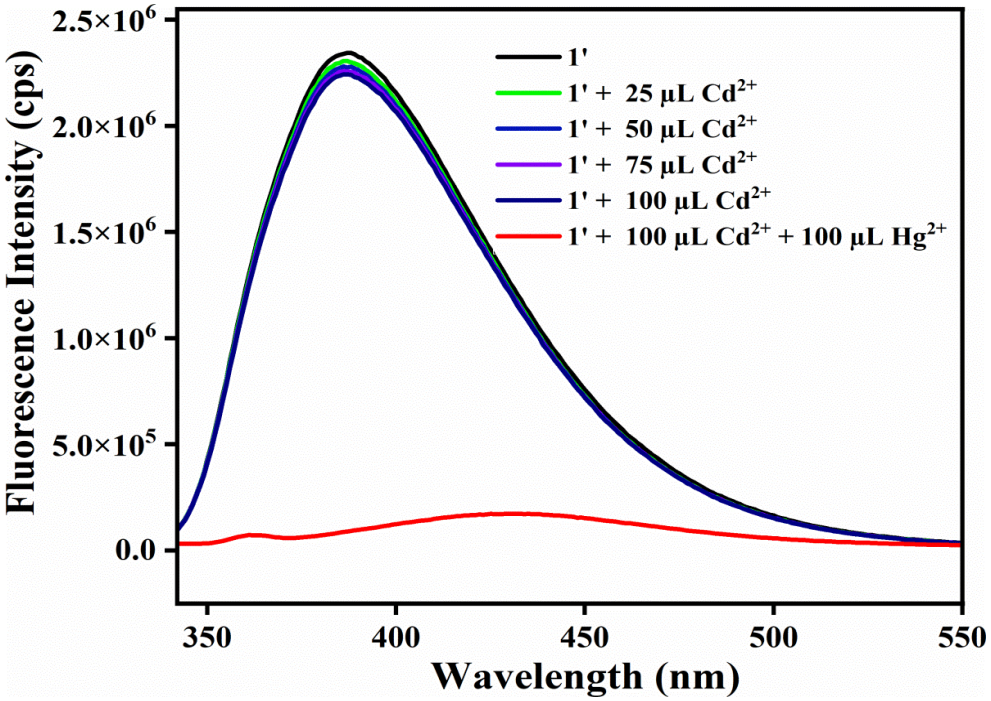

Figure S21. Fluorometric turn-off response of **1'** towards Hg^{2+} (10 mM) in the presence of Cd^{2+} (10 mM) in aqueous medium.

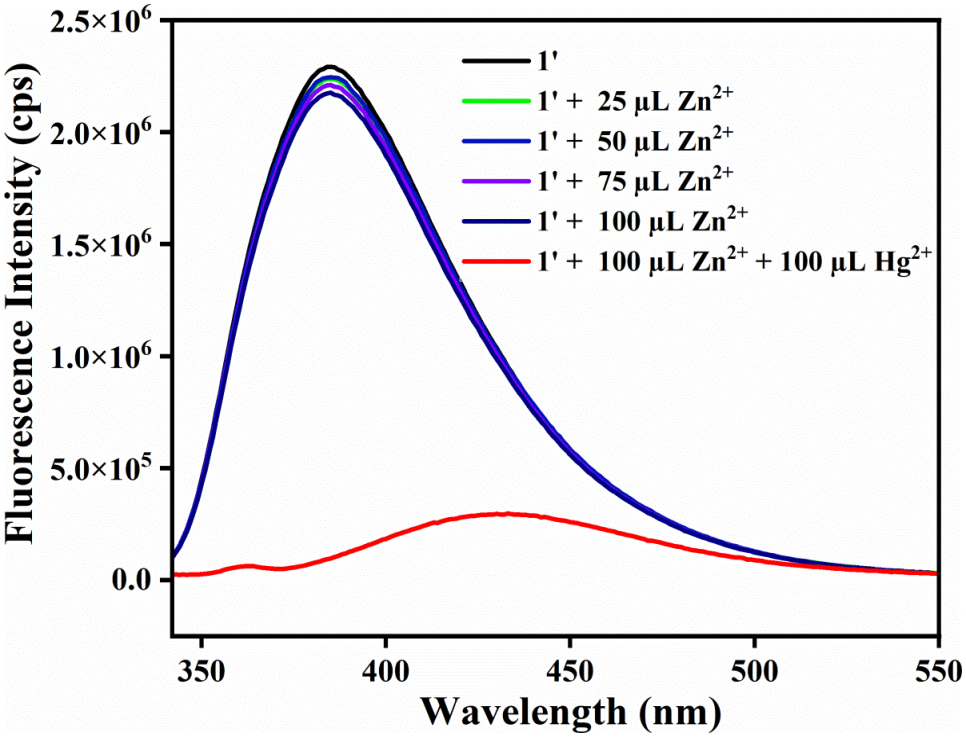

Figure S22. Fluorometric turn-off response of **1'** towards Hg^{2+} (10 mM) in the presence of Zn^{2+} (10 mM) in aqueous medium.

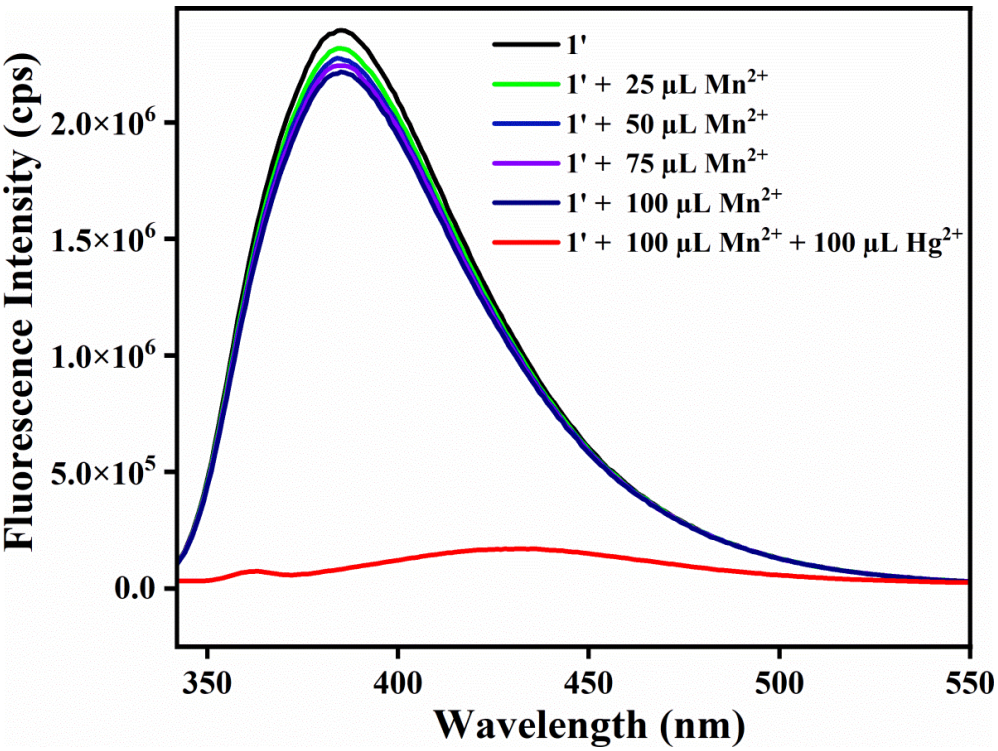

Figure S23. Fluorometric turn-off response of **1'** towards Hg^{2+} (10 mM) in the presence of Mn^{2+} (10 mM) in aqueous medium.

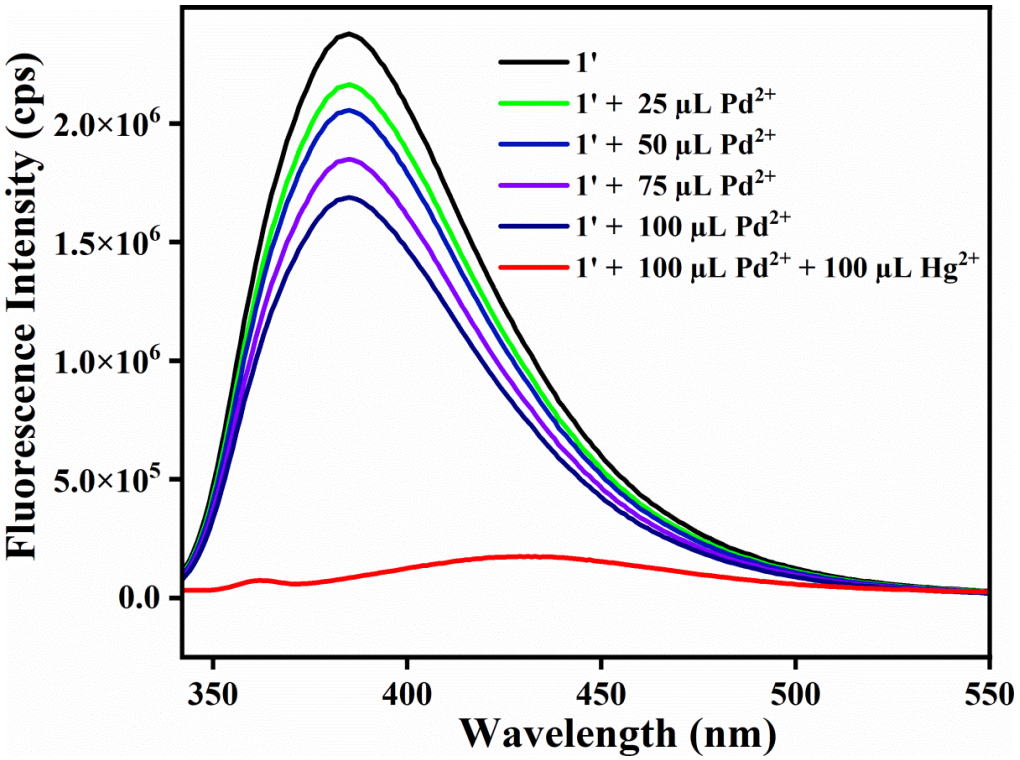

Figure S24. Fluorometric turn-off response of **1'** towards Hg^{2+} (10 mM) in the presence of Pd^{2+} (10 mM) in aqueous medium.

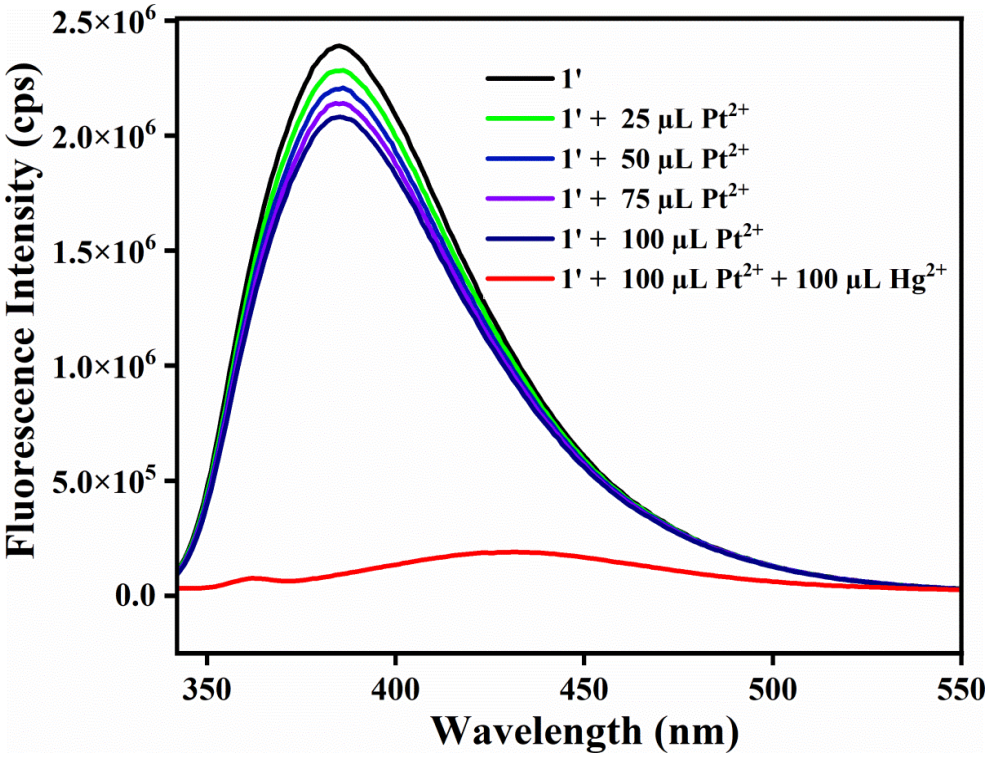

Figure S25. Fluorometric turn-off response of **1'** towards Hg^{2+} (10 mM) in the presence of Pt^{2+} (10 mM) in aqueous medium.

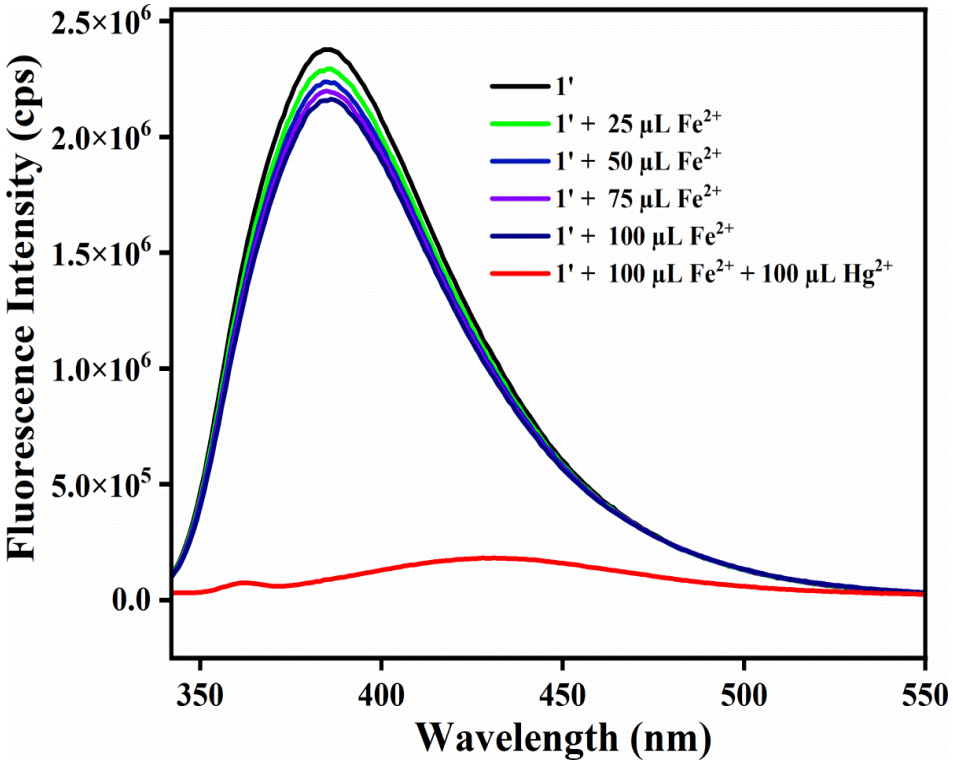

Figure S26. Fluorometric turn-off response of **1'** towards Hg^{2+} (10 mM) in the presence of Fe^{2+} (10 mM) in aqueous medium.

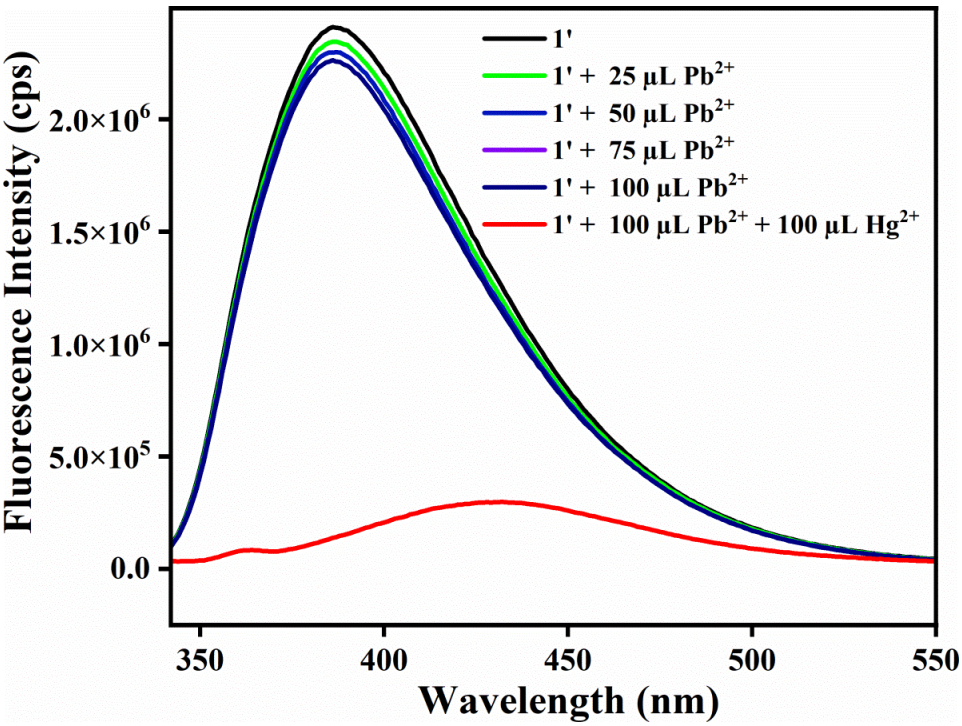

Figure S27. Fluorometric turn-off response of **1'** towards Hg^{2+} (10 mM) in the presence of Pb^{2+} (10 mM) in aqueous medium.

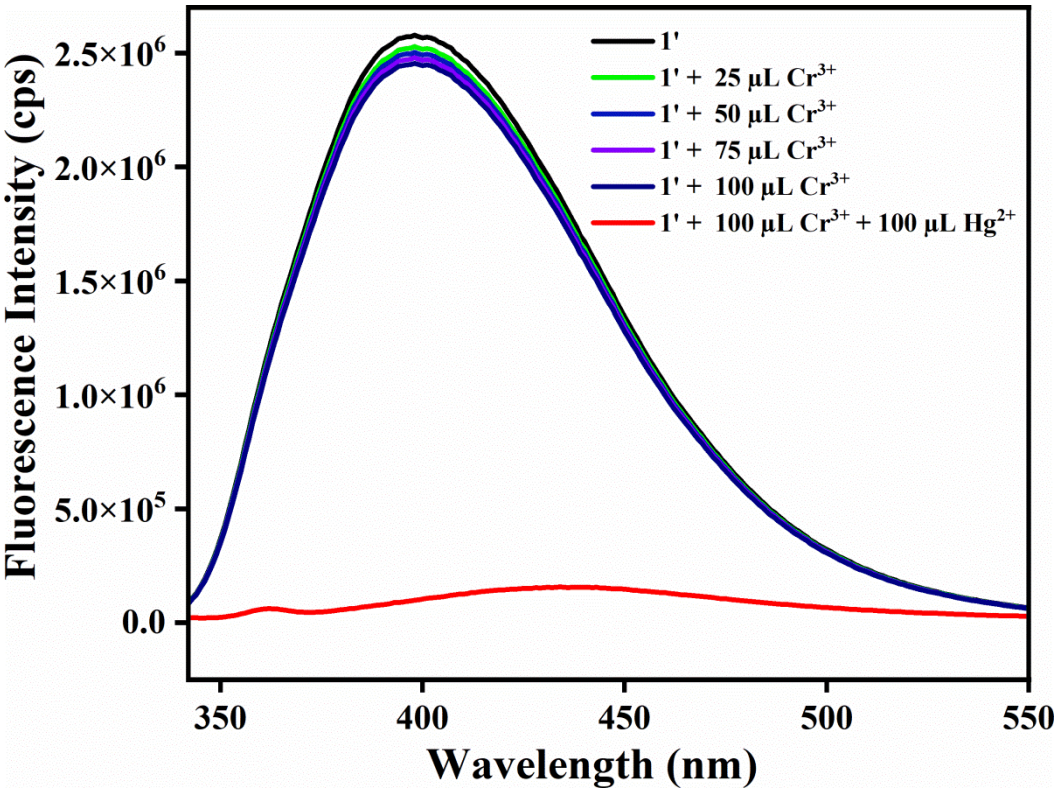

Figure S28. Fluorometric turn-off response of **1'** towards Hg^{2+} (10 mM) in the presence of Cr^{3+} (10 mM) in aqueous medium.

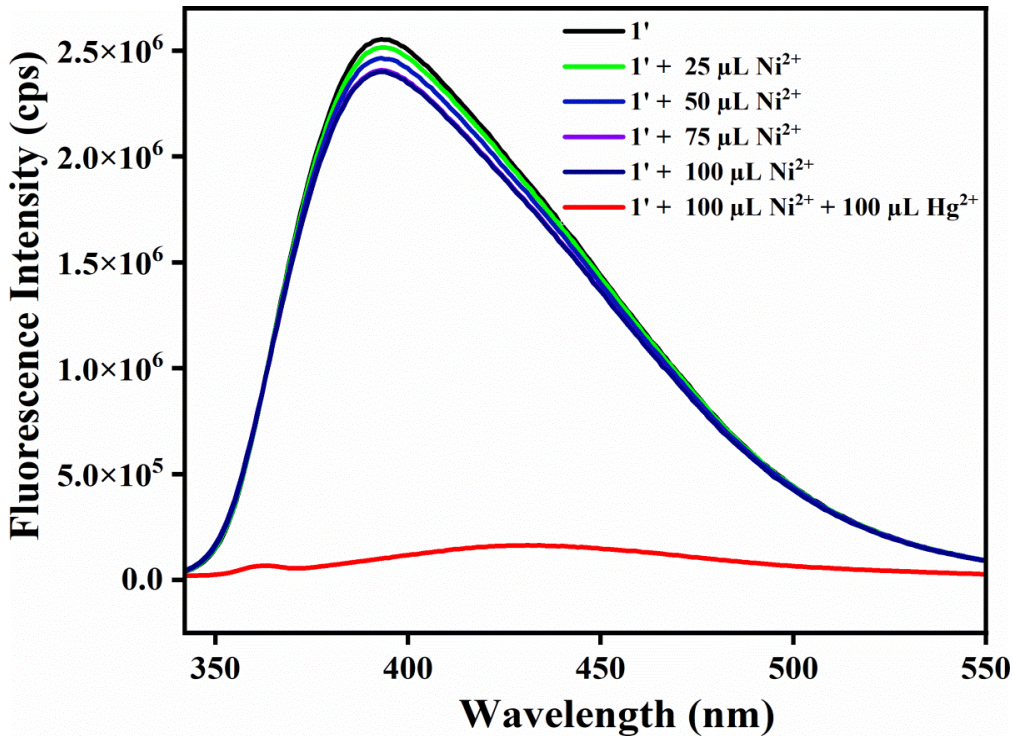

Figure S29. Fluorometric turn-off response of **1'** towards Hg^{2+} (10 mM) in the presence of Ni^{2+} (10 mM) in aqueous medium.

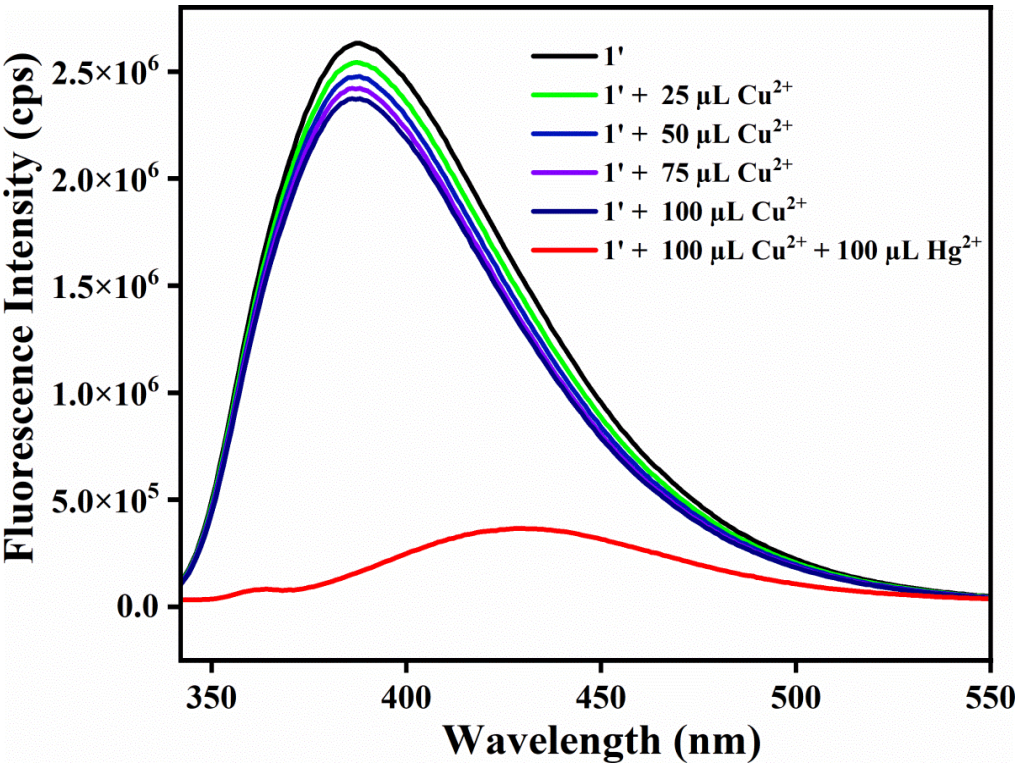

Figure S30. Fluorometric turn-off response of **1'** towards Hg^{2+} (10 mM) in the presence of Cu^{2+} (10 mM) in aqueous medium.

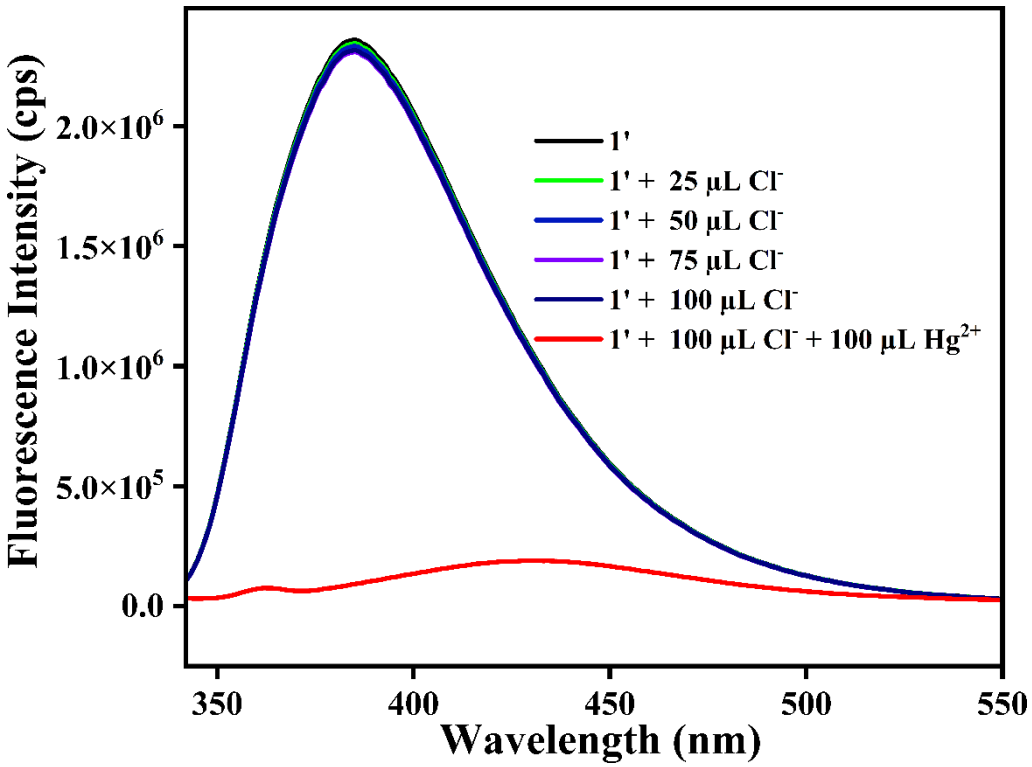

Figure S31. Fluorometric turn-off response of **1'** towards Hg^{2+} (10 mM) in the presence of Cl^- (10 mM) in aqueous medium.

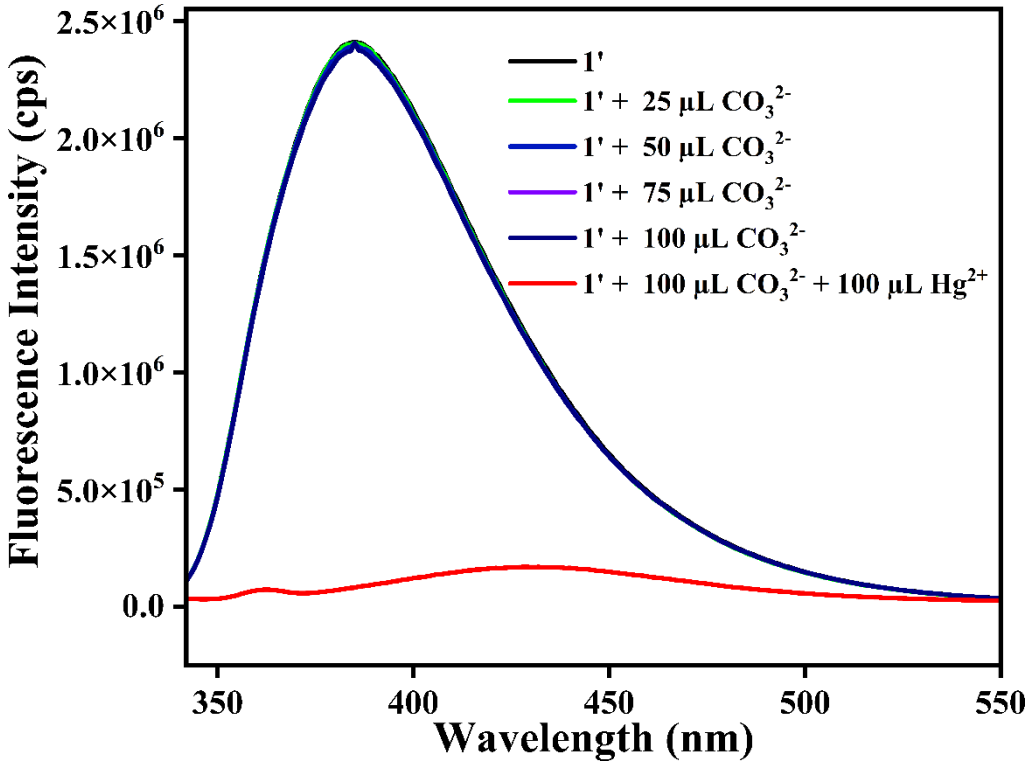

Figure S32. Fluorometric turn-off response of **1'** towards Hg^{2+} (10 mM) in the presence of CO_3^{2-} (10 mM) in aqueous medium.

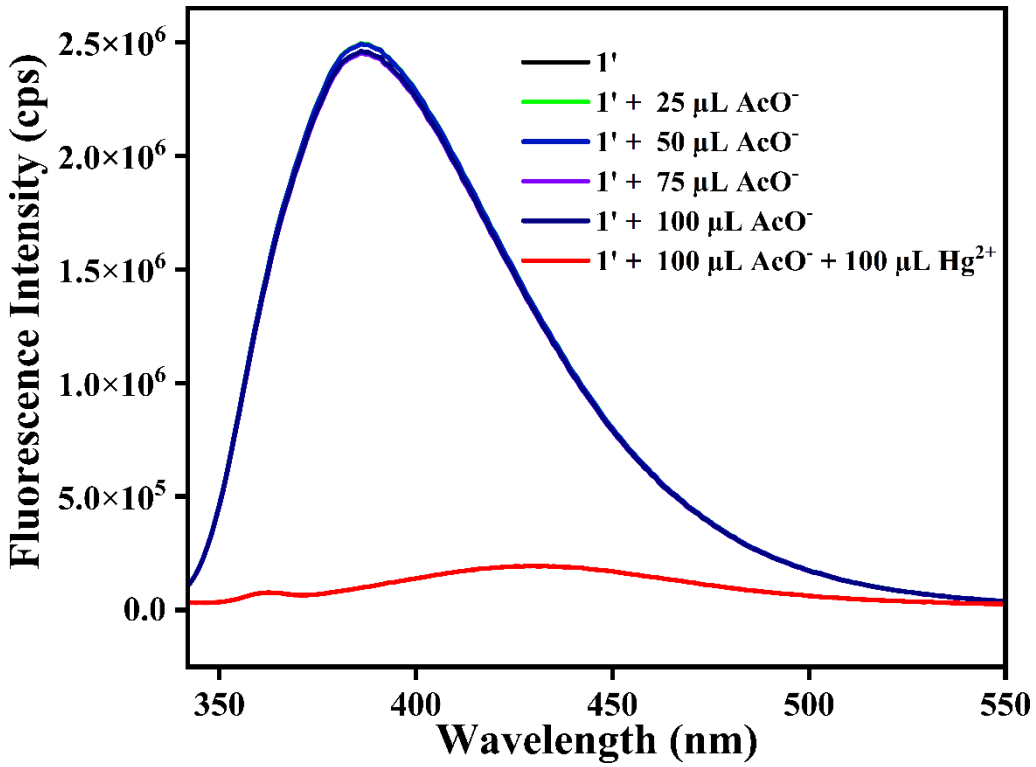

Figure S33. Fluorometric turn-off response of **1'** towards Hg^{2+} (10 mM) in the presence of $CH3COO^-$ (10 mM) in aqueous medium.

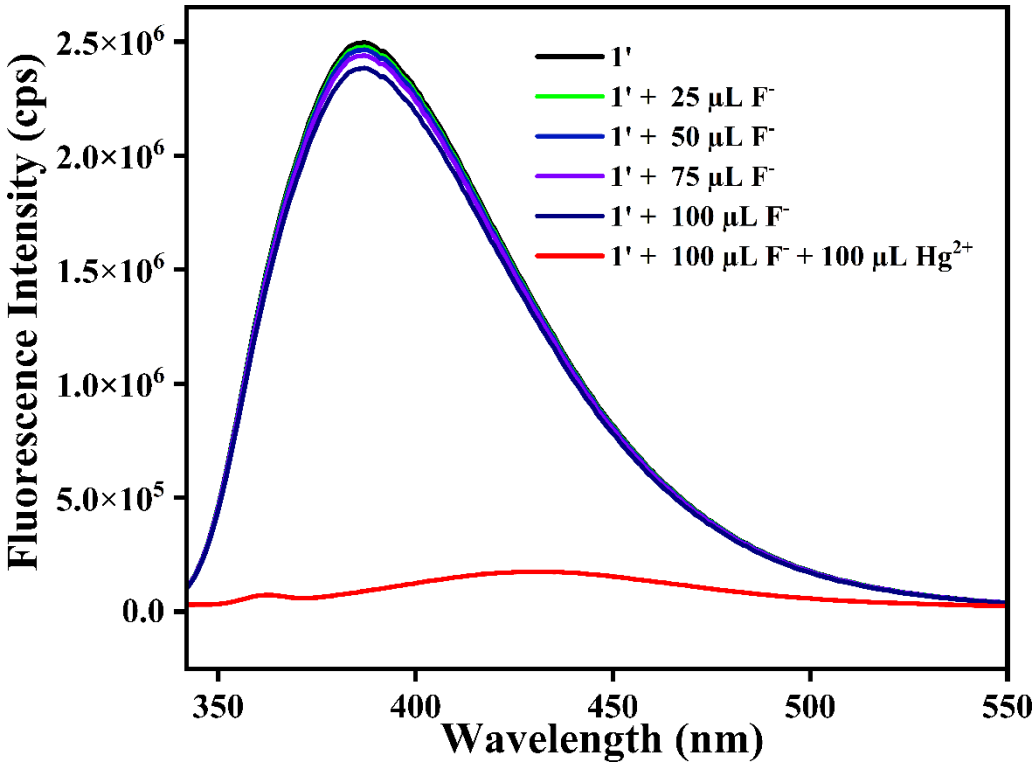

Figure S34. Fluorometric turn-off response of **1'** towards Hg^{2+} (10 mM) in the presence of F^- (10 mM) in aqueous medium.

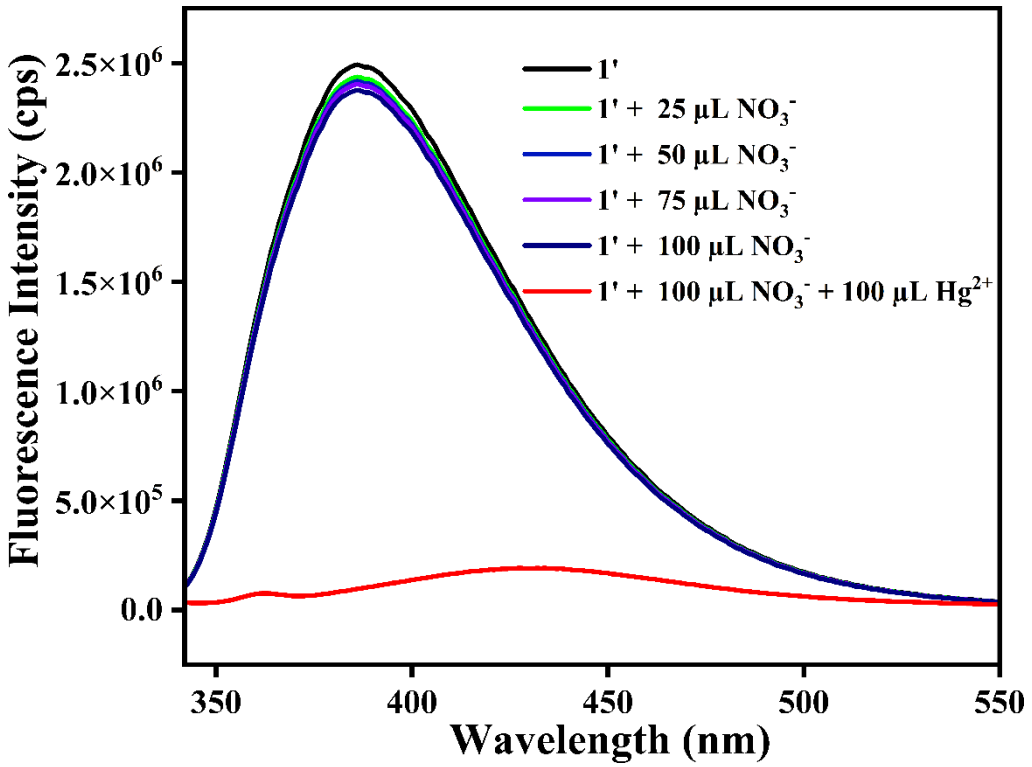

Figure S35. Fluorometric turn-off response of **1'** towards Hg^{2+} (10 mM) in the presence of NO_3^- (10 mM) in aqueous medium.

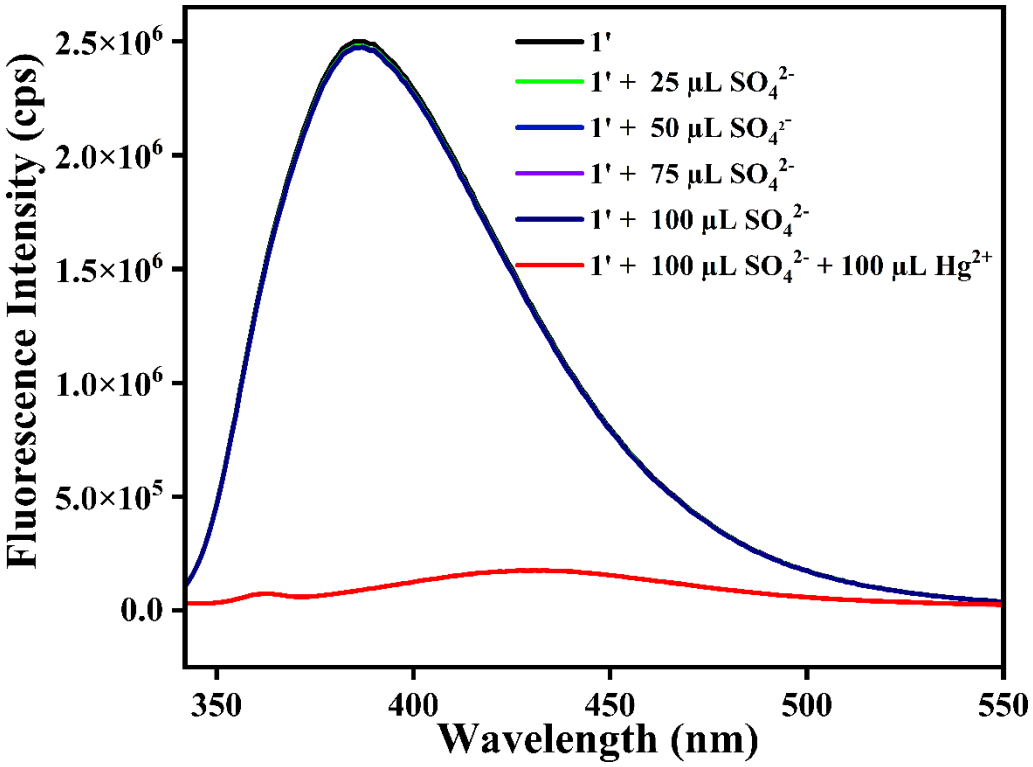

Figure S36. Fluorometric turn-off response of **1'** towards Hg^{2+} (10 mM) in the presence of SO_4^{2-} (10 mM) in aqueous medium.

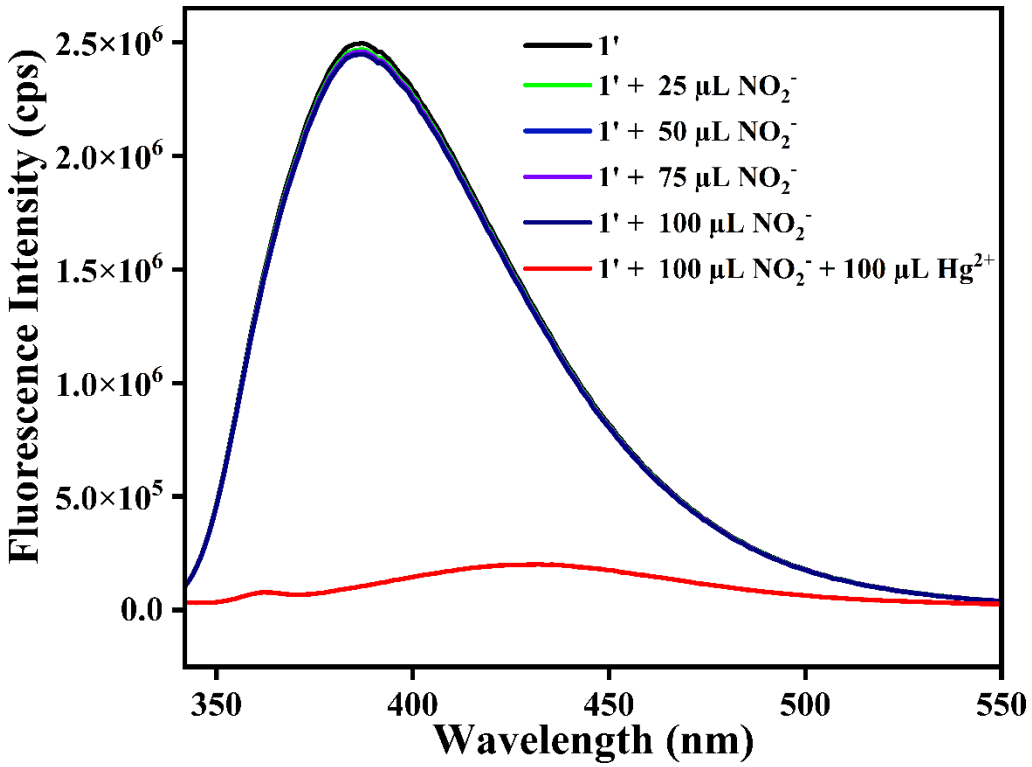

Figure S37. Fluorometric turn-off response of **1'** towards Hg^{2+} (10 mM) in the presence of NO_2^- (10 mM) in aqueous medium.

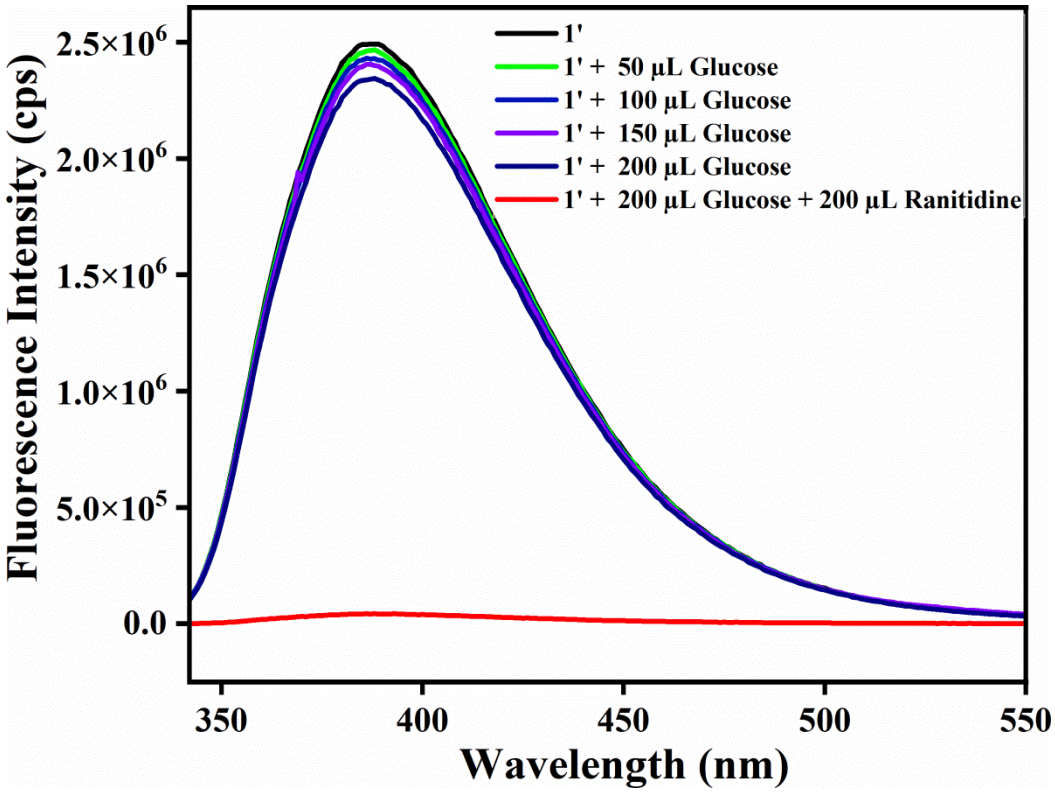

Figure S38. Fluorometric turn-off response of **1'** towards ranitidine (5 mM) in the presence of glucose (5 mM) in HEPES buffer medium.

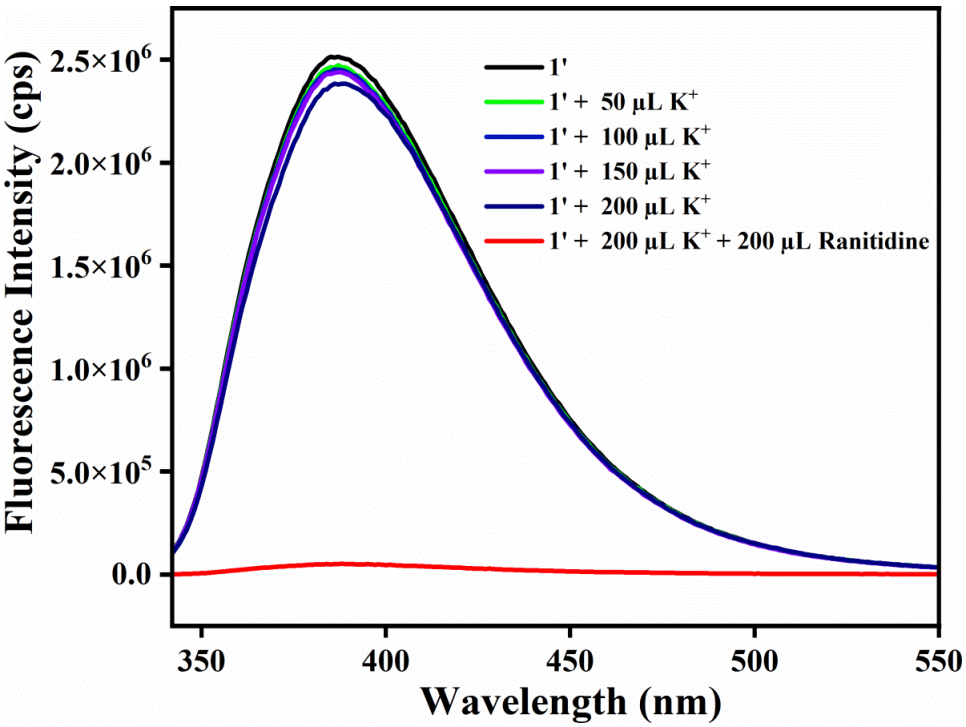

Figure S39. Fluorometric turn-off response of **1'** towards ranitidine (5 mM) in the presence of K^+ (5 mM) in HEPES buffer medium.

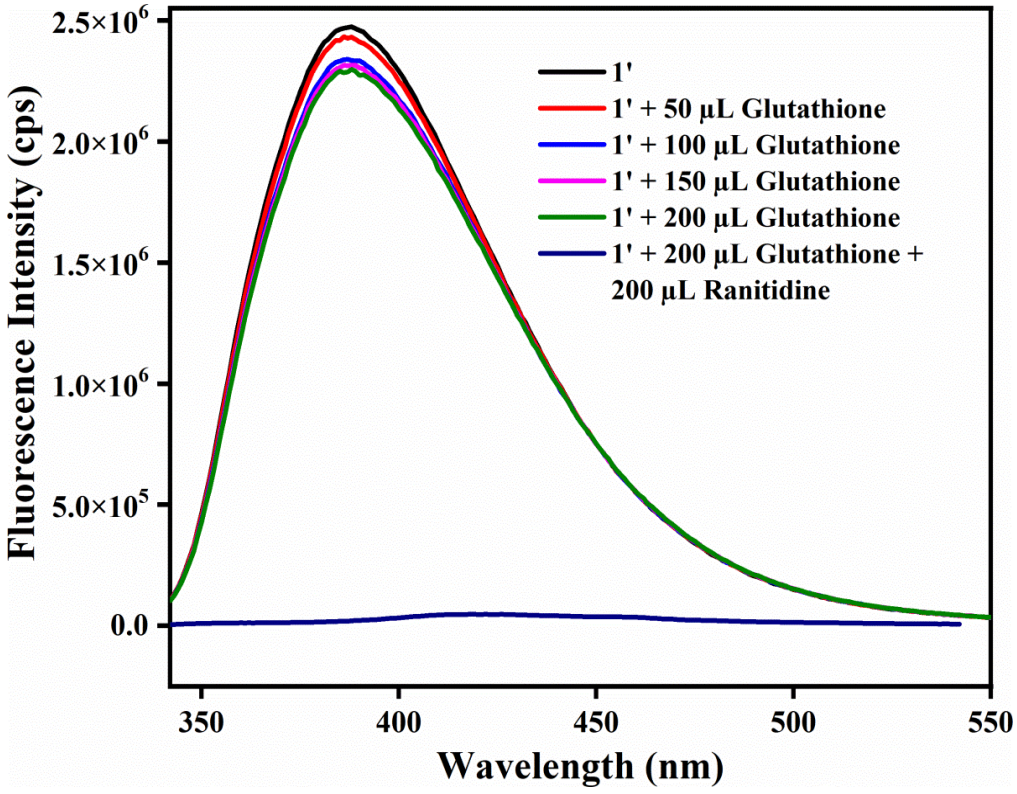

Figure S40. Fluorometric turn-off response of **1'** towards ranitidine (5 mM) in the presence of glutathione (5 mM) in HEPES buffer medium.

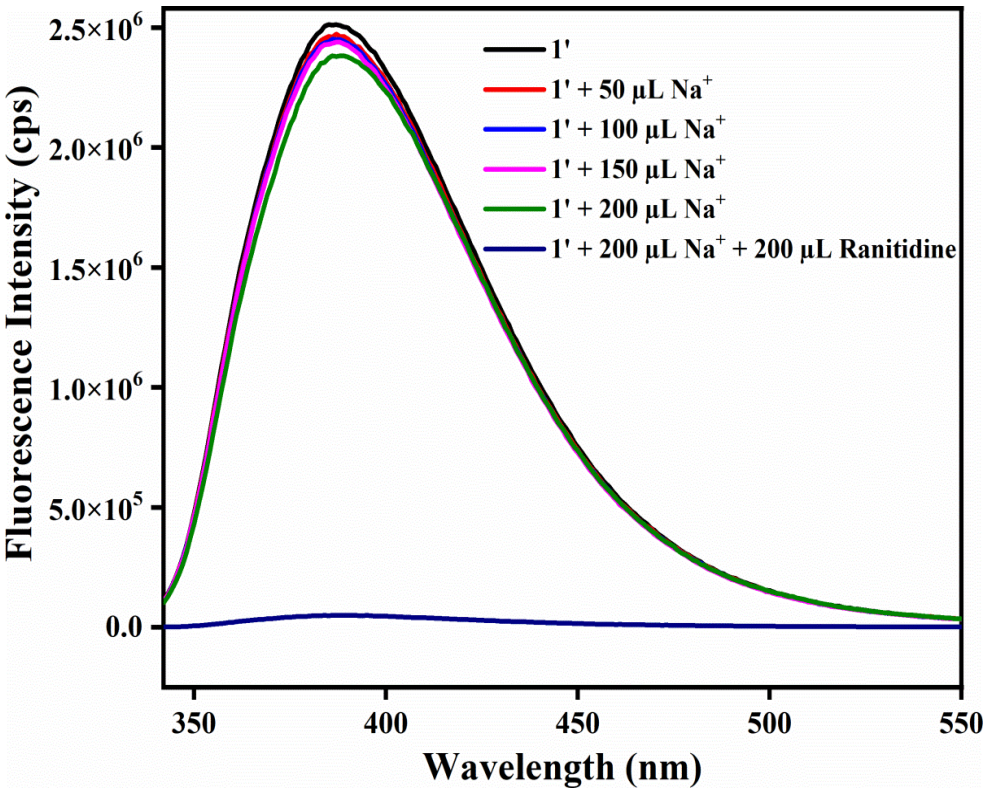

Figure S41. Fluorometric turn-off response of **1'** towards ranitidine (5 mM) in the presence of Na^+ (5 mM) in HEPES buffer medium.

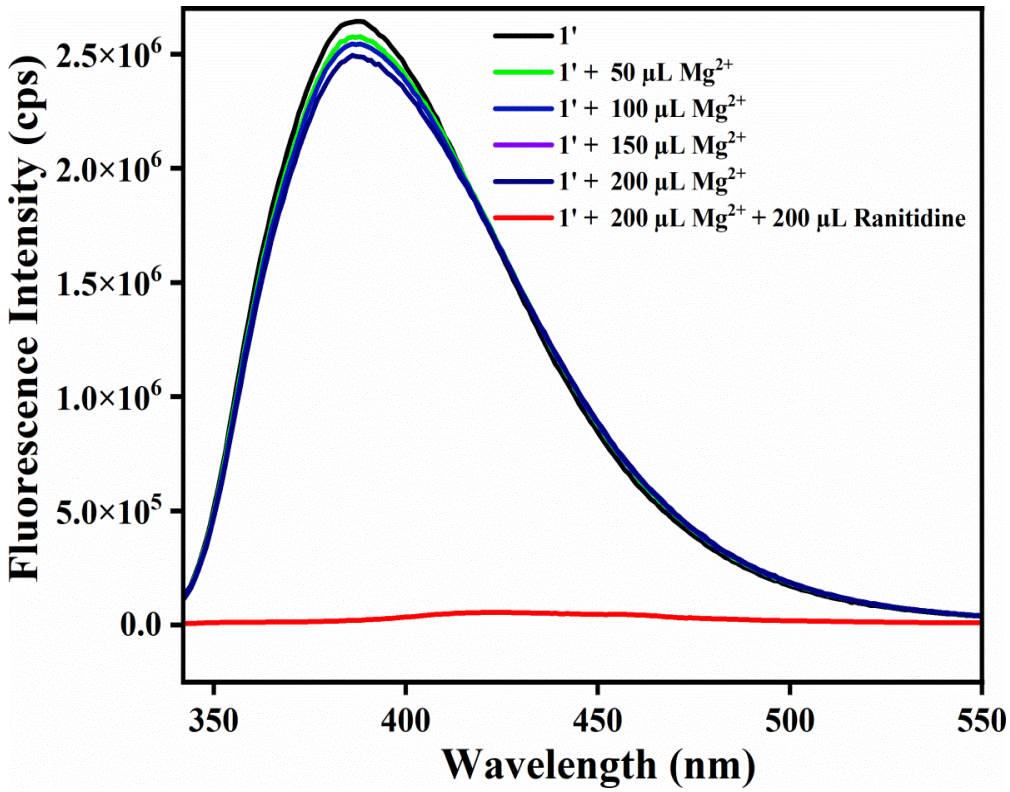

Figure S42. Fluorometric turn-off response of **1'** towards ranitidine (5 mM) in the presence of Mg^{2+} (5 mM) in HEPES buffer medium.

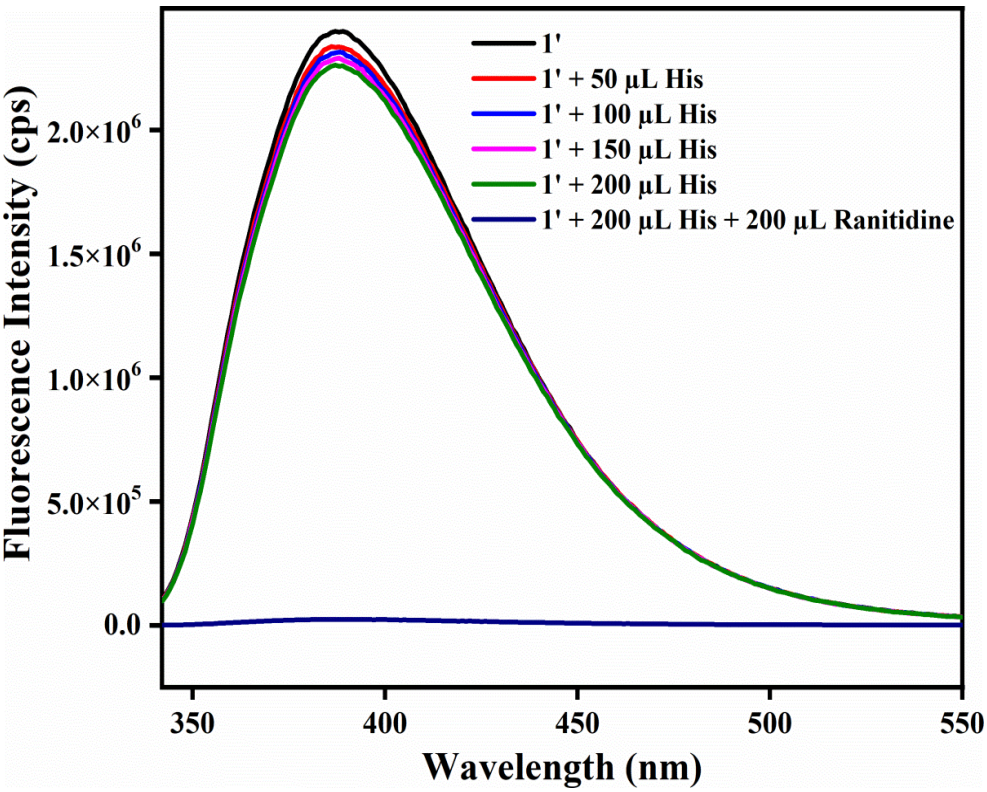

Figure S43. Fluorometric turn-off response of **1'** towards ranitidine (5 mM) in the presence of histidine (5 mM) in HEPES buffer medium.

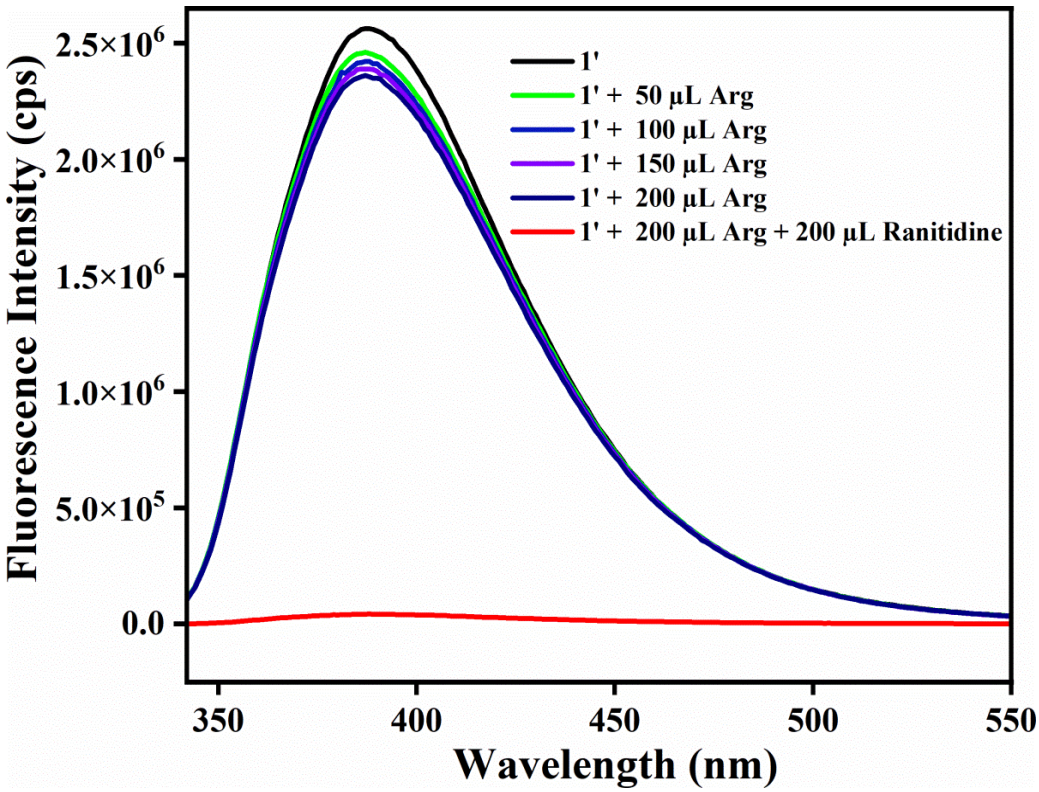

Figure S44. Fluorometric turn-off response of **1'** towards ranitidine (5 mM) in the presence of arginine (5 mM) in HEPES buffer medium.

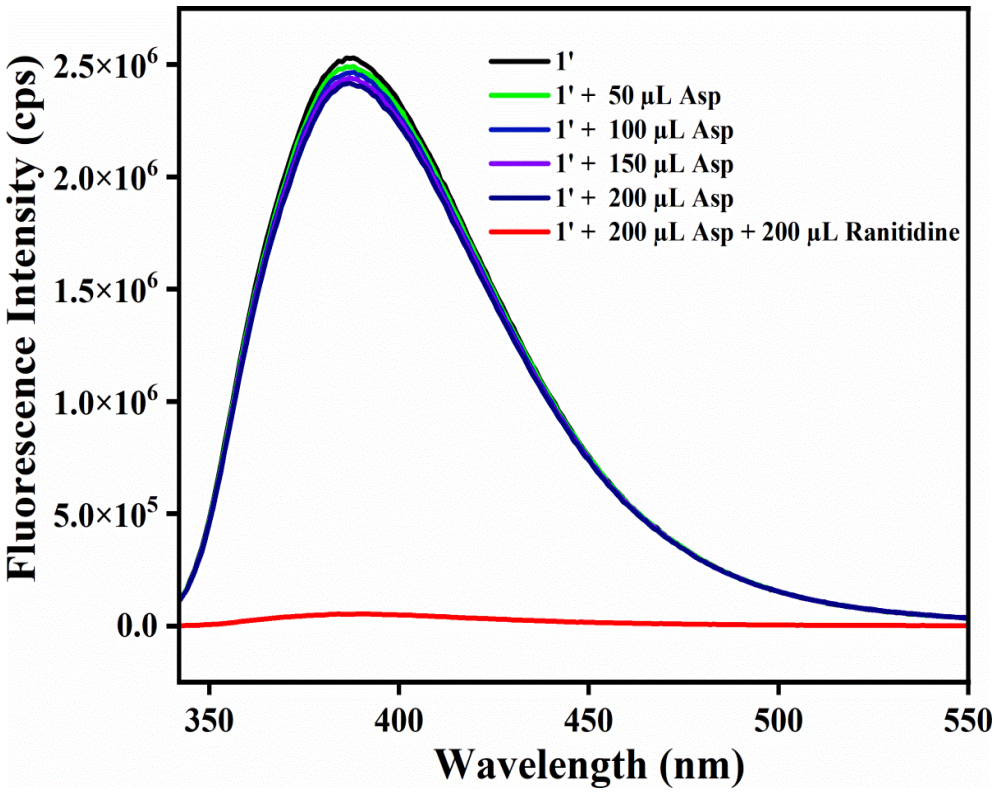

Figure S45. Fluorometric turn-off response of **1'** towards ranitidine (5 mM) in the presence of aspartic acid (5 mM) in HEPES buffer medium.

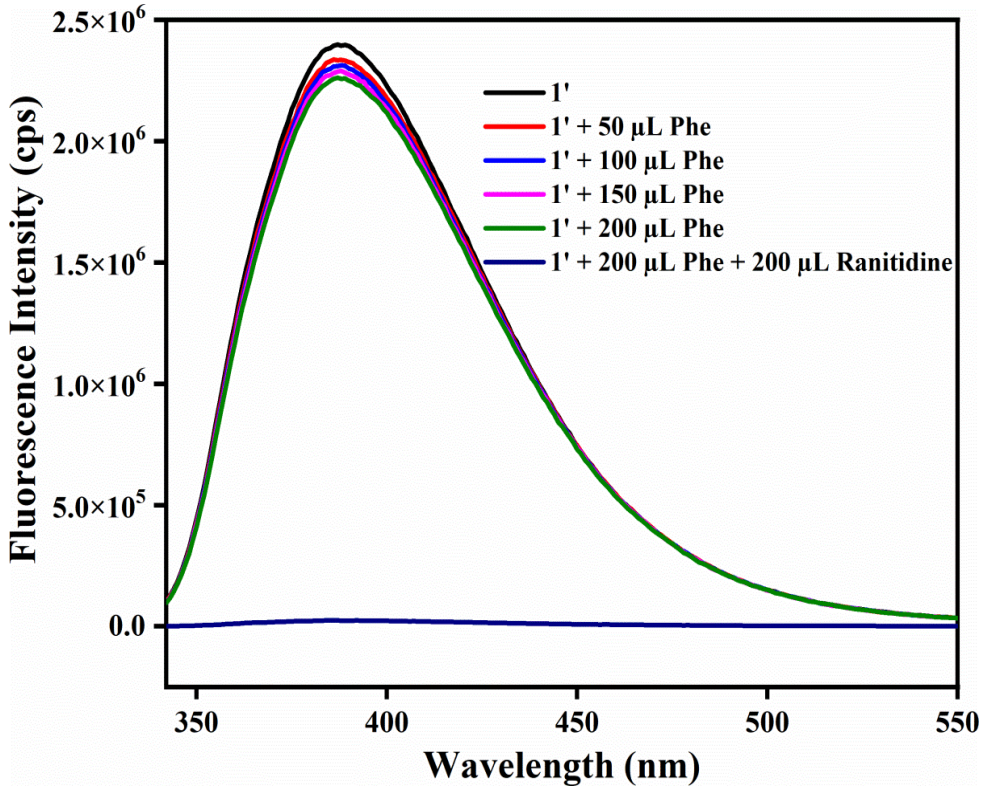

Figure S46. Fluorometric turn-off response of **1'** towards ranitidine (5 mM) in the presence of phenyl alanine (5 mM) in HEPES buffer medium.

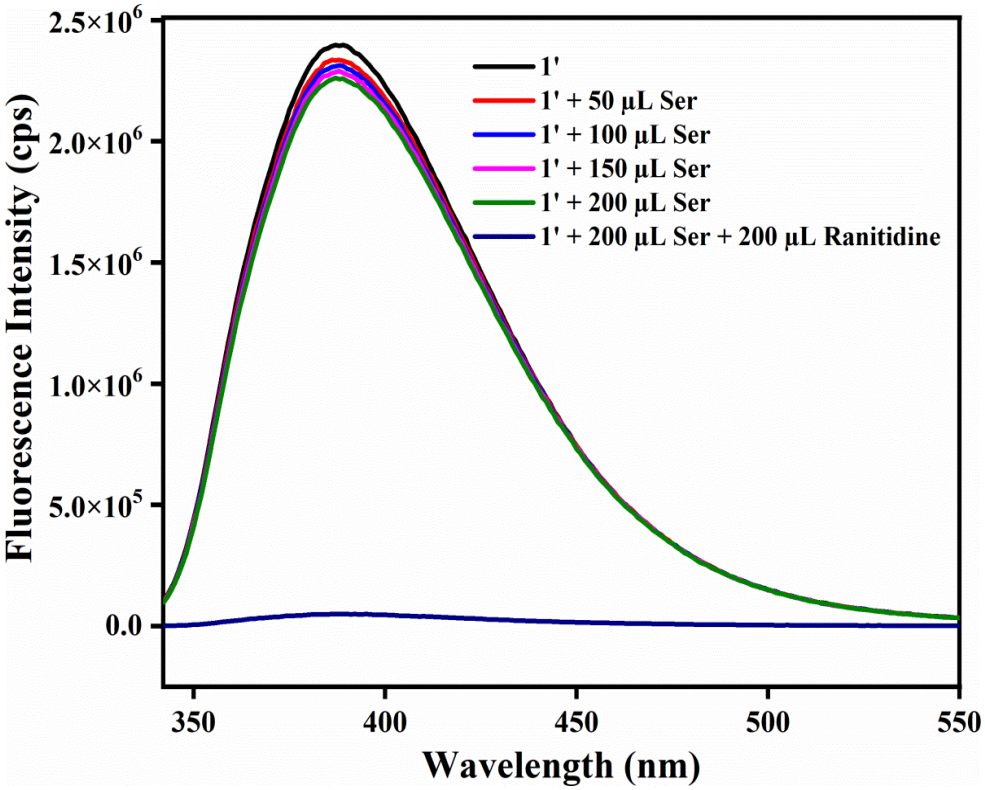

Figure S47. Fluorometric turn-off response of **1'** towards ranitidine (5 mM) in the presence of serine (5 mM) in HEPES buffer medium.

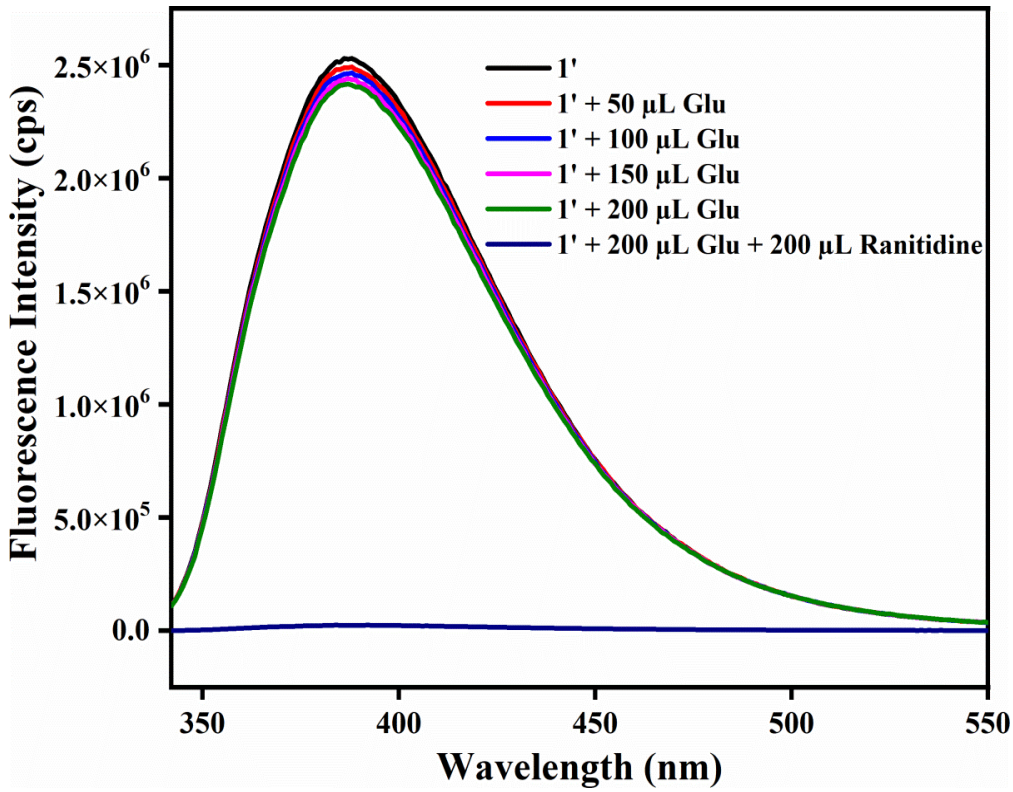

Figure S48. Fluorometric turn-off response of **1'** towards ranitidine (5 mM) in the presence of glutamic acid (5 mM) in HEPES buffer medium.

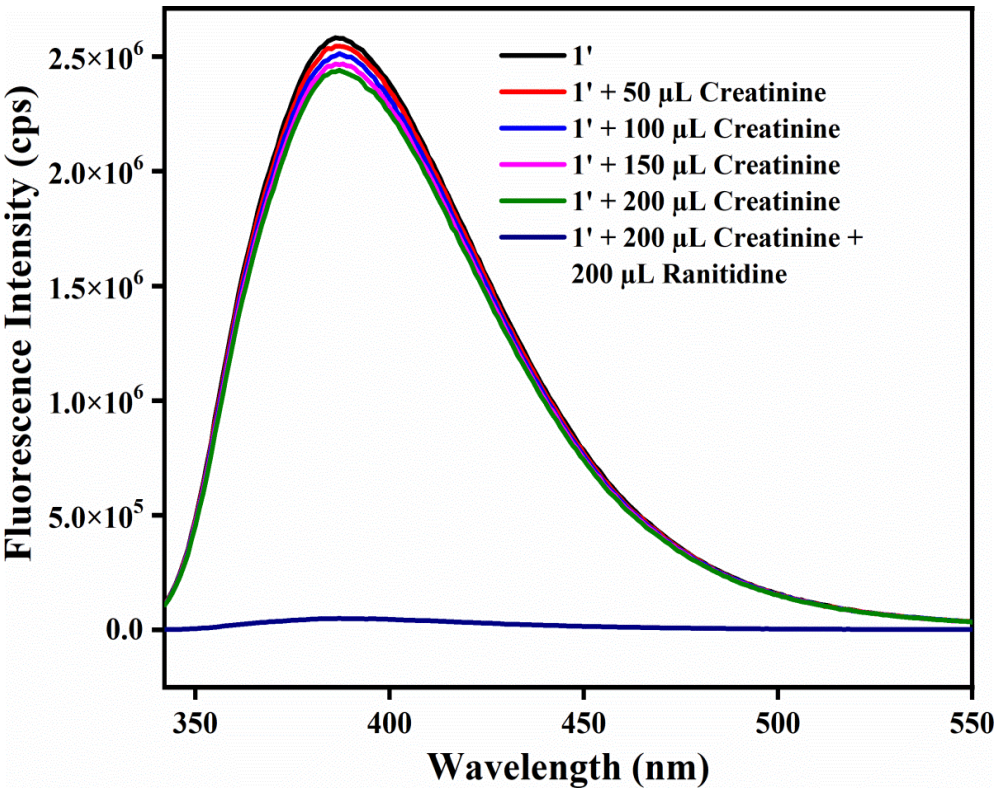

Figure S49. Fluorometric turn-off response of **1'** towards ranitidine (5 mM) in the presence of creatinine (5 mM) in HEPES buffer medium.

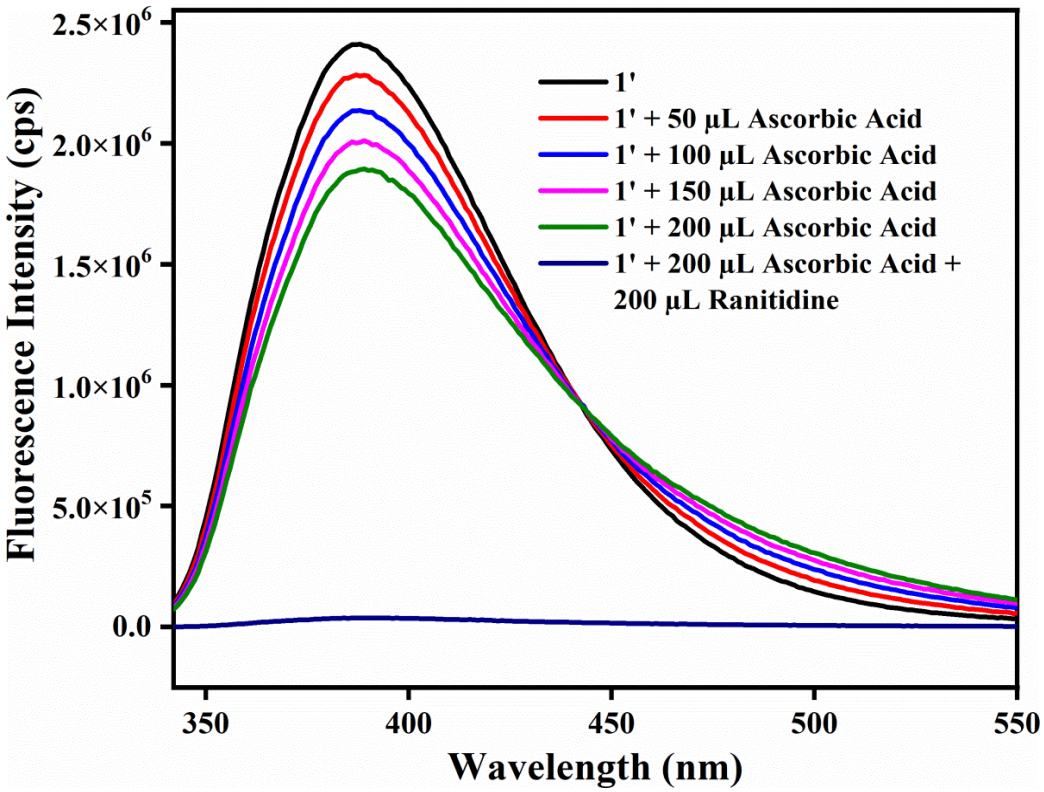

Figure S50. Fluorometric turn-off response of **1'** towards ranitidine (5 mM) in the presence of ascorbic acid (5 mM) in HEPES buffer medium.

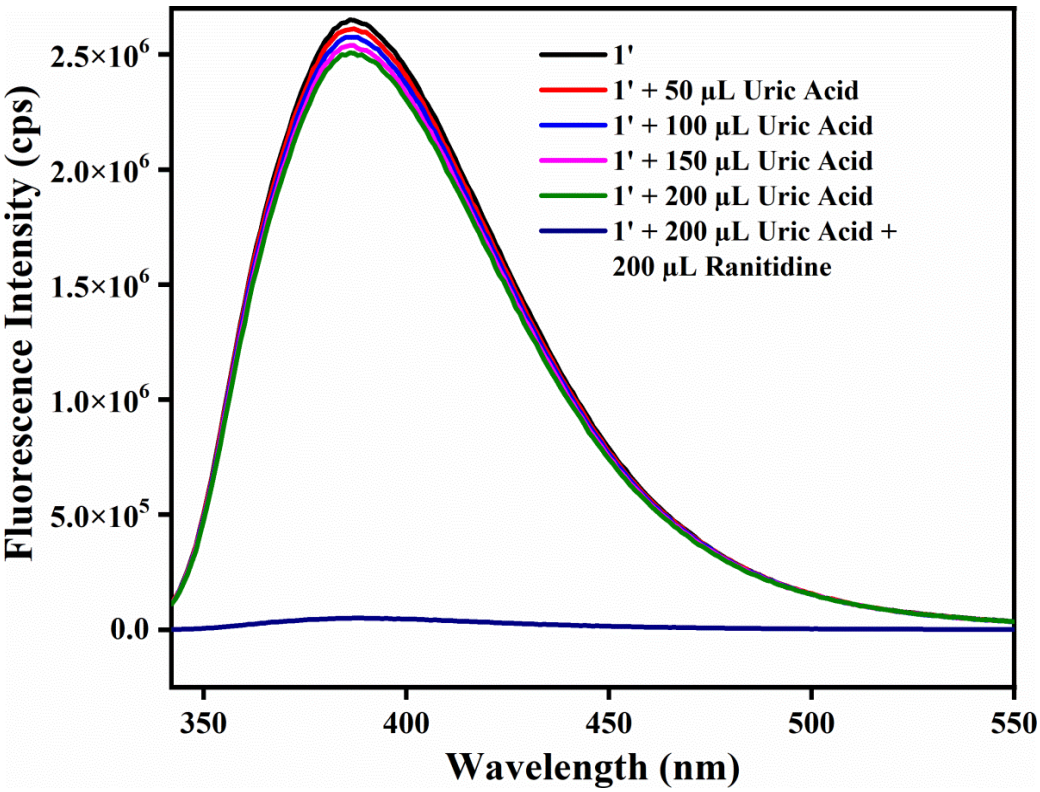

Figure S51. Fluorometric turn-off response of **1'** towards ranitidine (5 mM) in the presence of uric acid (5 mM) in HEPES buffer medium.

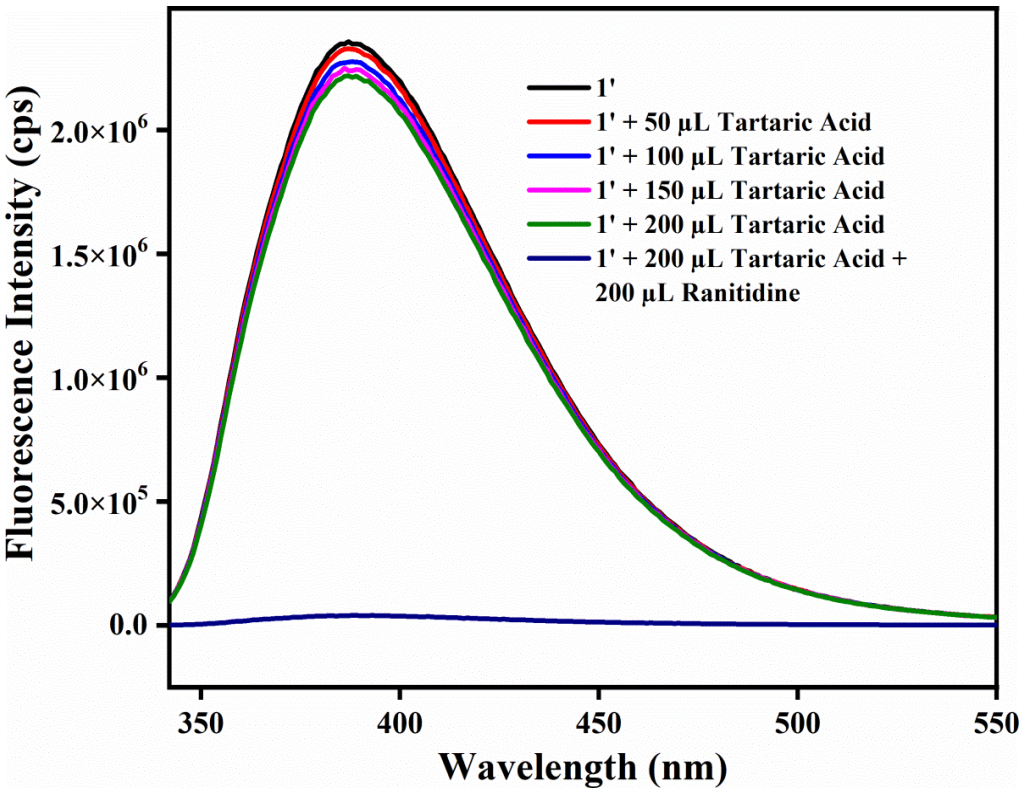

Figure S52. Fluorometric turn-off response of **1'** towards ranitidine (5 mM) in the presence of tartaric acid (5 mM) in HEPES buffer medium.

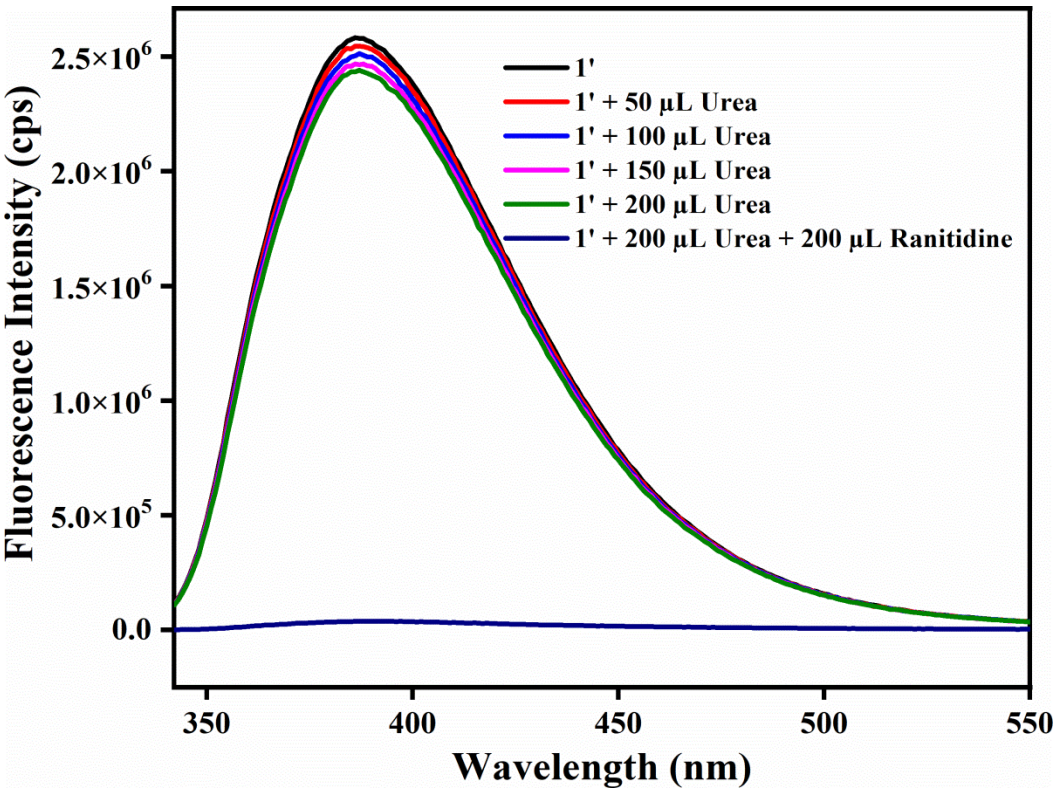

Figure S53. Fluorometric turn-off response of **1'** towards ranitidine (5 mM) in the presence of urea (5 mM) in HEPES buffer medium.

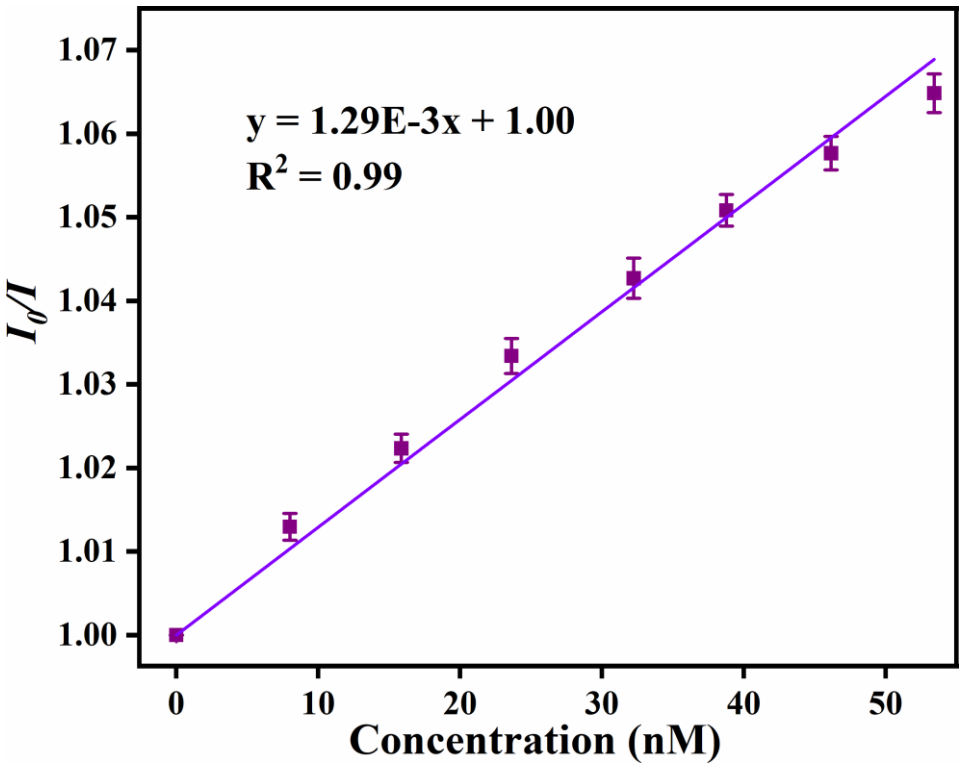

Figure S54. Stern-Volmer plot for the fluorescence quenching of **1'** in presence of Hg^{2+} in aqueous medium (with error bar).

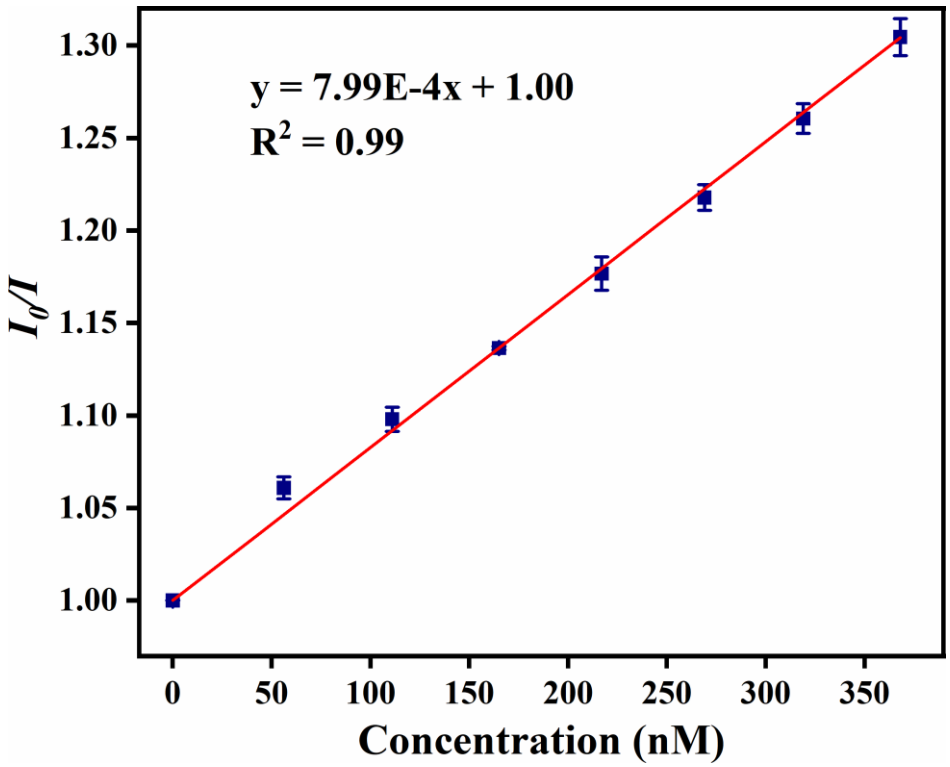

Figure S55. Stern-Volmer plot for the fluorescence quenching of **1'** in presence of ranitidine in HEPES buffer medium (with error bar).

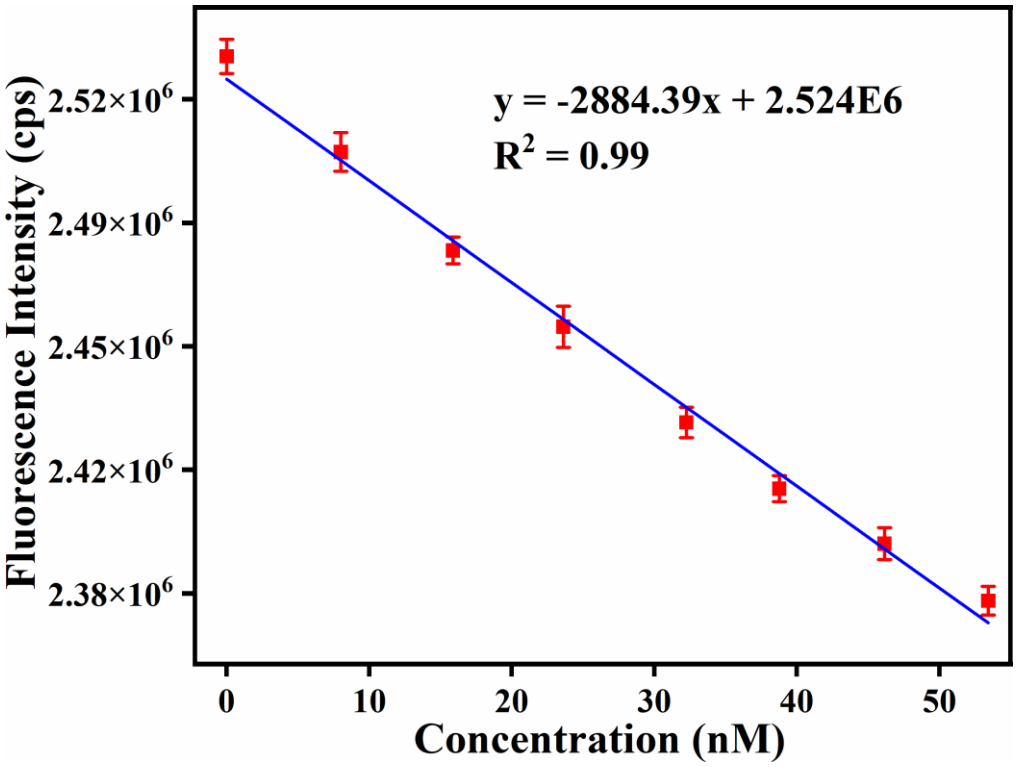

Figure S56. Change of fluorescence intensity of **1'**as a function of the concentration of Hg^{2+} in aqueous medium (with error bar).

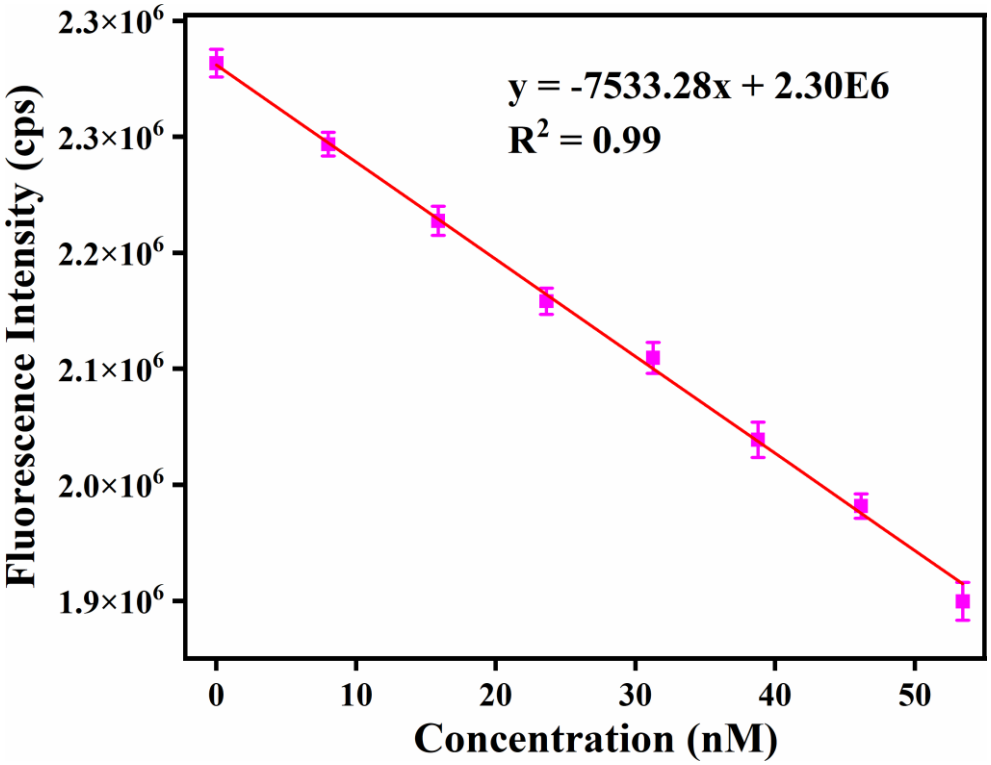

Figure S57. Change of fluorescence intensity of **1'** as a function of the concentration of ranitidine in HEPES buffer medium (with error bar).

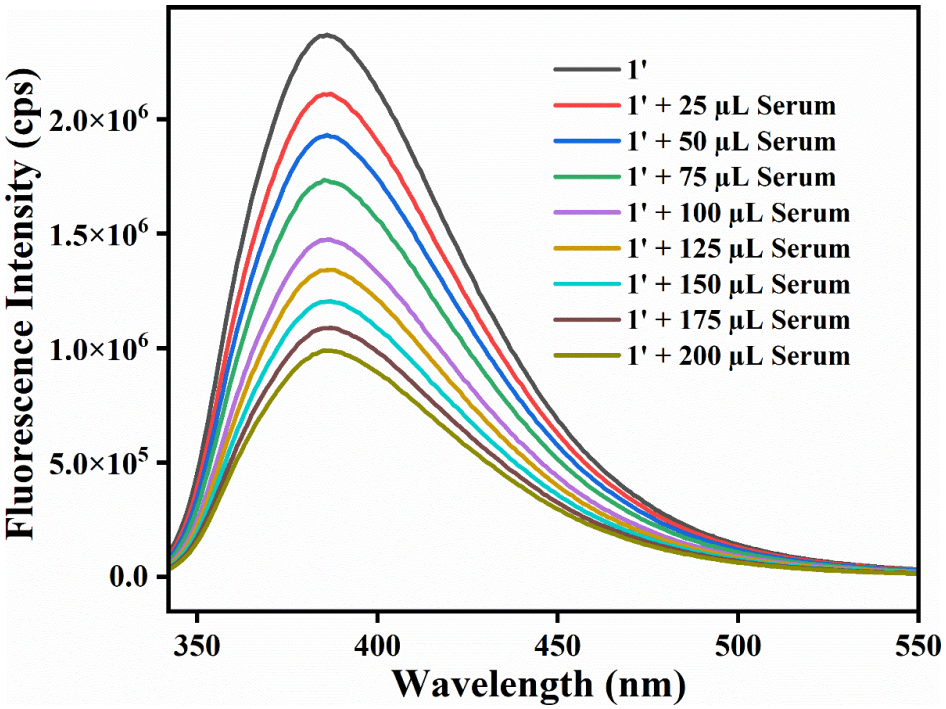

Figure S58. Fluorometric turn-off response of **1'** towards 1 mM of ranitidine-spiked serum solution.

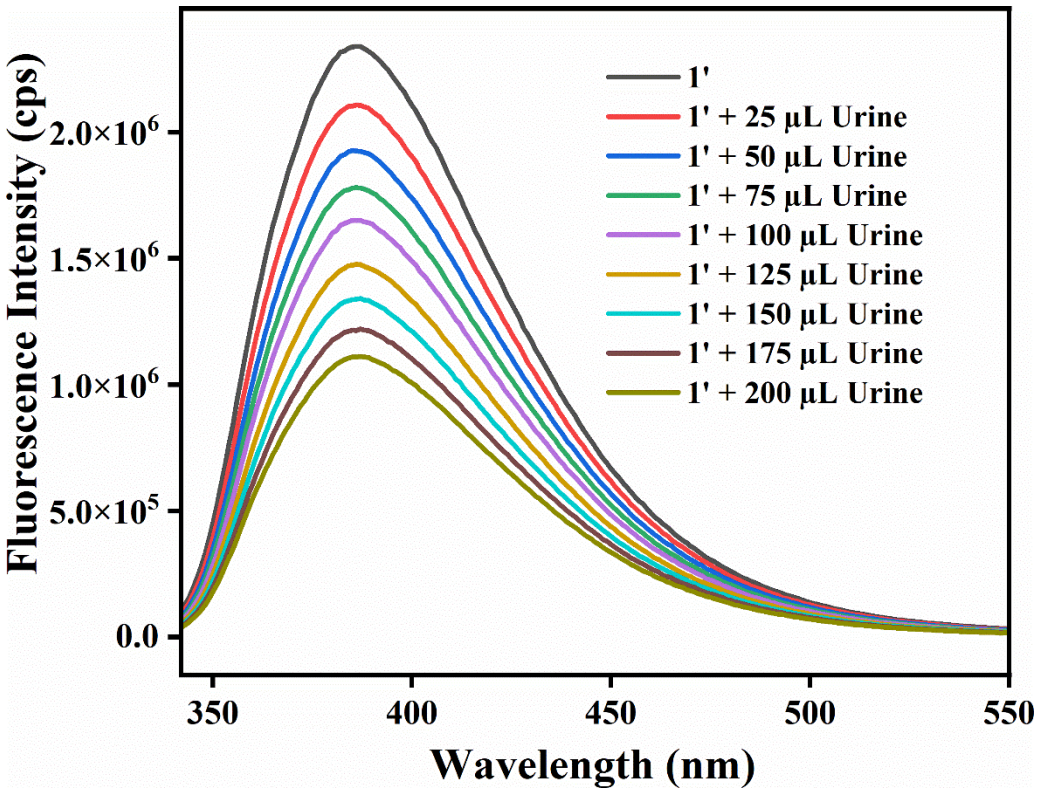

Figure S59. Fluorometric turn-off response of **1'** towards 1 mM of ranitidine-spiked urine solution.

Table S1. Fluorometric detection of ranitidine in human serum sample by **1'**.

Ranitidine Spiked (µM)	Ranitidine Found (µM)	Recovery (%)	RSD (%) (n=3)
12.74	13.26	104.08	1.13
25.16	24.71	98.21	0.99
37.27	38.16	102.39	2.12

Table S2. Fluorometric detection of ranitidine in human urine sample by **1'**.

Ranitidine Spiked (µM)	Ranitidine Found (µM)	Recovery (%)	RSD (%) (n=3)
12.74	12.36	97.01	3.10
25.16	25.53	101.47	1.97
37.27	38.42	103.08	0.78

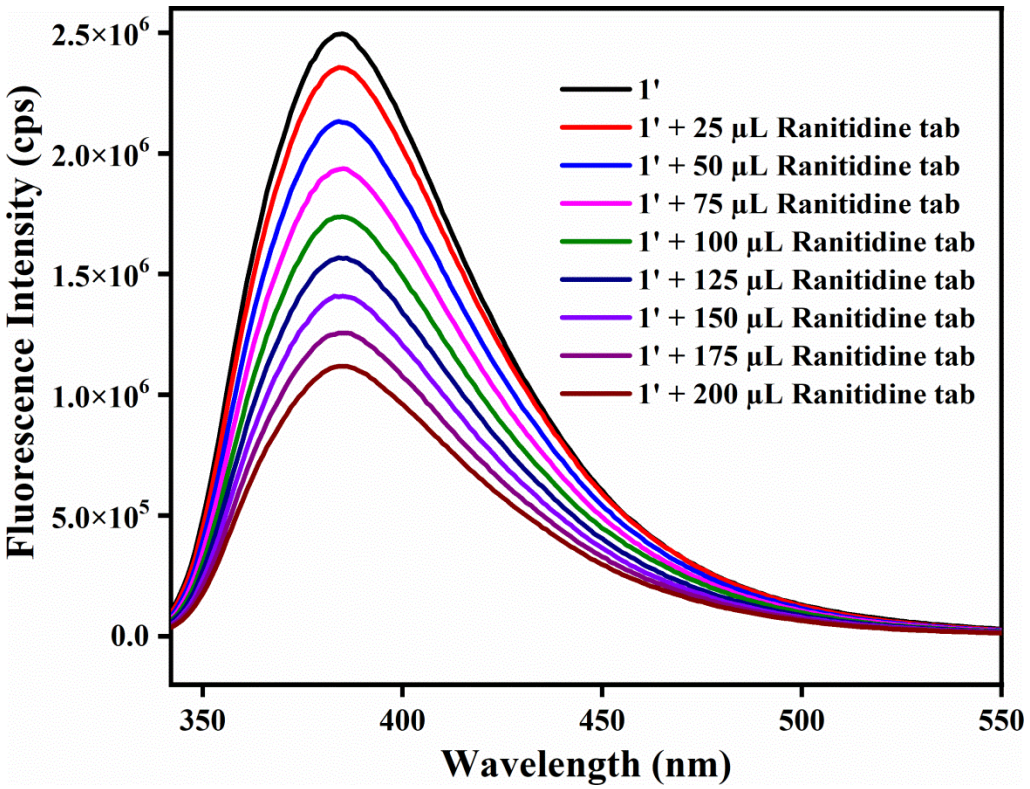

Figure S60. Fluorometric turn-off response of **1'** towards 1 mM of ranitidine tablet extract.

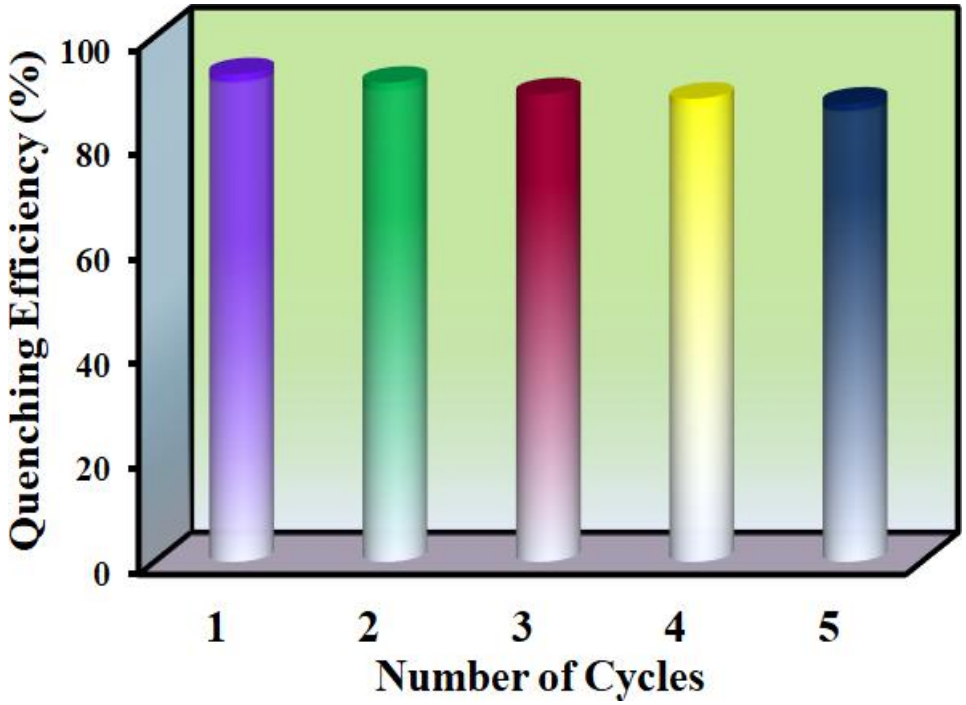

Figure S61. Recyclability test of probe **1'** for the sensing of Hg^{2+} in aqueous medium.

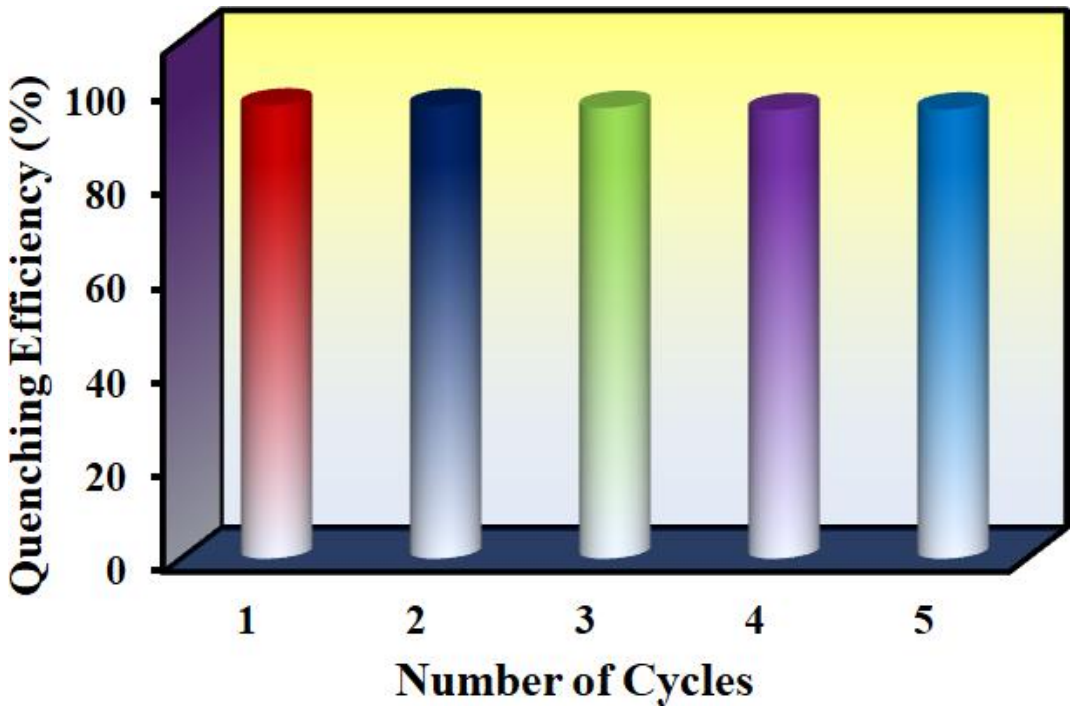

Figure S62. Recyclability test of probe **1'** for the sensing ranitidine in HEPES buffer medium.

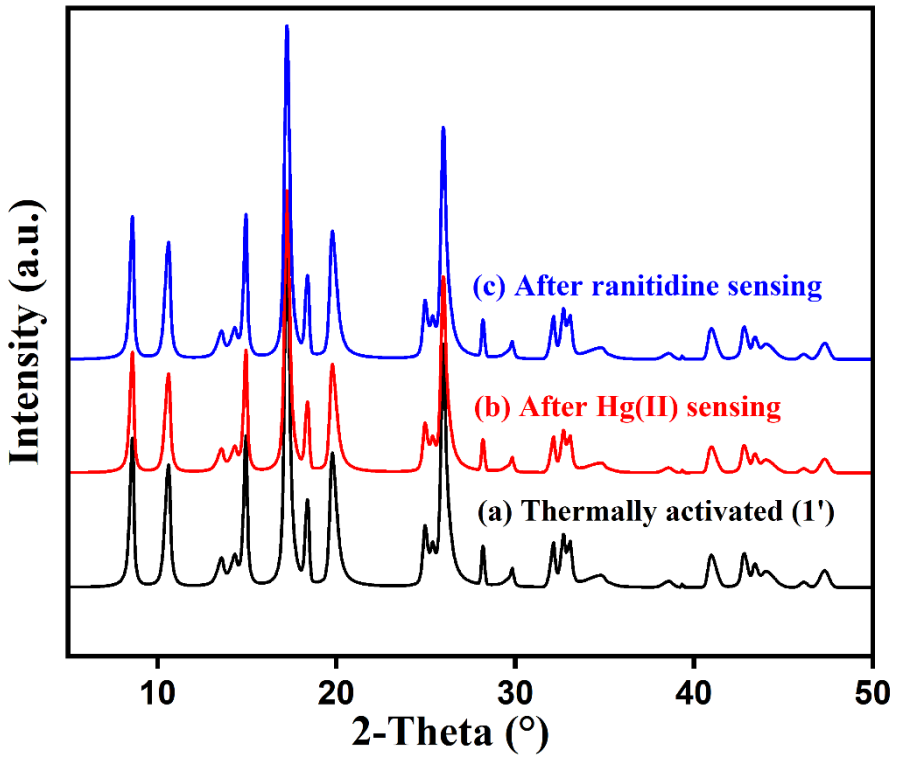

Figure S63. PXRD patterns of **1'** before sensing (a), after sensing of Hg^{2+} in aqueous medium (b) and after the sensing of ranitidine in HEPES buffer medium (c).

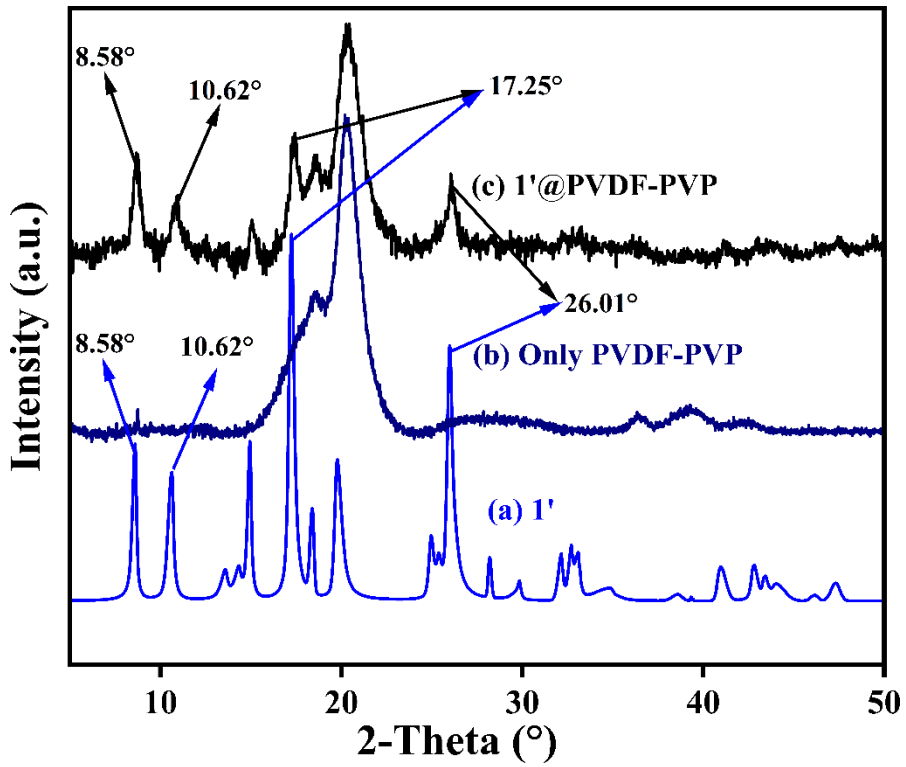

Figure S64. PXRD patterns of (a) pristine MOF **1'**, (b) PVDF-PVP, and (c) **1'**@ PVDF-PVP polymer composite.

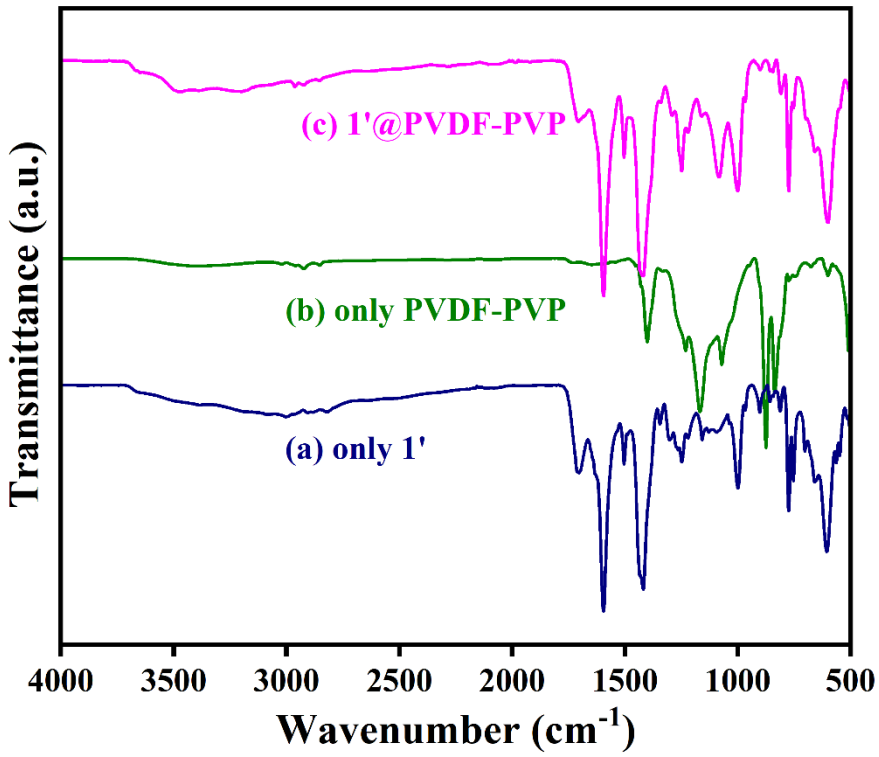

Figure S65. ATR-IR spectra of (a) pristine MOF **1'**, (b) PVDF-PVD, and (c) **1'**@ PVDF-PVD polymer composite.

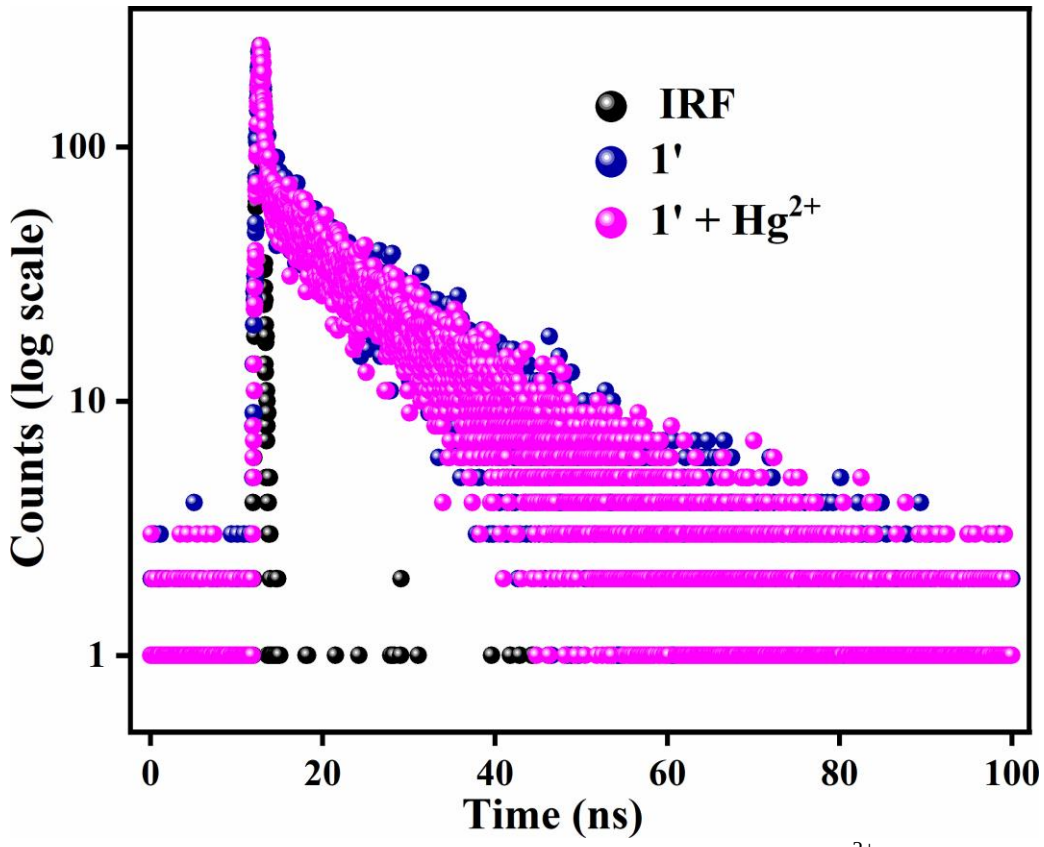

Figure S66. Lifetime decay profile of **1′** in absence and presence of Hg^{2+} solution (λ_{ex} = 322 nm, monitored at 336 nm).

Table S3. Fluorescence lifetimes of **1′** before and after the addition of Hg^{2+} solution (λ_{ex} = 336 nm, pulsed diode laser).

Volume of Hg^{2+} solution added (μL)	f_1	f_2	τ_1 (ns)	τ_2 (ns)	$<\tau>$* (ns)	χ^2
0	0.155	0.854	0.301	13.112	11.31	1.003
100	0.149	0.849	0.349	12.290	11.17	1.005

* $<\tau> = f_1\tau_1 + f_1\tau_2$

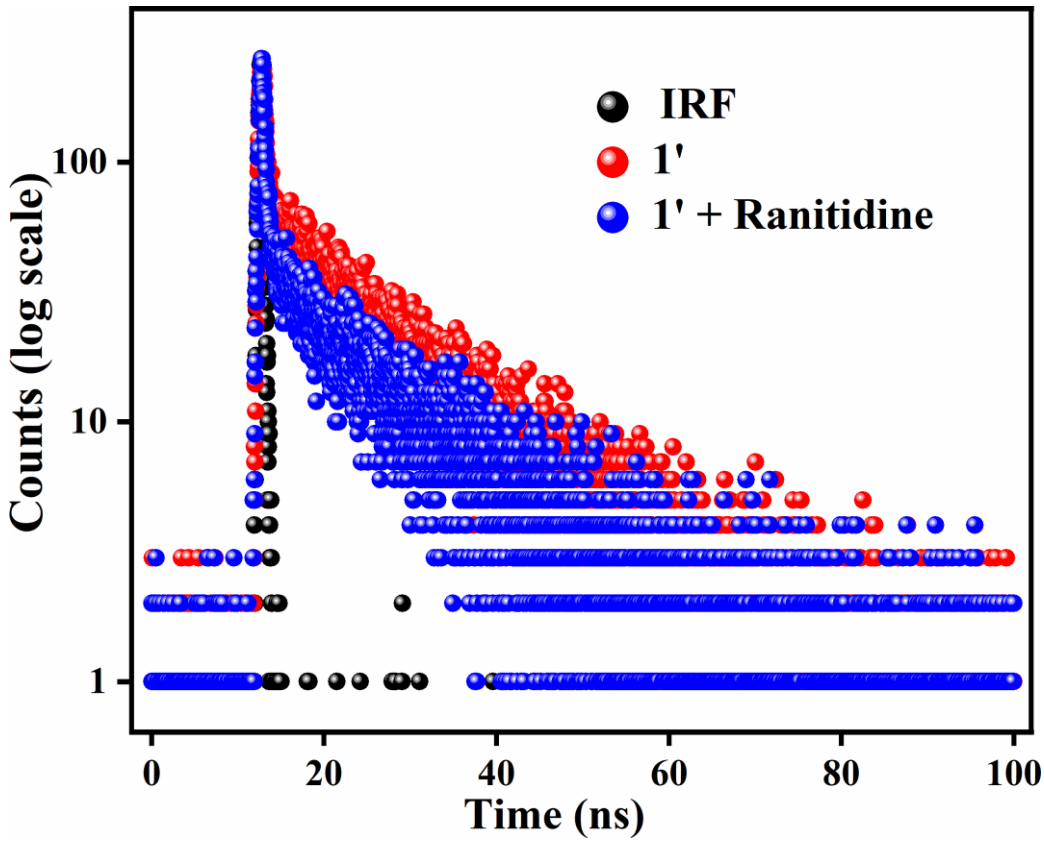

Figure S67. Lifetime decay profile of **1′** in absence and presence of ranitidine solution (λ_{ex} = 322 nm, monitored at 336 nm).

Table S4. Fluorescence lifetimes of **1′** before and after the addition of ranitidine solution (λ_{ex} = 336 nm, pulsed diode laser).

Volume of ranitidine solution added (μL)	f_1	f_2	τ_1 (ns)	τ_2 (ns)	$<\tau>$* (ns)	χ^2
0	0.163	0.837	0.291	13.132	11.04	1.008
200	0.244	0.809	0.273	13.199	10.74	1.007

* $<\tau> = f_1\tau_1 + f_1\tau_2$

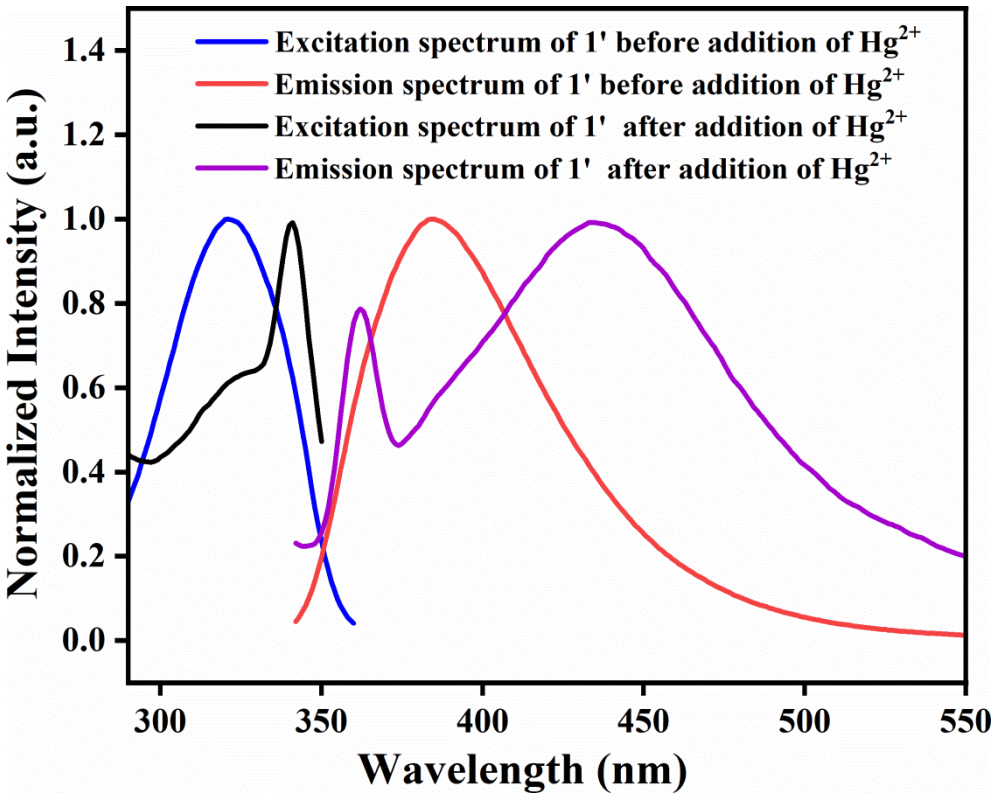

Figure S68. Change of excitation and emission spectra of **1'** in presence of Hg^{2+}.

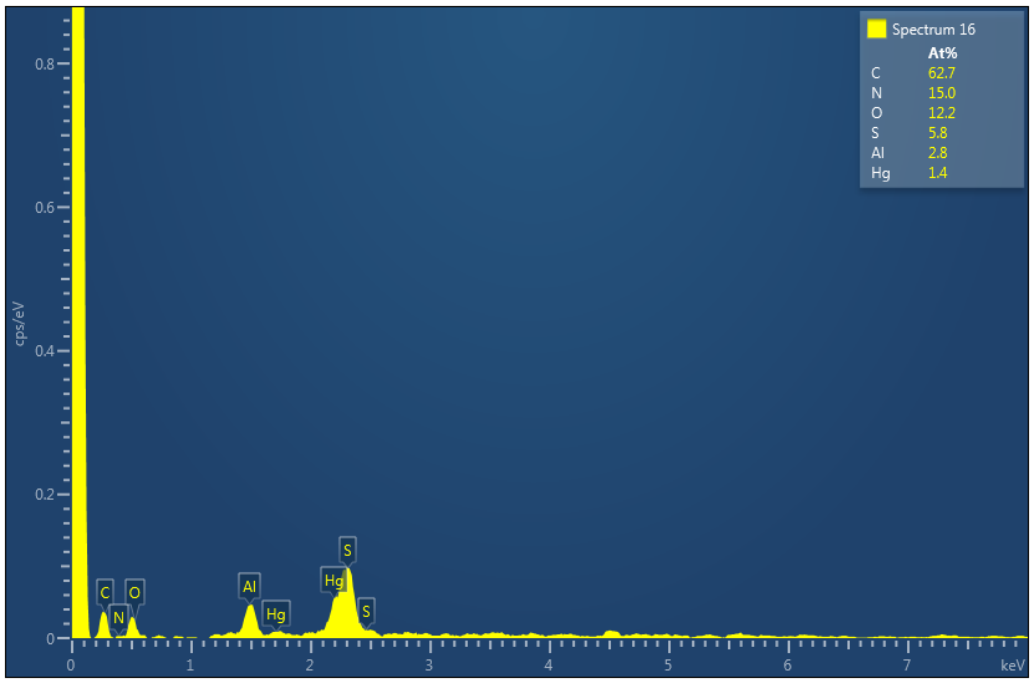

Figure S69. EDX spectrum of **1'** after sensing of Hg^{2+} (without washing).

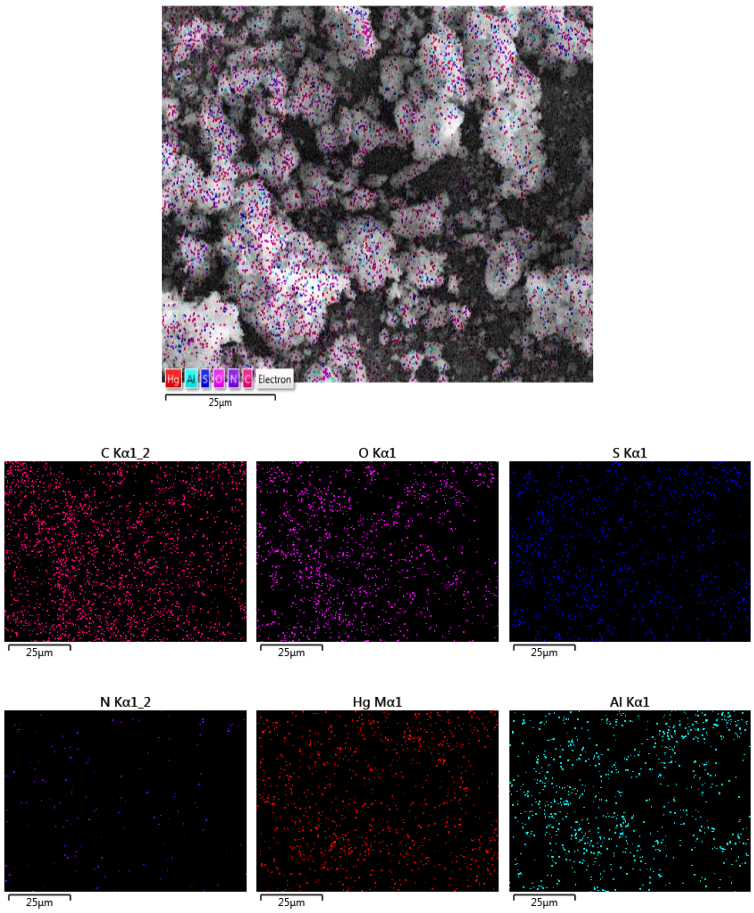

Figure S70. EDX elemental mapping of **1'** after sensing of Hg^{2+} (without washing).

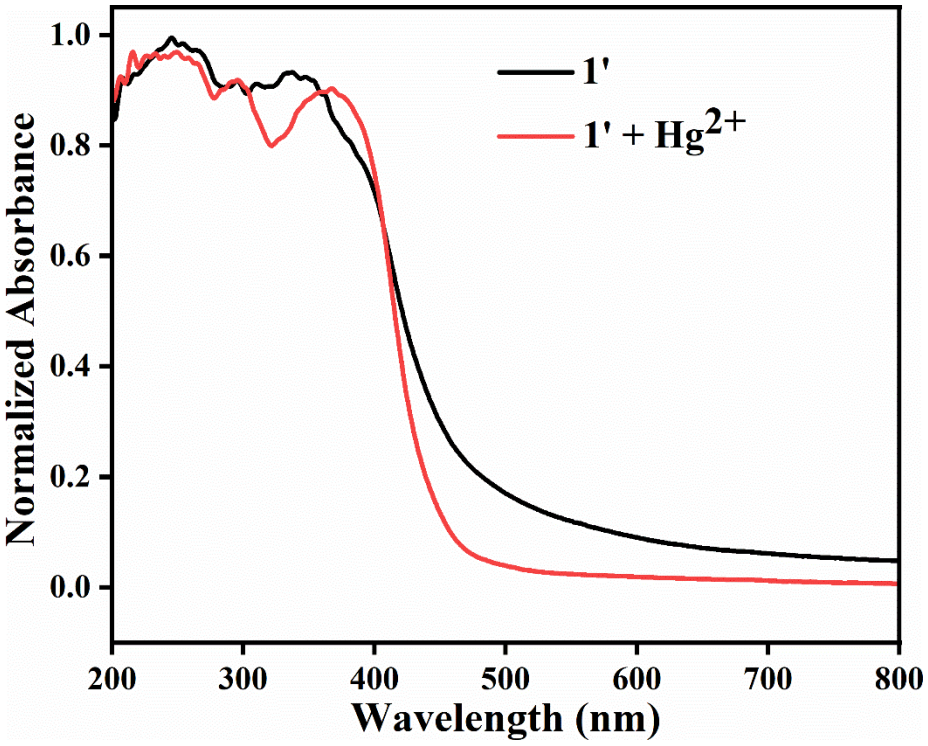

Figure S71. Solid state UV-Vis spectra of **1'** before after treatment Hg^{2+}.

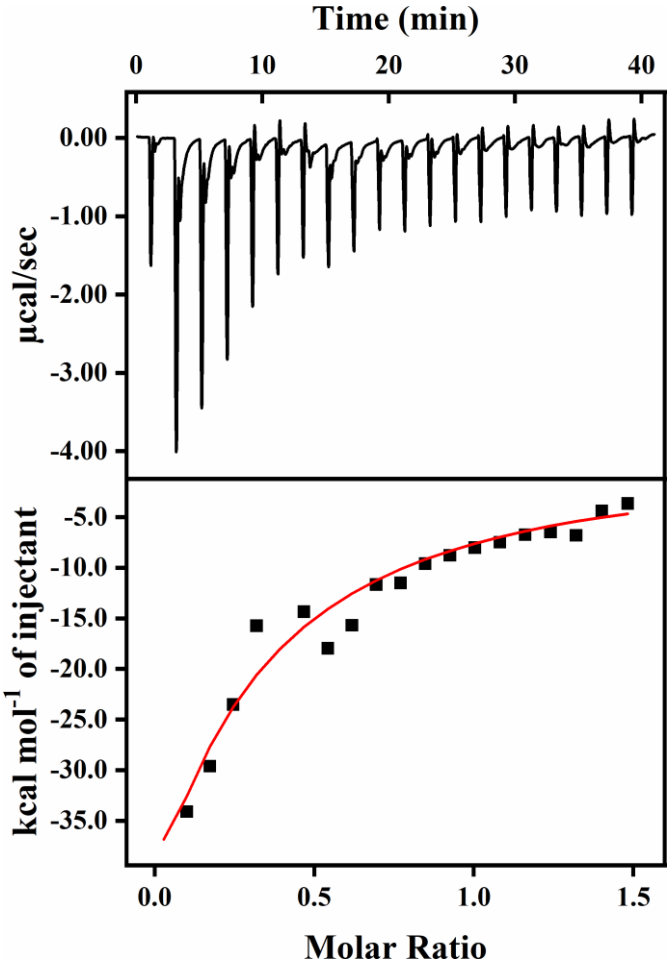

Figure S72. Isothermal titration calorimetry (ITC) for the gradual addition of Hg^{2+} solution to the linker solution.

Table S5. ITC Thermogram enthalpy and entropy values for the addition of Hg^{2+} solution to the linker solution.

Binding Constant (K_i) (M^{-1})	Enthalpy Change (ΔH) ($cal \cdot mol^{-1}$)	Entropy Change (ΔS) ($cal \cdot mol^{-1} \cdot deg^{-1}$)
1.18E4 ± 8.13E3	-6.56E9 ± 6.13E14	-2.16E7

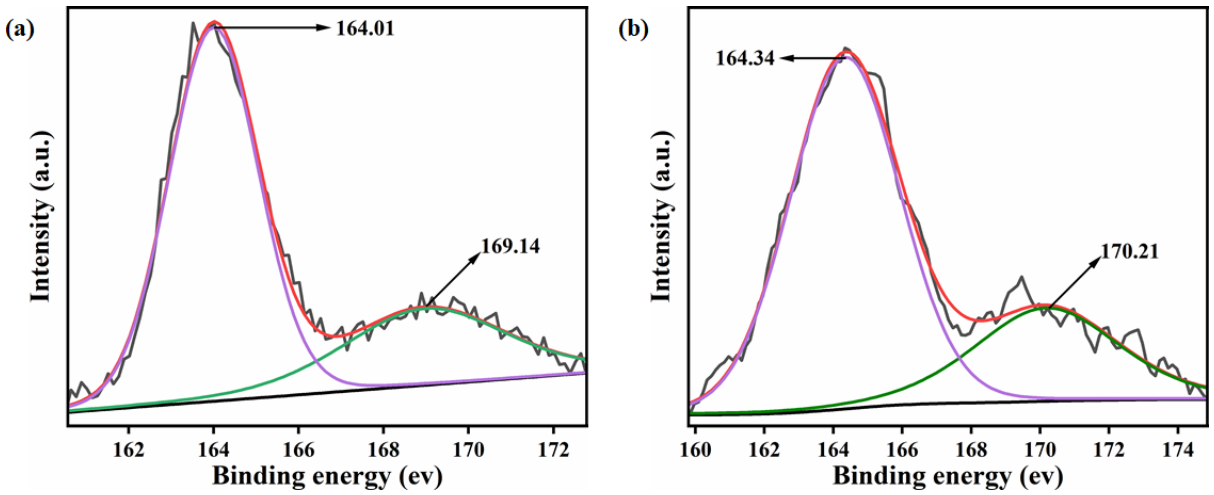

Figure S73. Fitted XPS spectra of S (2p) before (a) and after (b) addition of Hg^{2+} in **1'**.

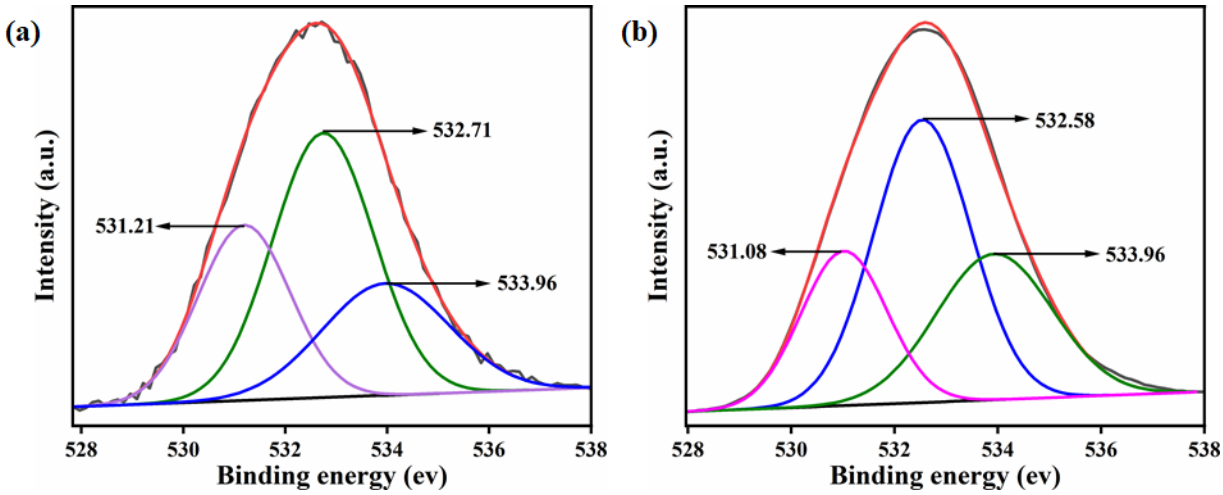

Figure S74. Fitted XPS spectra of O (1s) before (a) and after (b) addition of Hg^{2+} in **1'**.

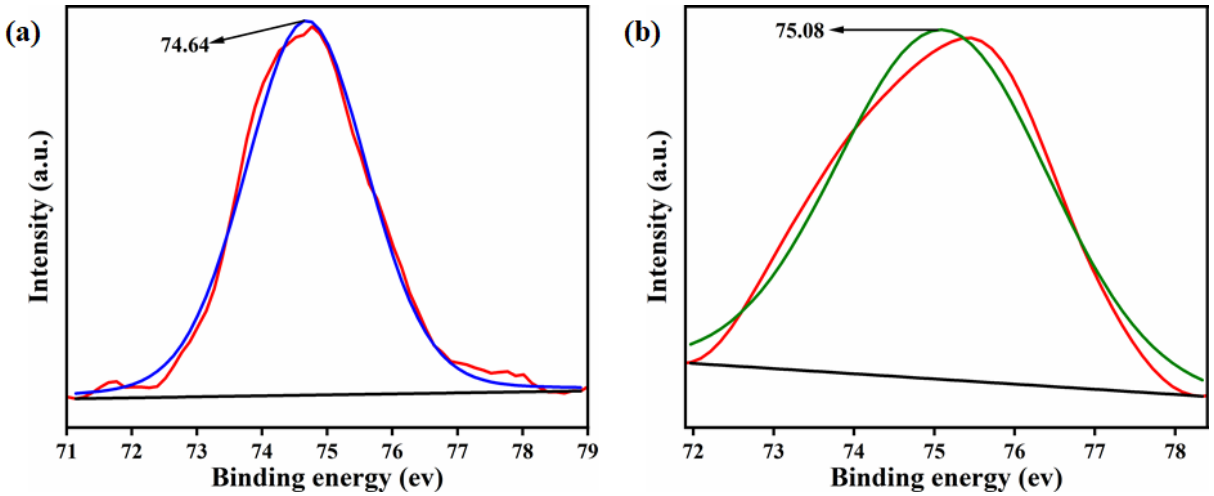

Figure S75. Fitted XPS spectra of Al (2p) before (a) and after (b) addition of Hg^{2+} in **1'**.

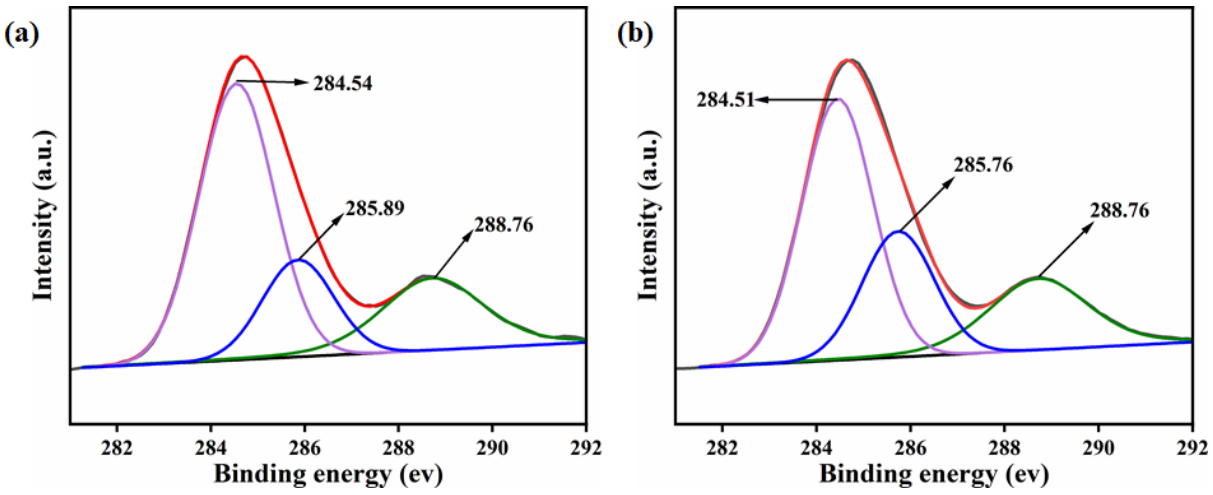

Figure S76. Fitted XPS spectra of C (1s) before (a) and after (b) addition of Hg^{2+} in **1'**.

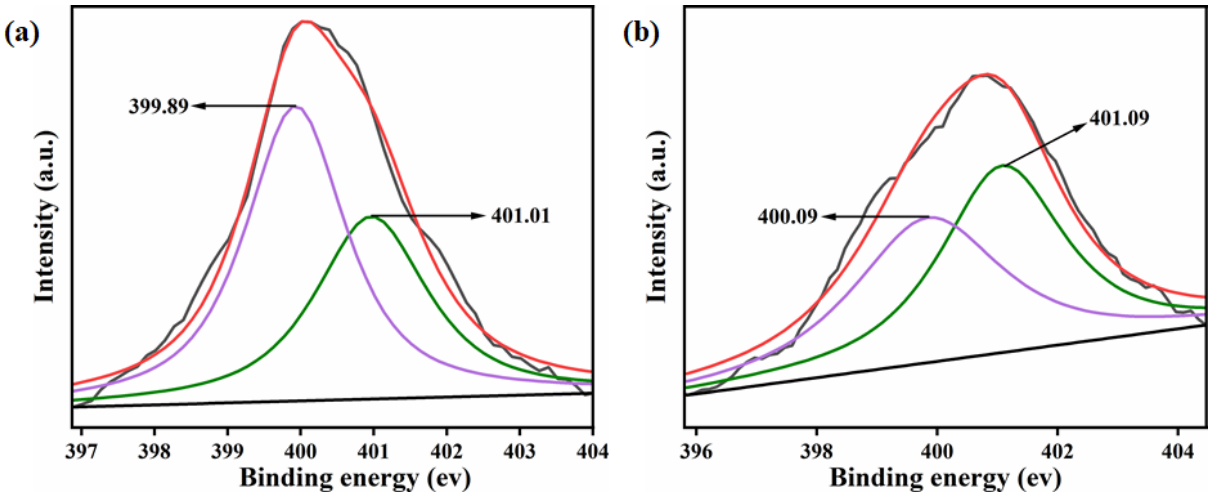

Figure S77. Fitted XPS spectra of N (1s) before (a) and after (b) addition of Hg^{2+} in **1'**.

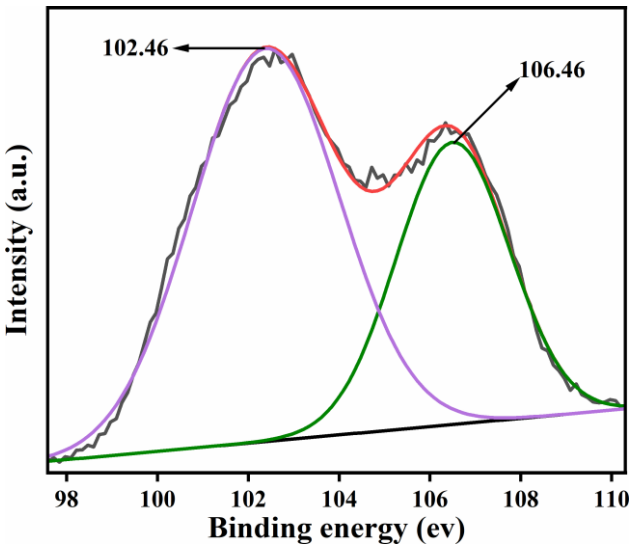

Figure S78. Fitted XPS spectra of Hg (4f) after addition of Hg^{2+} in **1'**.

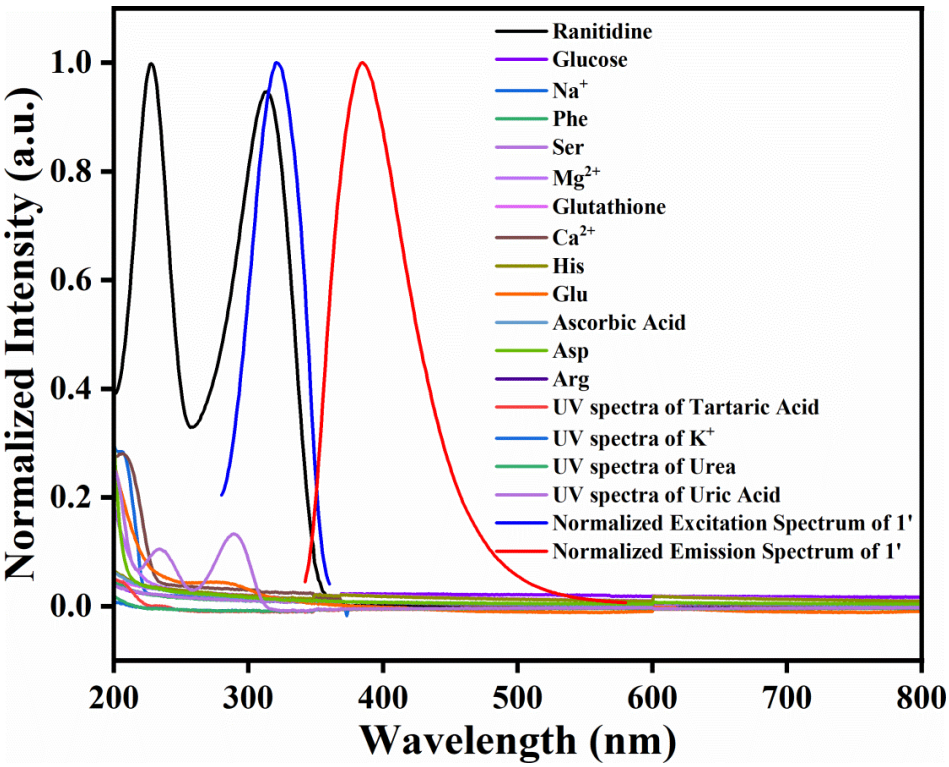

Figure S79. Spectral overlap of excitation/emission spectra of **1'** with the absorption spectrum of ranitidine and others analytes.

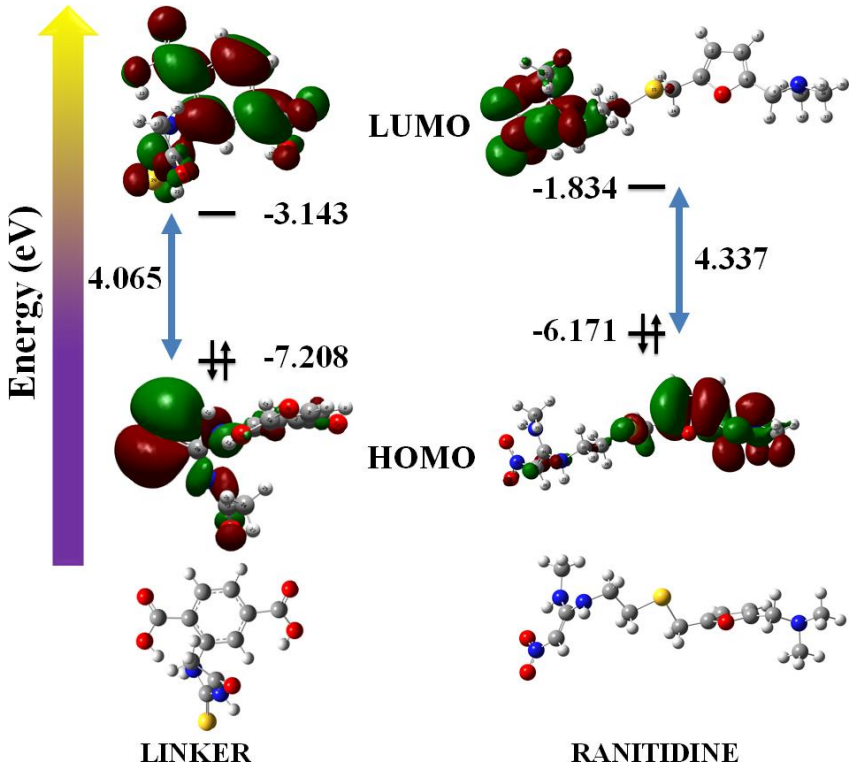

Figure S80. HOMO and LUMO energy levels of the free linker of MOF and ranitidine.

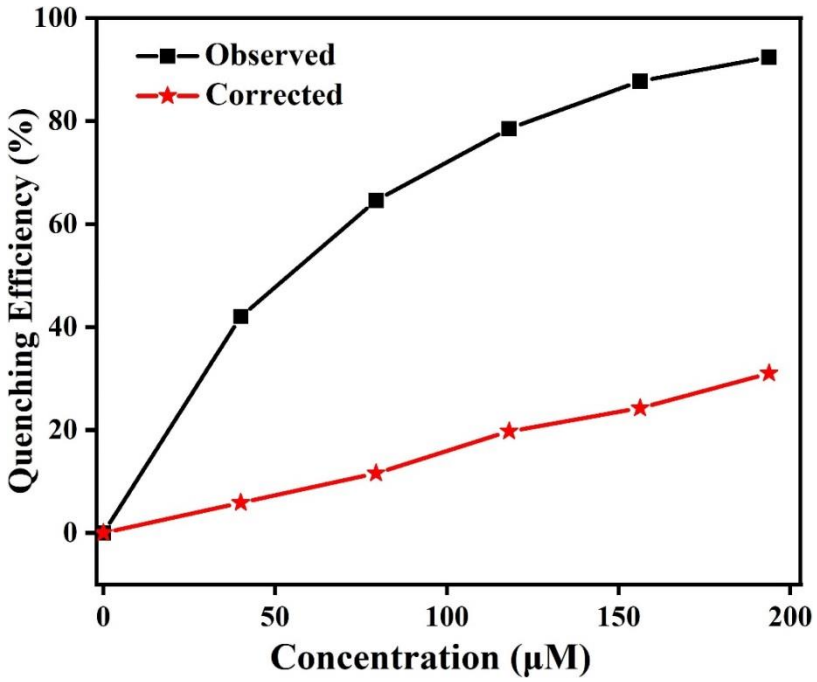

Figure S81. Observed and corrected quenching efficiency for ranitidine sensing.

Table S6. IFE correction table for ranitidine sensing.

[6-MP] (µM)	A_{ex}	A_{em}	Correction Factor (CF)	$F_{observed}$	$F_{corrected}$	$F_{corrected(0)}$/ $F_{corrected}$
0	0.20971	0.03454	1.30020	1260290	1638638	1
40	0.67556	0.07492	2.11130	730705	1542741	1.06216
79	1.22726	0.08406	3.24420	446504	1448552	1.13122
118	1.91371	0.09331	4.85981	270593	1315032	1.24608
156	3.16226	0.10532	8.02824	154642	1241506	1.31987
194	4.21394	0.11819	11.82211	95620	1130433	1.44956

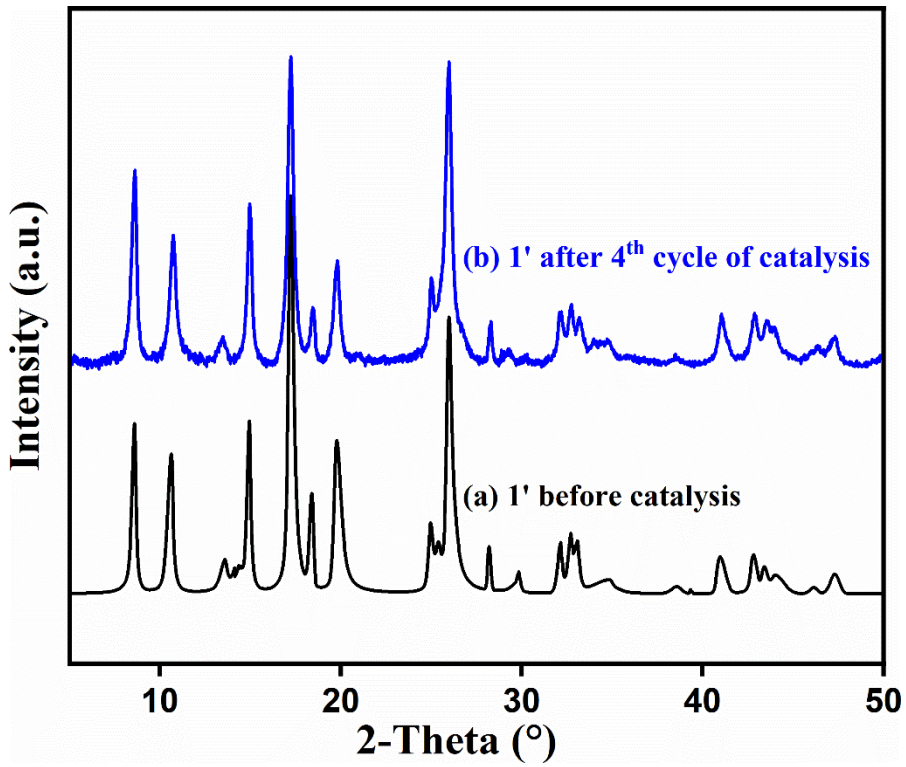

Figure S82. PXRD pattern of **1'** before and after 4th cycle of catalysis.

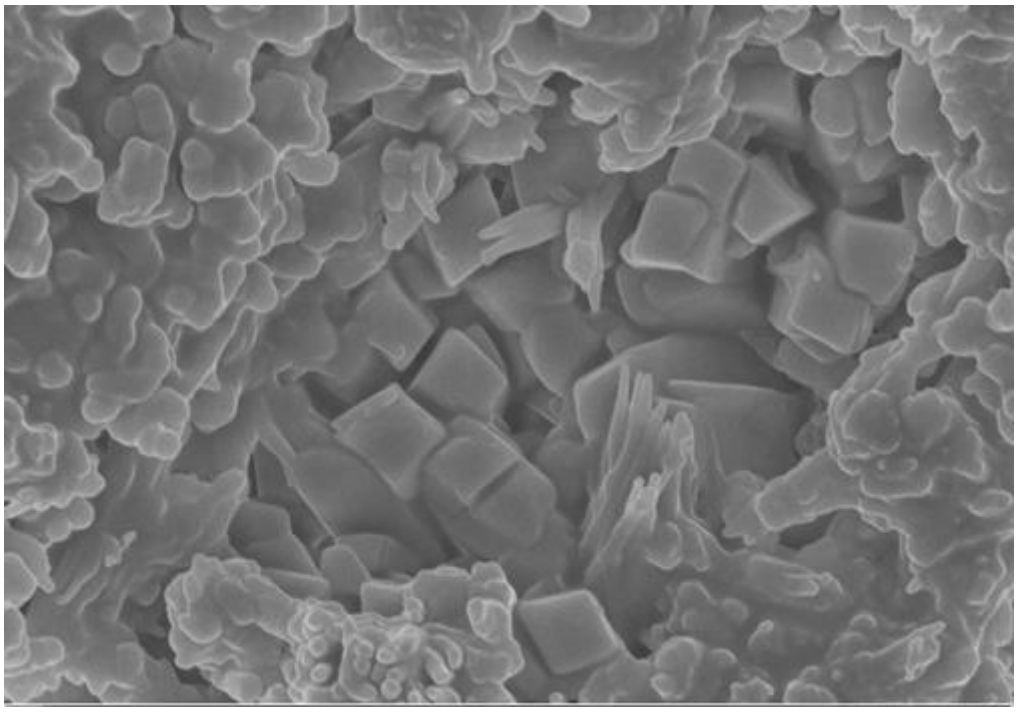

Figure S83. FESEM images of **1'** after 4th cycle of catalysis.

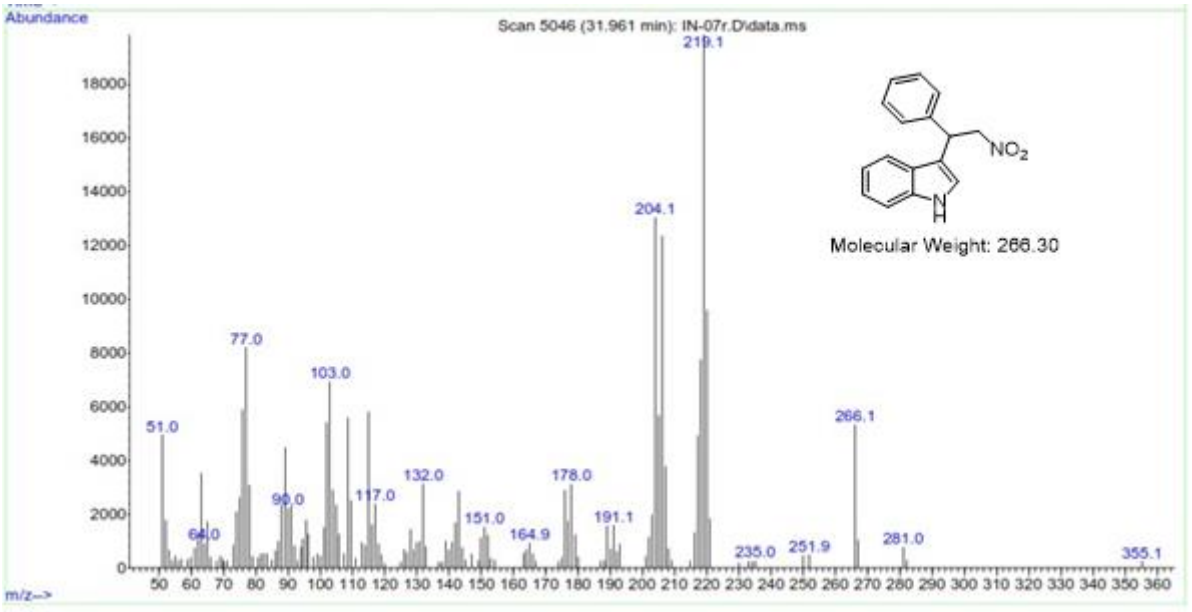

Figure S84. GC-MS trace of 3-(2-nitro-1-phenylethyl)-1H-indole.

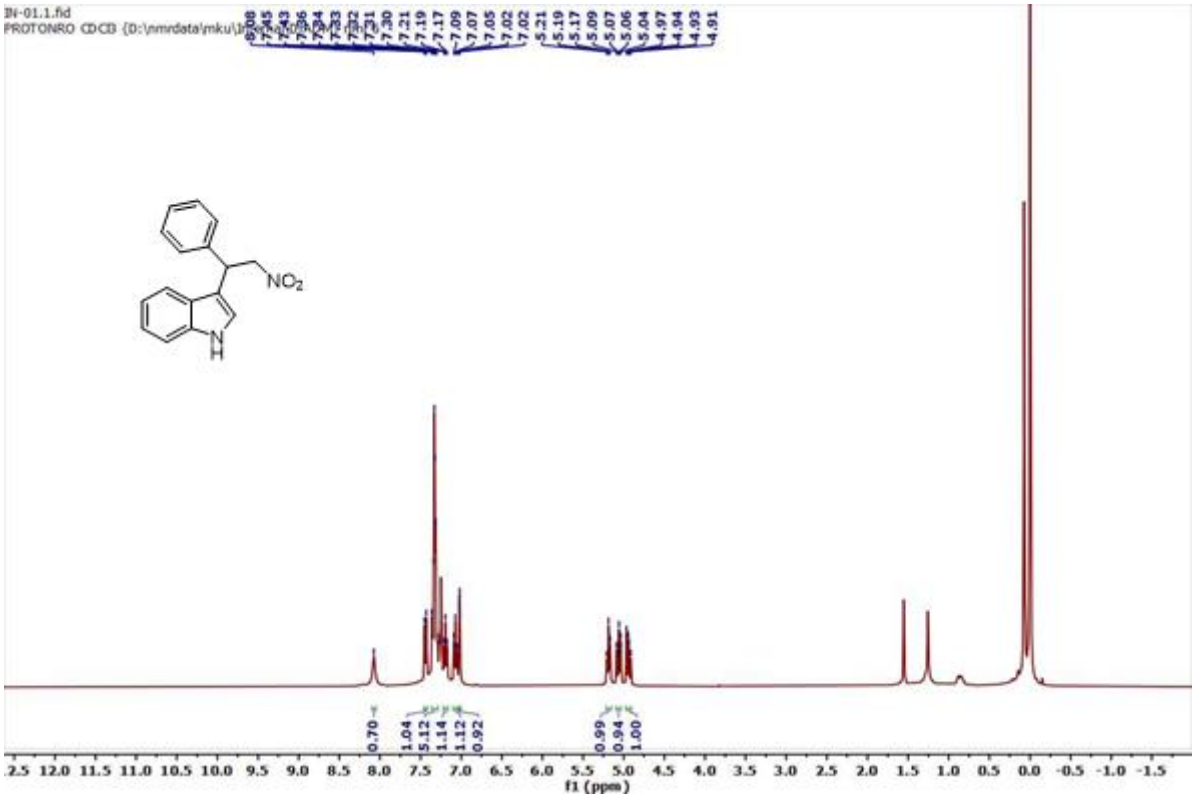

Figure S85. ^{1}H NMR of 3-(2-nitro-1-phenylethyl)-1H-indole. ^{1}H NMR (400 MHz, $CDCl_3$) δ 4.93(q, 1H), 5.06(q, 1H), 5.19(t, 1H), 7.02(d,1H), 7.07(t, 1H) 7.19(t, 1H), 7.33(m, 5H), 7.44(d, 1H), 8.08(s, 1H)

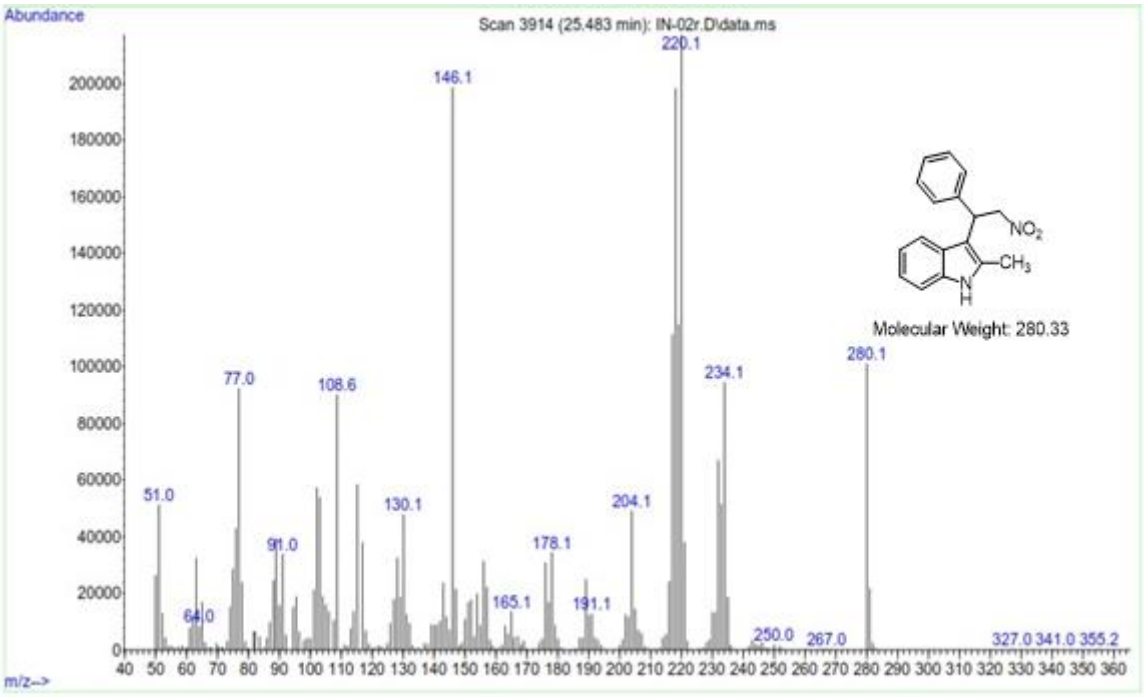

Figure S86. GC-MS trace of 2-methyl-3-(2-nitro-1-phenylethyl)-1H-indole.

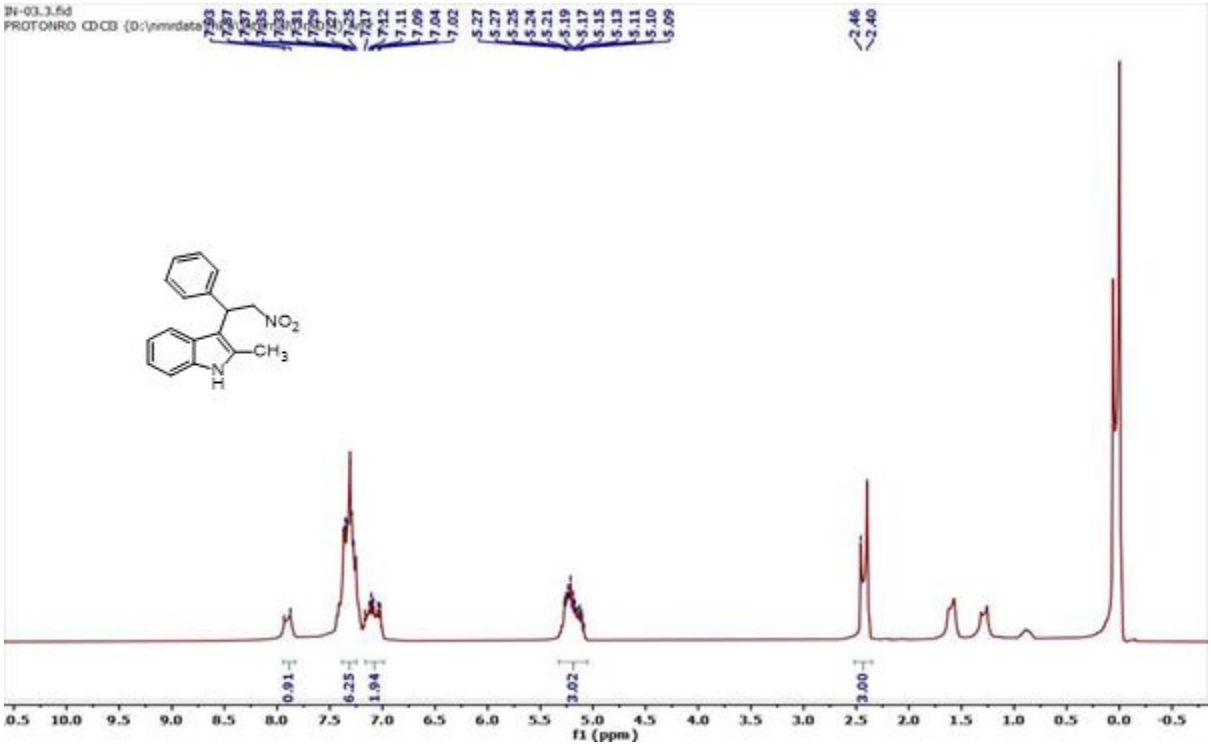

Figure S87. ^{1}H NMR of 2-methyl-3-(2-nitro-1-phenylethyl)-1H-indole ^{1}H NMR (400 MHz, $CDCl_3$) δ 2.43(d, 3H), 5.19(m, 3H), 7.10(m, 1H), 7.31(m, 6H), 7.89(d,1H).

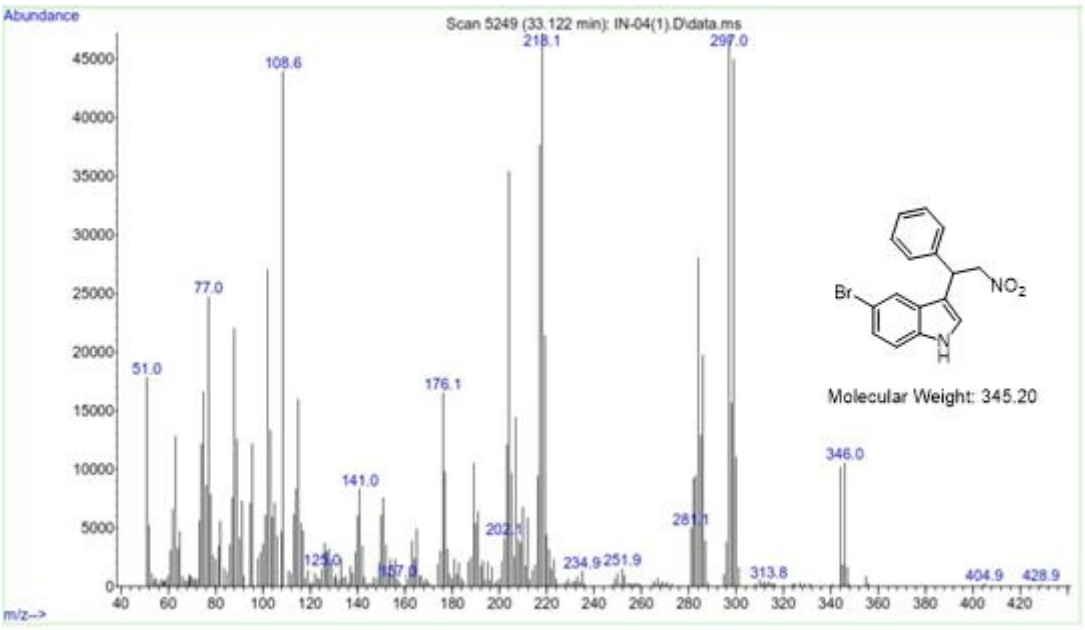

Figure S88. GC-MS trace of 5-bromo-3-(2-nitro-1-phenylethyl)-1H-indole.

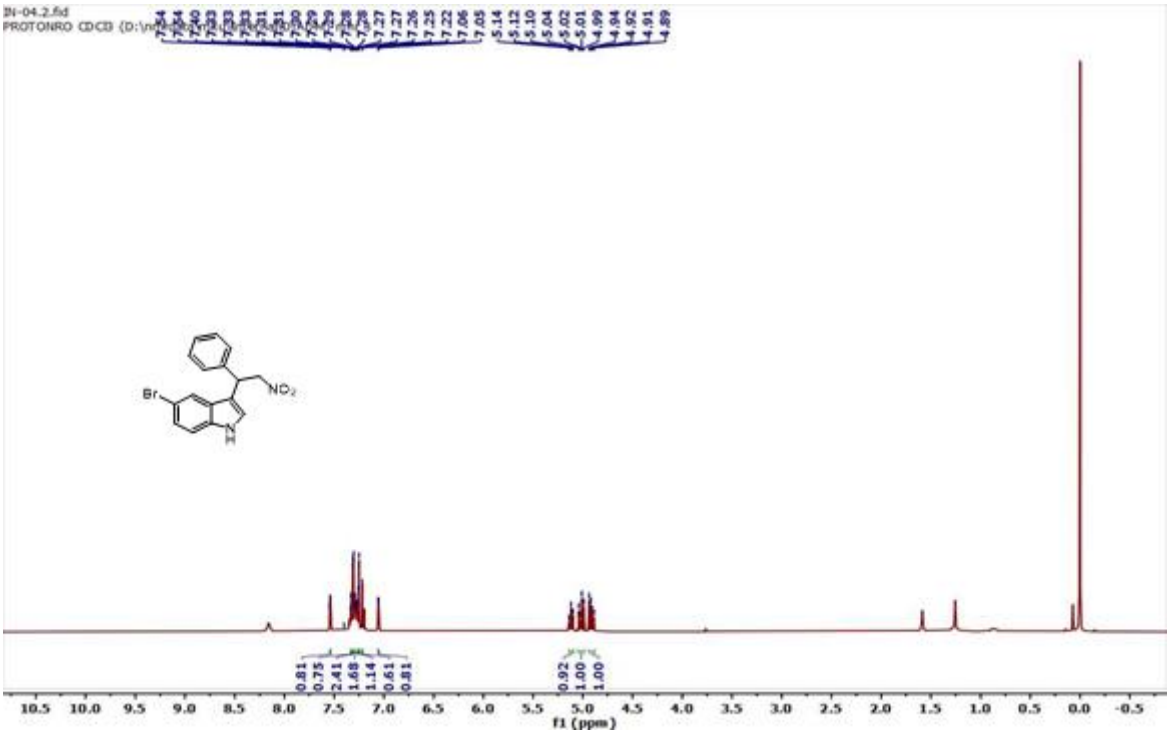

Figure S89. ^{1}H NMR of 5-bromo-3-(2-nitro-1-phenylethyl)-1H-indole. ^{1}H NMR (400 MHz, $CDCl_3$) δ 4.91(q, 1H), 5.02(q, 1H), 5.12(t, 1H), 7.05(d,1H), 7.22(s, 1H) 7.26(t, 1H), 7.28(m, 2H), 7.31(d, 2H), 7.33(t, H), 7.54(d, 1H).

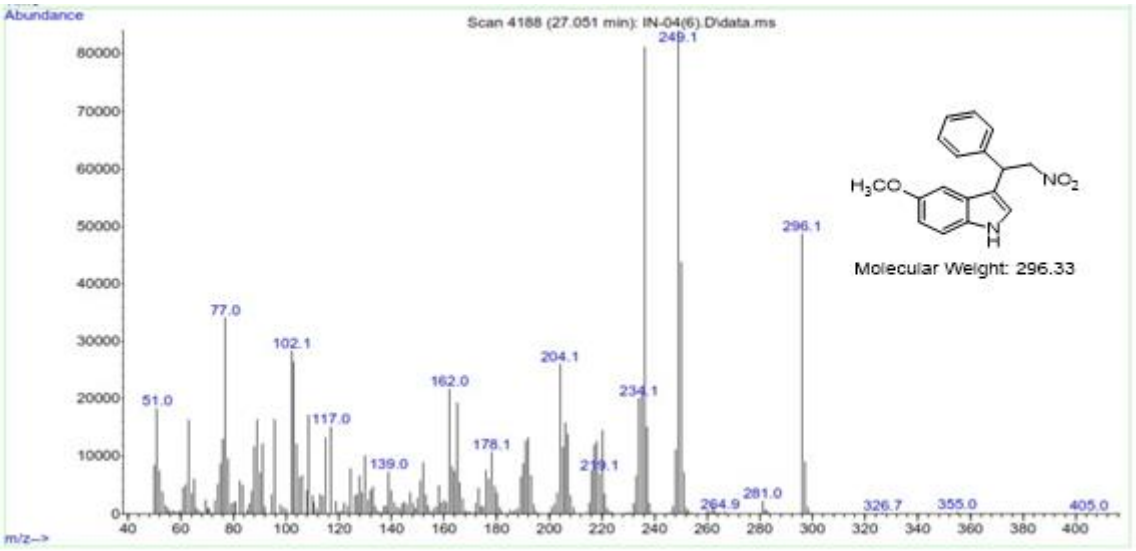

Figure S90. GC-MS trace of 5-methoxy-3-(2-nitro-1-phenylethyl)-1H-indole.

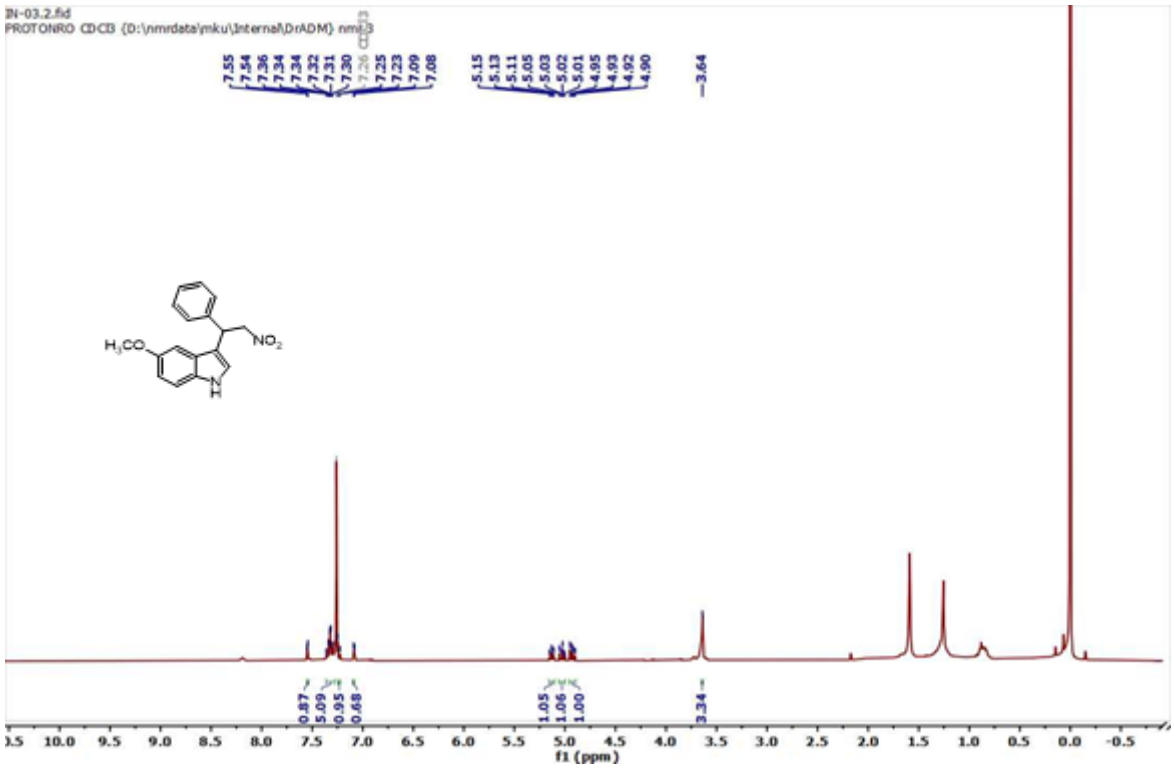

Figure S91. ^{1}H NMR of 5-methoxy-3-(2-nitro-1-phenylethyl)-1H-indole. ^{1}H NMR (400 MHz, $CDCl_3$): δ 3.64(s, 3H), 4.92(q, 1H), 5.03(q, 1H), 5.13(t, 1H), 7.08(d,1H), 7.25(s, 1H) 7.30(s, 1H), 7.33(m, 5H), 7.55(s, 1H).

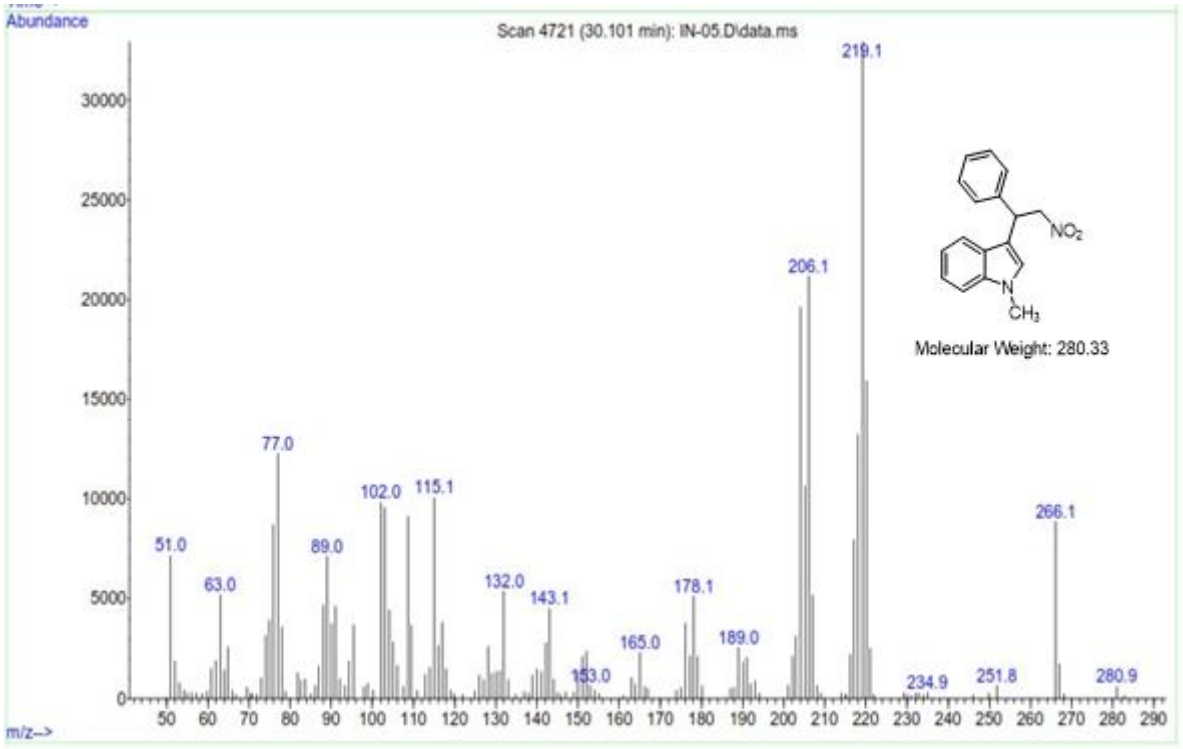

Figure S92. GC-MS trace of 1-methyl-3-(2-nitro-1-phenylethyl)-1H-indole.

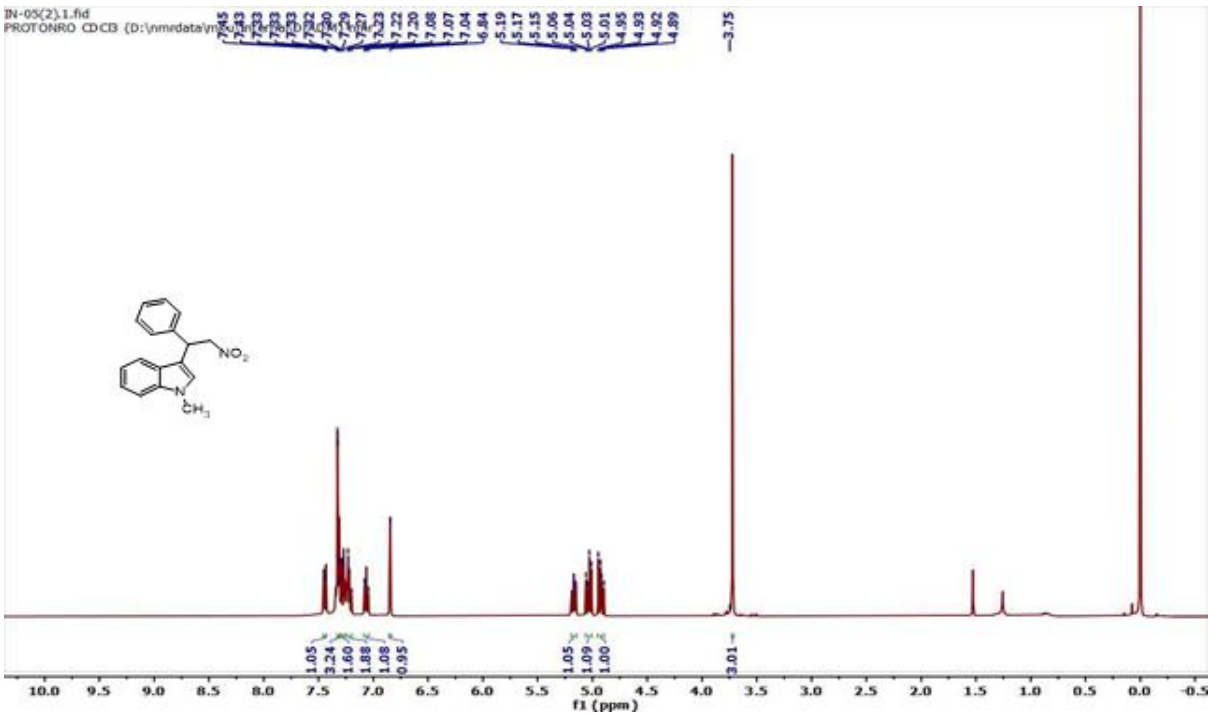

Figure S93. ^{1}H NMR of 1-methyl-3-(2-nitro-1-phenylethyl)-1H-indole: ^{1}H NMR (400 MHz, $CDCl_3$) δ 3.75(s, 3H), 4.92(q, 1H), 5.03(q, 1H), 5.13(t, 1H), 6.84(s, 1H), 7.07(t,1H), 7.21(t, 2H) 7.29(d,2H) 7.33(m, 3H), 7.43(d, 1H).

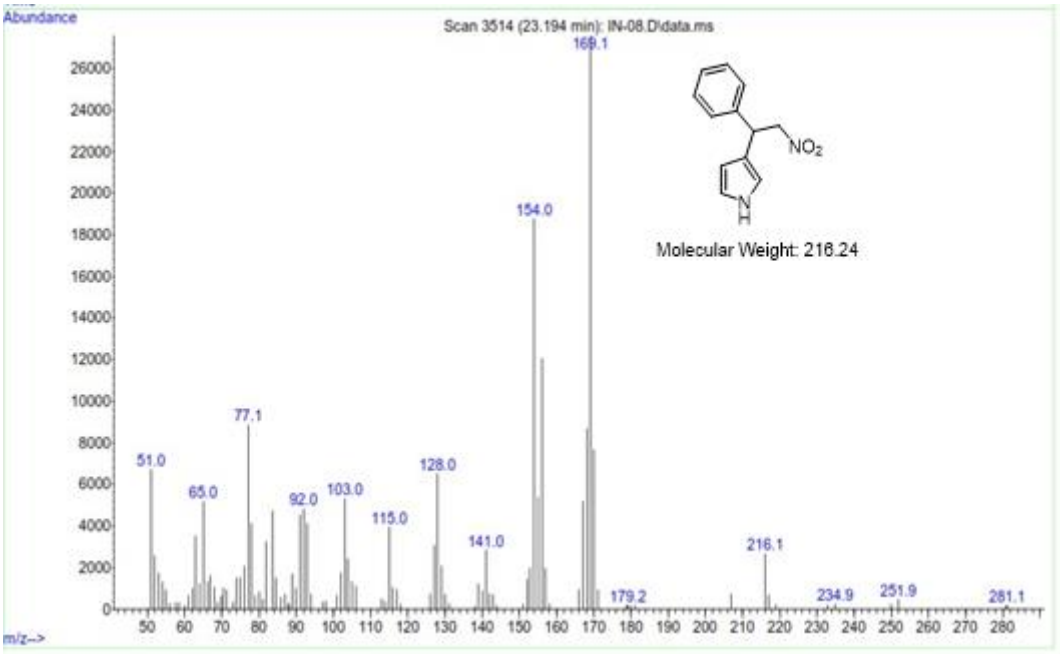

Figure S94. GC-MS trace of 3-(2-nitro-1-phenylethyl)-1H-pyrrole.

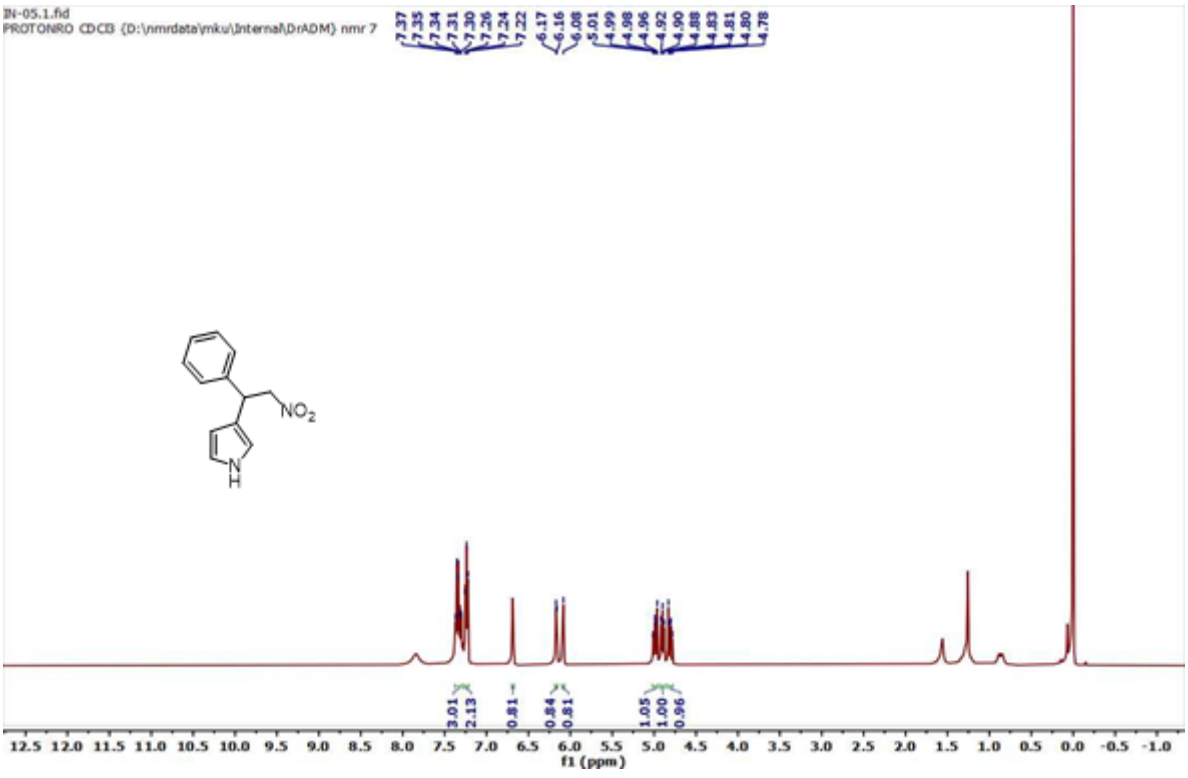

Figure S95. ^{1}H NMR of 3-(2-nitro-1-phenylethyl)-1H-pyrrole: ^{1}H NMR (400 MHz, $CDCl_3$) δ 3.75(s, 3H), 4.92(q, 1H), 5.03(q, 1H), 5.13(t, 1H), 6.84(s, 1H), 7.07(t,2H), 7.21(t, 2H) 7.33(m, 3H).

Table S7. Comparison of the response time, detection limit, K_{SV} and sensing media used for the reported MOF based fluorometric sensors for Hg^{2+} sensing.

Sl. No.	MOFs	Sensing Medium	K_{SV} (M^{-1})	LOD (nM)	Response Time (min)	Ref.
1	[PCN-221]	water	4021.9	10	1	2
2	$[Ni(3\text{-}bpd)_2(NCS)_2]_n$	water	-	-	120	3
3	[Cu(Dcbb)(Bpe)]·Cl	HEPES buffer	-	3.2	30	4
4	UiO-66@ Butyne	water	-	10.9	3	5
5	$Ln(TATAB)(DMF)_4(H_2O)(MeOH)_{0.5}$	water	4851	4.4	-	6
6	Eu^{3+}/CDs@MOF-253	water	-	47.88	3	7
7	$[Cu(Cdcbp)(H_2O)2\cdot 2H2O]_n$	water	-	2.3	2	8
8	NH2-MIL-53(Al)	water	5.7×10^4	150	-	9
9	$[Cu(Cbdcp)(Dps)(H_2O)_3]\cdot 6H_2O_n$	HEPES buffer	-	2.6	10	10
10	Cd−EDDA	water	4.3×10^3	2	0.25	11
11	Al-MOF (TAM)	water	-	2.94	0.5	12
12	$[Zn(L)(BBI).(H_2O)_2]$ $[Cd(L)(TPOM)_{0.75}]$	water	-	-	-	13
13	$Zn(tpbpc)_2$	water	6.2×10^3	320	60	14
14	P/UiO-66-NH_2	Tis-HCl Buffer	-	17.6	-	15
15	**$[Al(OH)(BDC\text{-}NHCSNHCOCH_3)]\cdot H_2O$ (1)**	**water**	**1.29×10^6**	**7.3**	**0.16**	**this work**

Table S8. Comparison of the response time, detection limit, K_{SV} and sensing media used for the reported MOF based fluorometric sensors for ranitidine sensing.

Sl. No.	MOFs	Sensing Medium	K_{SV} (M^{-1})	LOD (nM)	Response Time (min)	Ref.
1	AP-NSCDs	MeCN	-	100 nM	-	16
2	CDs	phophate buffer	-	30 µM	4	17
3	CdS QDs	Tris-HCl buffer	-	120 µM	-	18

4	Tyr@AuNP	phophate buffer	-	174 nM	3	19
5	**[Al(OH)(BDC-NHCSNHCOCH$_3$)]·H$_2$O (1)**	**water**	**7.99×10^5**	**3.4** nM	**0.08**	**this work**

References:

1. Douglass, I. B.; Dains, F., Some derivatives of benzoyl and furoyl isothiocyanates and their use in synthesizing heterocyclic compounds1. *J. Am. Chem.* **1934,** *56*, 719-721.
2. Moradi, E.; Rahimi, R.; Safarifard, V., Porphyrinic zirconium-based MOF with exposed pyrrole Lewis base site as an efficient fluorescence sensing for Hg2+ ions, DMF small molecule, and adsorption of Hg2+ ions from water solution. *J. Solid State Chem. Sci.* **2020,** *286*, 121277.
3. Halder, S.; Mondal, J.; Ortega-Castro, J.; Frontera, A.; Roy, P., A Ni-based MOF for selective detection and removal of Hg 2+ in aqueous medium: a facile strategy. *Dalton Trans.* **2017,** *46*, 1943-1950.
4. Hu, P.-P.; Liu, N.; Wu, K.-Y.; Zhai, L.-Y.; Xie, B.-P.; Sun, B.; Duan, W.-J.; Zhang, W.-H.; Chen, J.-X., Successive and specific detection of Hg2+ and I–by a DNA@ MOF biosensor: experimental and simulation studies. *Inorg. Chem.* **2018,** *57*, 8382-8389.
5. Samanta, P.; Desai, A. V.; Sharma, S.; Chandra, P.; Ghosh, S. K., Selective recognition of Hg2+ ion in water by a functionalized metal–organic framework (MOF) based chemodosimeter. *Inorg. Chem.* **2018,** *57*, 2360-2364.
6. Xia, T.; Song, T.; Zhang, G.; Cui, Y.; Yang, Y.; Wang, Z.; Qian, G., A terbium metal–organic framework for highly selective and sensitive luminescence sensing of Hg2+ ions in aqueous solution. *Chem. Eur. J.* **2016,** *22* (51), 18429-18434.
7. Xu, X.-Y.; Yan, B., Fabrication and application of a ratiometric and colorimetric fluorescent probe for Hg 2+ based on dual-emissive metal–organic framework hybrids with carbon dots and Eu 3+. *J. Mater. Chem. C* **2016,** *4*, 1543-1549.
8. Huang, N.-H.; Li, R.-T.; Fan, C.; Wu, K.-Y.; Zhang, Z.; Chen, J.-X., Rapid sequential detection of Hg2+ and biothiols by a probe DNA—MOF hybrid sensory system. *J. Inorg. Biochem.* **2019,** *197*, 110690.
9. Zhang, L.; Wang, J.; Du, T.; Zhang, W.; Zhu, W.; Yang, C.; Yue, T.; Sun, J.; Li, T.; Wang, J., NH2-MIL-53 (Al) metal–organic framework as the smart platform for simultaneous high-performance detection and removal of Hg2+. *Inorg. Chem.* **2019,** *58*, 12573-12581.
10. Huang, N.-H.; Liu, Y.; Li, R.-T.; Chen, J.; Hu, P.-P.; Young, D. J.; Chen, J.-X.; Zhang, W.-H., Sequential Ag+/biothiol and synchronous Ag+/Hg 2+ biosensing with zwitterionic Cu 2+-based metal–organic frameworks. *Analyst* **2020,** *145*, 2779-2788.
11. Wu, P.; Liu, Y.; Liu, Y.; Wang, J.; Li, Y.; Liu, W.; Wang, J., Cadmium-based metal–organic framework as a highly selective and sensitive ratiometric luminescent sensor for mercury (II). *Inorg. Chem.* **2015,** *54*, 11046-11048.
12. Radwan, A.; El-Sewify, I. M.; Shahat, A.; Azzazy, H. M.; Khalil, M. M.; El-Shahat, M. F., Multiuse Al-MOF chemosensors for visual detection and removal of mercury ions in water and skin-whitening cosmetics. *ACS Sustainable Chem. Eng.* **2020,** *8* (40), 15097-15107.
13. Zhao, Y.; Xu, X.; Qiu, L.; Kang, X.; Wen, L.; Zhang, B., Metal–organic frameworks constructed from a new thiophene-functionalized dicarboxylate: luminescence sensing and pesticide removal. *ACS Appl. Mater. Interfaces* **2017,** *9*, 15164-15175.

14. Xiao, J.; Liu, J.; Gao, X.; Ji, G.; Wang, D.; Liu, Z., A multi-chemosensor based on Zn-MOF: Ratio-dependent color transition detection of Hg (II) and highly sensitive sensor of Cr (VI). *Sens. Actuators B: Chem.* **2018,** *269*, 164-172.
15. Wu, L. L.; Wang, Z.; Zhao, S. N.; Meng, X.; Song, X. Z.; Feng, J.; Song, S. Y.; Zhang, H. J., A metal–organic framework/DNA hybrid system as a novel fluorescent biosensor for mercury (II) ion detection. *Chem. Eur. J.* **2016,** *22*, 477-480.
16. Lv, S.; Wang, P.; Liu, D.; Liu, X.; Zhou, Z., Aminophenol functionalized carbon quantum dots as fluorescent sensor for nitroalkenes. *Microchem. J.* **2023,** *189*, 108569.
17. Mohammadi, N.; Akhgari, F.; Samadi, N., A Green and Simple Carbon-dot-based Fluorescent Probe for Selective and Sensitive Detection of Ranitidine Hydrochloride. *Anal. Bioanal. Chem. Res.* **2021,** *8*, 525-536.
18. Gore, A. H.; Mote, U. S.; Tele, S. S.; Anbhule, P. V.; Rath, M. C.; Patil, S. R.; Kolekar, G. B., A novel method for ranitidine hydrochloride determination in aqueous solution based on fluorescence quenching of functionalised CdS QDs through photoinduced charge transfer process: Spectroscopic approach. *Analyst* **2011,** *136*, 2606-2612.
19. Hameed, M. K.; Parambath, J. B.; Kanan, S. M.; Mohamed, A. A., FRET-based fluorescent probe for drug assay from amino acid@ gold-carbon nanoparticles. *Anal. Bioanal. Chem. Res.* **2021,** *413*, 1117-1125.